Integrated Seismic Interpretation along with Attributes and Post Stack Inversion, Petrophysical Analysis, Rock Physics based Facies Modeling, Full Wave Inversion based Velocity Model Building

&

3D Survey Planning of Sinjhoro Area, Lower Indus Basin Pakistan.

USAMA YOUNAS

BS Geophysics

2016-2020

Department of Earth Sciences

Quaid-i-Azam University

Islamabad, Pakistan.

CERTIFICATE

This dissertation submitted by USAMA YOUNAS S/O MUHAMMAD YOUNAS is accepted in its present form by the Department of Earth Sciences, Quaid-i-Azam University Islamabad as satisfying the requirement for the award of BS degree in Geophysics.

RECOMMENDED BY

Prof. Dr. M. Gulraiz Akhter _____

(Supervisor)

Dr. Amir Ali _____

(Chairman Department of Earth Sciences)

External Examiner _____

"Research Is the Joy of

Discovering

Something new"

ACKNOWLEDGEMENT

In the name of Allah Almighty, the most Gracious, the most Compassionate. Almighty, on whom ultimately, we depend for sustenance and guidance. I bear witness that Hazrat Muhammad (PBUH) is the last messenger, whose life is role model for the whole mankind till the Day of Judgment. I thank Allah Almighty for giving me strength and skill to finalize this study.

I acknowledge the cooperation extended by the Department of Earth Sciences at Quaid-i- Azam University Islamabad. Principally I would like to manifest my appreciation to my Supervisor; Professor Dr. Muhammad Gulraiz Akhter for having faith in me by giving me a chance to do my dissertation under the guidance of Dr. Khalid Amin Khan.

I would like to pay special thanks to my mentor Dr. Khalid Amin Khan who always inspired me by stories of great scientists and helped me to learn new things. He always encouraged my mind to think more creative, hands to play with softwares and heart to love.

I must acknowledge some persons who helped me in all aspects of thesis work and encouraged me to finish this research in time. Rana Salman, Ajam Abbas, Sana Kayani and Amber Latif. Their moral and technical support was very beneficial for my research work and to enhance my knowledge, without them it wouldn’t have been possible.

This Work is dedicated to

My Beloved Parents

&

Siblings

whose support, encouragement, guidance

and prays make me able to achieve such success and honor.

Abstract

Sinjhoro is a developed field of Oil and Gas accumulations with structural and stratigraphic traps in the Lower Indus Basin. The present study pertains to integrated seismic interpretation along with attributes analysis and post stack inversion, petrophysical analysis coupled with rock physics techniques, velocity model building using horizon-based interpolation and full wave inversion. It also includes 3D seismic survey planning for future exploration. The data used for this research work consist of thirteen seismic lines along with velocity data and well logs of 4 wells.

The seismic interpretation shows horst and graben structures bounded by normal faults. After time to depth conversion,using the velocity model, the true structural geometry is obtained in the form of depth sections. The horizons were identified using formation tops from wells and their depths were confirmed through correlation with synthetic seismogram generated from sonic and density logs. Crustal extension analysis has also been carried out on the depth section which indicates an extensional regime.

Petrophysics is the one of the most reliable tools for the confirmation of the type of hydrocarbon and for marking the proper zone of the interest for the presence of the hydrocarbon through combination of different logs. Petrophysics and rock physics analysis along with facies modeling and empirical relations of logs are performed on the Chak 5 Dim South-01 well and zone of interest identified where the fluid saturations and porosities are calculated.

Seismic velocities have been calibrated through borehole velocities from sonic logs and velocity model has been built using spatio-temporal as well as horizon-based interpolation algorithms and finally improved with full wave inversion. 2D synthetic seismic has been generated from these velocity models through convolution with a Ricker wavelet. The results indicate that horizon-based interpolation generates the best velocity model and therefore it is used in time to depth conversion.

Post stack seismic inversion analysis has been carried out for better understanding of the behavior of impedance in the reservoir and seal rocks. In addition, AVA synthetic gathers have been generated which indicate class II type of gas sands.

As part of the study a 3D seismic survey has been planned keeping in view the existing data to increase the probability of success for field development and reservoir characterization.

Table of Contents

Chapter 1: Introduction

Oil and Gas are considered as lifeblood of modern industrialized civilization. These are the most valuable and essential energy resources on the planet Earth. Geophysicists are using different geophysical methods to explore these energy resources lying deep into the subsurface of Earth. Seismic method is one of the most widely used geophysical methods for exploration of hydrocarbons. Seismic technology has evolved rapidly in the last decade and can provide stunning images of the subsurface.

The **seismic method** is rather simple in concept, an energy source is used to produce seismic waves (similar to sound) that travel through the earth and the motion or pressure variations are converted to electrical signal recorded by electronic instruments (Gadallah & Fisher, 2009).

The seismic method has three principal applications:

1. Delineation for near-surface geology for engineering studies, and coal, and mineral exploration within a depth of up to 1km: The seismic method applied to the near- surface studies is known as engineering seismology.
2. Hydrocarbon exploration and development is carried out within a depth of up to 10 Km in sedimentary basins. The seismic method applied to the exploration and development of oil and gas fields is known as exploration seismology.
3. Investigation of the earth's crustal structure within a depth of up to 100 Km: The seismic method applied to the crustal and earthquake studies is known as earthquake seismology (Yilmaz, 2001).

1.1 Seismic Reflection

Seismic Reflection determines the Earth's deep layer structure which is a geophysical prospecting method based on the fact that the velocity of transmission of shock waves through the Earth vary with the elastic constants and the densities of the rocks through which the waves pass. (Kearey, 2002).

1.2 Seismic Refraction

Seismic Refraction is a surface geophysics method that utilizes the refraction of seismic waves on geological layers and rock units to characterize subsurface geologic conditions. The method involves a geophysical principal governed by Snell's Law. The seismic Refraction method is

based on the measurement of the travel times of refracted waves refracted at the interfaces between subsurface layers of differing velocities.

1.3 Seismic Acquisition

Seismic acquisition is the process of collecting seismic data on both land and ocean. This usually involves injecting energy into the ground in the form of elastic waves, using vibroseis or buried dynamite on land, or air gun arrays at sea. The waves propagate into the Earth and reflect, refract or diffract from subsurface heterogeneities. Energy that returns to the surface is recorded at geophone (for land) or hydrophone (for ocean), These are the devices that converts ground movement (velocity) into voltage. Which may be recorded at a recording station. The deviation of this measured voltage from the base line is called the seismic response and is analysed to understand the structure of the earth. Seismic Data can be acquired depending upon the objective of the survey and economy of the drilling company such as 2D, 3D and 4D.

1.4 2-D Seismic

In 2-D reflection seismic surveying both the energy source and the geophones (numbering up to a hundred or more per shot) are moved along a straight line. The resultant product can be thought of as a vertical cross-section of the subsurface beneath the survey line.

1.5 3-D Seismic

3-D seismic survey is a set of numerous closely spaced seismic lines that provide a high spatially sampled measure of subsurface reflectivity. A 3-D seismic data provides more thorough analysis than 2-D seismic data. Shooting a 3-D seismic survey has both exploration and exploitation benefits. 3D surveys (acquired on dense grids) provide high-resolution 3D images which reveal fine-scale geological structure for exploration in more complex settings. In a worldwide study one large company registered an increase in their success rate for 13% in 1991 using 2D data to 44% in 1996 using 3D technology extensively (Ayler, 1997).

1.6 4-D Seismic or Time-lapse

The differences observed in 3-D seismic surveys recorded over the same field with a separation period of several years show the progress of depletion and flooding practices. Such surveys are called “4-D” or “time lapse” surveys.

The objective is to determine the changes occurring in the reservoir as a result of hydrocarbon production or injection of water or gas into the reservoir by comparing the repeated datasets.

1.7 Petroleum Potential of Pakistan

Pakistan is blessed with enormous hydrocarbon potential most of which is still untapped. According to technical evaluations the original recoverable reserves were 1,246,.877million barrels of oil and 57.436 Tcf of gas. The current recoverable reserves are 347.878 million barrels of oil and 19.541Tcf of gas. (Ministry of Energy, Petroleum Division, Government of Pakistan).

Pakistan has a large sedimentary area of 872,268 Sq. Kms in which only 1094 Exploratory and 1443 Appraisal/ Development wells have been drilled so far with an average well drilling density of 3.0 wells per 1000 Sq. Kms. These wells have resulted in 394 discoveries and about 95% of these wells are concentrated in the Indus Basin, Balochistan, Khyber Pakhtunkhwa, while Offshore area is virtually unexplored.(Ministry of Energy Petroleum division Government of Pakistan).

Indus and Baluchistan basin are separated by Ornach Bela transform fault zone and the Pishin basin lies between Indus and Chamman transform fault. A variety of sub-basins, fold belts and monoclines with variable structural styles resulting from diverse geodynamic conditions have been identified in Baluchistan Basin and Indus Basin (Kadri, 1995).

1.8 Study Area

2D reflection survey was done in Sinjhoro, Sindh Pakistan. Sinjhoro area is present in Sanghar district of Sindh, Pakistan, about 12 km from Sanghar city, along Sanghar-Shahdad Pur Road and about 65 km northeast of Hyderabad City, Pakistan. Geographically the area falls in Lower Indus Basin. The Lower Indus Platform Basin is bounded to the North by the Central Indus Basin, to the Northwest by the Sulaiman Foldbelt Basin and the Kirthar Fold Belt Basin in the Southwest.

1.8.1 Geographical Coordinates

Latitude: 25.30°-26.29° N

Longitude: 68.25°-70.13° E

Elevation above sea level: 15 m.

1.8.2 Survey Information

It includes all the information about the lines, wells and base map of the study area. The seismic reflection data of the study area was obtained by Directorate General of Petroleum Concession

(DGPC) Pakistan in digital format for analysis and interpretation. This data was acquired by OGDCL Crew SP-7 in 2001-2002 and processed by OGDCL in 2003. Energy source used for the survey was 3KG of dynamite at 32 m hole depth. SP interval of the survey was 25m. The trend of the seismic dip and strike lines in SE-NW and SW-NE respectively. The SEG Y data of the seismic lines and wells mentioned in Table 1.1 was provided for this research work.

1.8.3 Base Map of Study Area

The navigation data of selected seismic lines and wells in the Sinjhoro Area, obtained from Directorate General of Petroleum Concessions (DGPC), is used to plot the base map using K-tron Precision Matrix an Integrated Geo Systems (Khan, 2000) application. Base map is considered as a principal module of interpretation as velocity and elevation contours are finally displayed on this map. The base map in survey grid with specialized location of source and receiver lines area is generated by plotting data in Universal Transverse Mercator (UTM, Zone 42) geodetic reference system is shown along with satellite imagery of the area.The seismic lines and wells used for marking the horizons are given in Table 1.1.

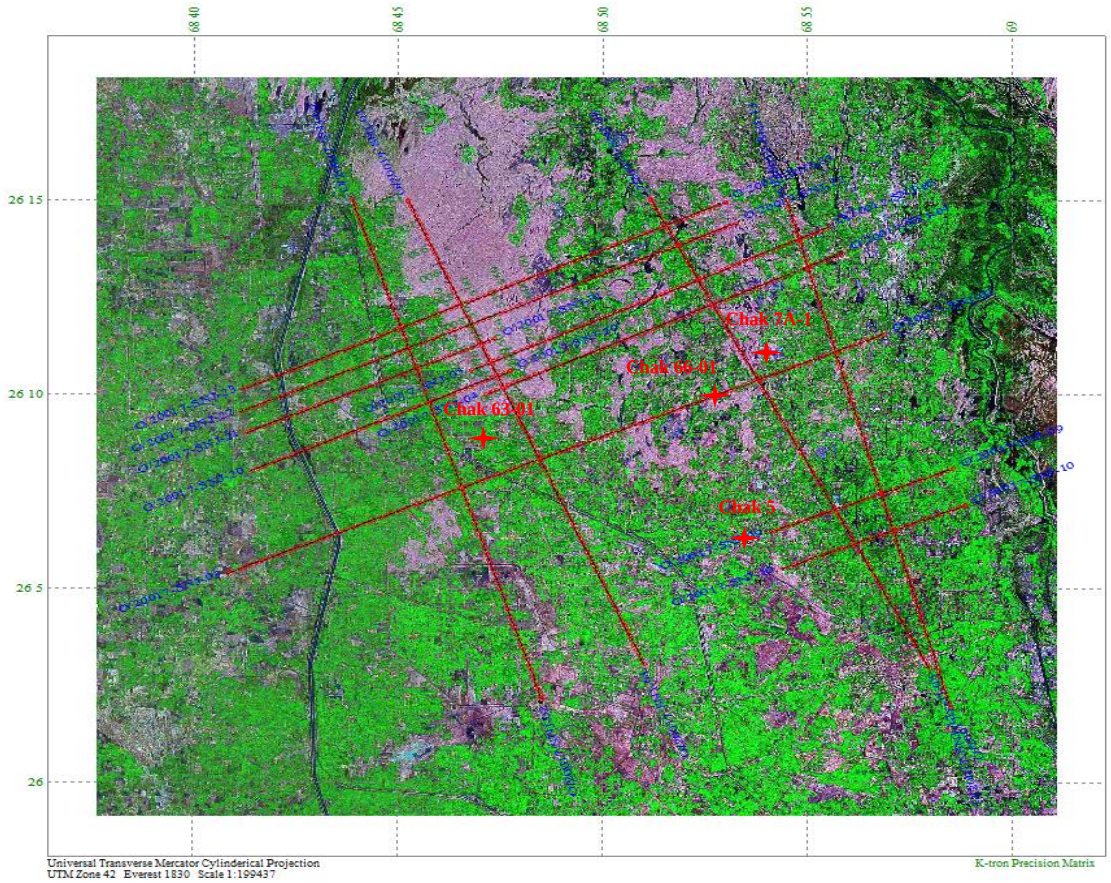

Fig 1.1: Base map posted on Satellite Image of the study area (Precision Matrix (Khan, 2000))

Table 1.1: Seismic Lines and Wells Information

Sr. No	Line No	Nature	Direction	Wells
1	**20017-SNJ-01**	**Strike**	**NW-SE**	
2	**20017-SNJ-03**	**Dip**	**SW-NE**	**CHAK-63-01**
3	**20017-SNJ-04**	**Dip**	**SW-NE**	**CHAK7A-01**
4	**20017-SNJ-05**	**Dip**	**SW-NE**	**CHAK66-01**
5	**20017-SNJ-08**	**Strike**	**NW-SE**	
6	**20017-SNJ-09**	**Dip**	**SW-NE**	**CHAK-5DIMSOUTH-01**
7	**20017-SNJ-10**	**Dip**	**SW-NE**	
8	**20017-SNJ-13**	**Strike**	**NW-SE**	
9	**20017-SNJ-19**	**Dip**	**SW-NE**	
10	**20017-SNJ-20**	**Dip**	**SW-NE**	
11	**20017-SNJ-21**	**Dip**	**SW-NE**	
12	**20017-SNJ-22**	**Dip**	**SW-NE**	
13	**20017-SNJ-23**	**Dip**	**SW-NE**	

1.9 Seismic Acquisition Parameters

Detail of seismic acquisition parameters is as below.

1.9.1 Source

Energy source	Dynamite
Charge Pattern	1 hole
Average Shot Depth	30 meters
S.P Interval	50 meters

1.9.2 Instruments

System	SN-358
Format	32-SEG D / DMUX
Notch Filter	IN
Field Sampling Interval	2 Milli Second
Record Length	5 Seconds
No. of Data Traces	240

1.9.3 Cable

Spread	3012-37.5-X-37.5-3012

Station Interval	50 meters
Group Interval	25 meters
Type of Geophone	SM-4S SERCEL / 10 Hz
Geophones/Group	0212 Over 23.92 M
Geophone Interval	1.04 meter

Spread: Symmetric Split Spread

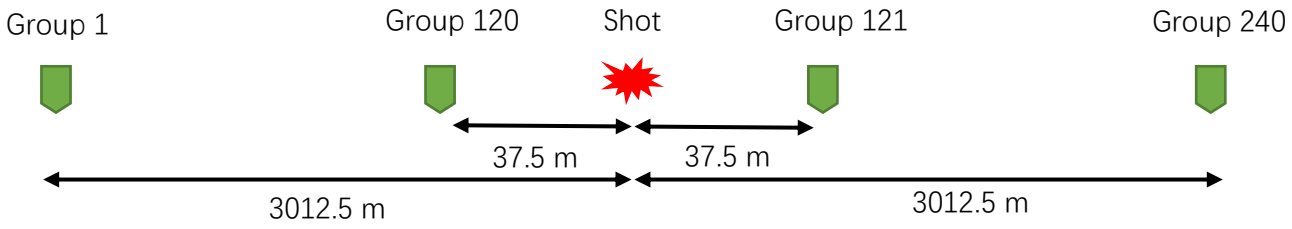

1.10 Seismic Processing

After the raw data has been collected from field, The data has been passed through the whole processing sequence that includes different data processing techniques which are used to suppress the noise and enhance the quality of the data for better interpretation. The raw seismic data is processed to enhance the signal to noise ratio and get the final seismic sections. The generalized processing sequence flow chart is given in Fig 1.2

This data was processed in 2001 with following general parameters.

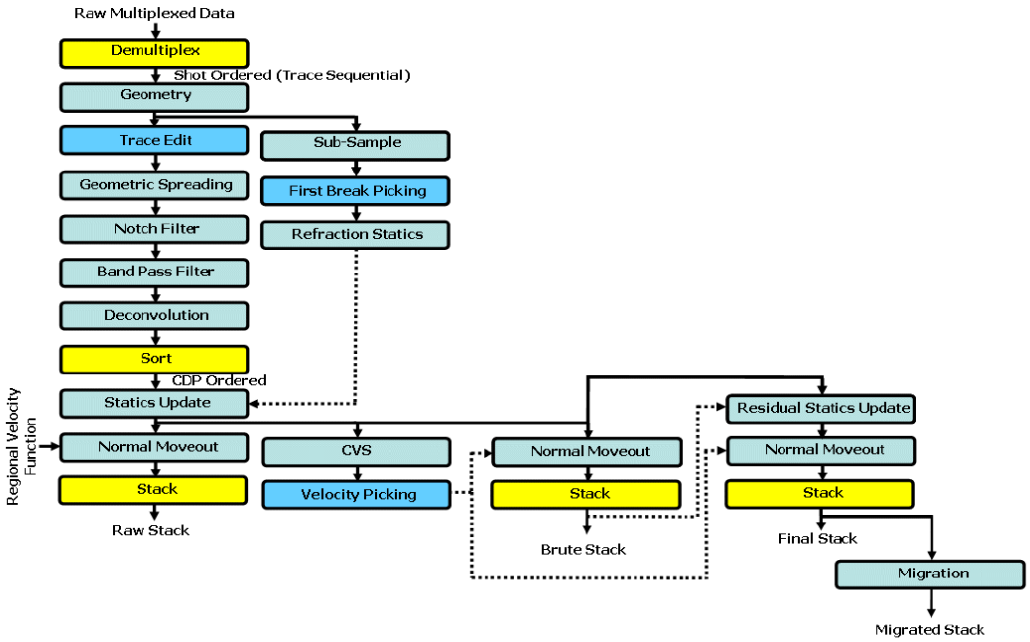

Fig 1.2: Generalized seismic processing sequence (Khan, 2009)

- ✓ **Process:** Migrated Stack
- ✓ **Fold:** 6000%
- ✓ **Datum Velocity:** 1800 m/sec
- ✓ **Datum Plane:** M.S.L
- ✓ **Processing Sampling Interval:** 4 Milli Second

Detailed processing sequence of this data is in table below.

Process Name		**Parameters**
Reformat to WGC CODE-4	✓	
Geometry Update • Bad trace edit • Uphole time statics update	✓	
Geometrical spreading Compensation	✓	
Notch filter 50	✓	50 Hz
CDP Sorting	✓	
Zone Anomaly Process	✓	
Surface Consistent Deconvolution	✓	
Objective Oriented Velocity analysis	✓	At Every 50 CDP
Surface Consistent Residual Statics	✓	Max Static Shift 24ms
Extensive Velocity Analysis	✓	At Every 50 CDP
Normal Moveout	✓	
Start time Mute	✓	
Datum Reduction	✓	
Stack	✓	
Finite Difference Migration	✓	
Band Pass Filter	✓	Low cut 10-14 Hz High Cut 45-40 Hz
Random Noise Attenuation	✓	
Time Variant Filter	✓	

1.11 Scales

- **Horizontal:** 36 Traces Per Inches
- **Vertical:** 2.5 Inches Per Second

1.12 Display Parameters

- **Display Amplitude:** 10 DB
- **Polarity:** Normal

1.13 Software Used

Details of software used in this research are given in the table below.

Software name	Use
Kingdom Suite	Seismic Interpretation and Attributes
Precision Matrix	Base Maps
X-Works	Velocity Model Building, Seismic Depth Sections and Full Wave Inversion.
Wavelets	Rockphysics, Facies modeling and AVA
Sigma 3D	Geodetic analysis and 3D Survey Planning
Hampson Russel by CGG	Seismic Post Stack Inversion
Golden Software Surfer	3D Surface Visualization

Chapter 2: General Geology and Stratigraphy

1.1 Introduction

Information about the geology of an area is very important in seismic survey. In the presence of challenging geological features, such as complex salt bodies, or naturally fractured reservoirs, there is a need to take multiple measurements from different directions (azimuths) to properly illuminate the structure and characterize the rock. The position and penetration of local faults and the presence of the unconformities between the rocks is very necessary from interpretation point of view. In many cases different lithologies can produce similar seismic signatures and vice versa. In order to deal with such complexities, an interpreter must have knowledge of the geology and its unconformities, stratification and major structures of the area under study.

Geology gives insight into the history of the Earth, as it provides the primary evidence for plate tectonics, the evolutionary history of life, and past climates. In modern times, geology is commercially important for mineral and hydrocarbon exploration and for evaluating water resources. It is also publicly important for the prediction and understanding of natural hazards.

2.2 Tectonic Framework of Pakistan

Pakistan emerges to be one of the most significant geographical patches of Asia (Fig 2.1). Unique feature of Pakistan is that it is located at the junction of these two diverse domains. The southern part of Pakistan belongs to Gondwanian Domain and is sustained by the Indo-Pakistan Crustal Plate. The northern most and western region of Pakistan fall in Tethyan Domain and presents a complicated geology. Pakistan comprises of three main geological subdivisions referred to as Laurasian, Tethyan and Gondwanaland domains (Kazmi et al., 1997).

Pakistan geologically overlaps both with the Indian and the Eurasian tectonic plates where its Sindh and Punjab provinces lie on the north-western corner of the Indian plate while Baluchistan and most of the Khyber-Pakhtunkhwa lie within the Eurasian plate which mainly comprises the Iranian plateau, some parts of the Middle East and Central Asia. The Northern Areas and Azad Kashmir lie mainly in Central Asia along the edge of the Indian

plate and hence are prone to violent earthquakes where the two tectonic plates collide forming youngest mountain system of the world.

The Tectonic Map of Pakistan along with sedimentary basins is shown in Fig. 2.1. Tectonics of Pakistan is characterized by two active convergent boundaries;

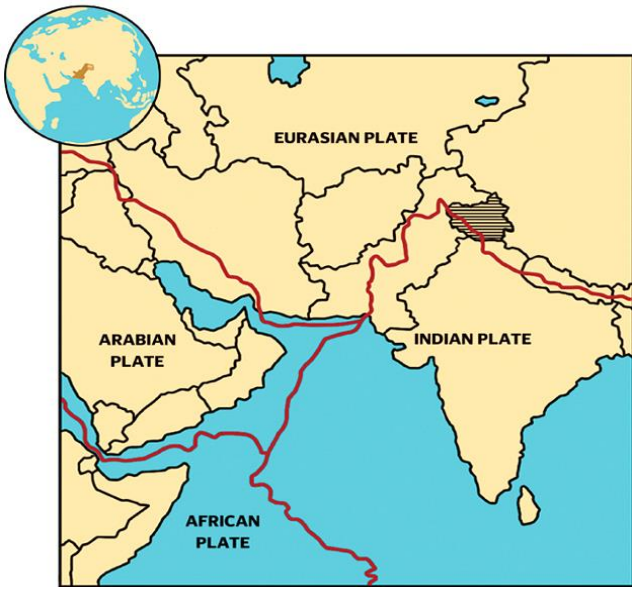

Fig 2.1 Regional Plates distribution of Pakistan

1. N-W Himalayan fold and Thrust belt is conspicuous feature of convergent continental plate boundary and it is characterized by number of active faults. In northern Pakistan there are three mountains ranges Hindukush, Karakorm and Himalayas.
2. In the southwest, there is an active boundary of oceanic lithosphere subducting arc trench gap sediments and continental sediments, the oceanic part of the Arabian plate passing under the Makran arc-trench gap and Afghan microplate.

2.3 Tectonic Zones of Pakistan

Based on Plate tectonic features, geological structure, orogenic history (age and nature of deformation, magmatism and metamorphism) and lithofacies, Pakistan may be divided into the following Tectonic zones.

a) Indus Platform and foredeep
b) East Baluchistan fold-and-thrust belt.
c) Northwest Himalayan fold-and-thrust belt.
d) Koshistan-Ladakh magmatic arc.
e) Karakoram block.
f) Kakar Khurasan flysch basin and Makran Accretionary Zone.
g) Chaghi magmatic arc.
h) Pakistan Offshore

The Study area lies in Indus Platform. The area is mostly dominated by normal faults and horst and graben structures are common in contrast to the major thrust common in the northern part of Pakistan. Fig 2.3 shows a model of horst and graben structures.

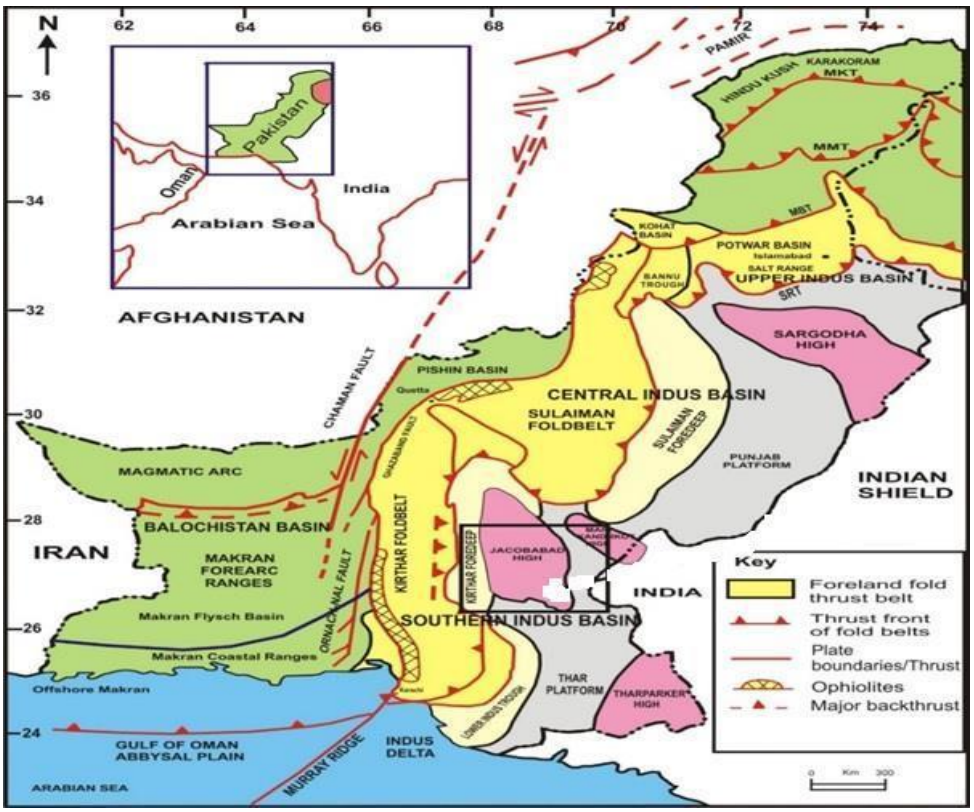

Fig 2.2 Tectonic and sedimentary basin map of Pakistan modified from Aziz and Khan 2003

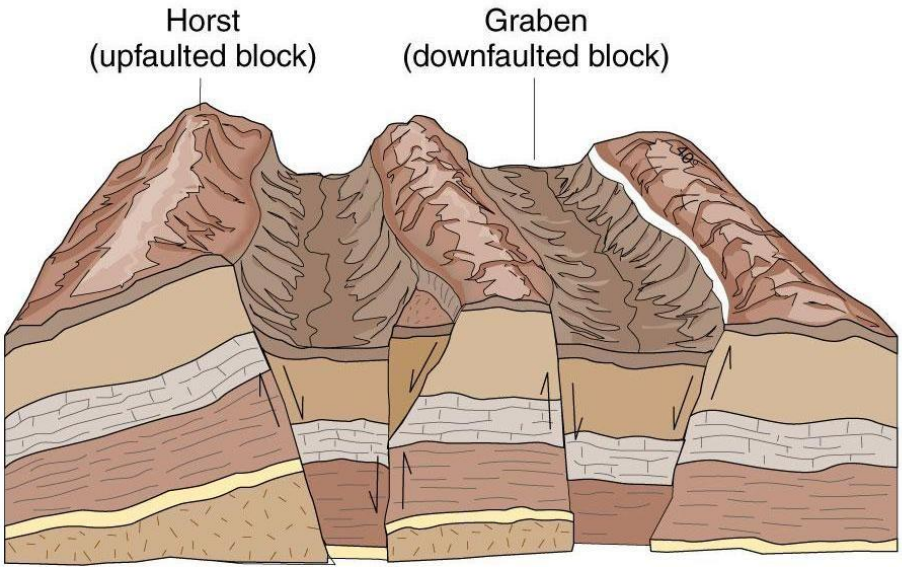

Fig 2.3 A model of Horst and Graben structures

2.4Structural Settings of Study Area

The basinal history of the study area is related mainly to rifting and break up of Gondwana in Jurassic period. The late Jurassic-Early Cretaceous rifting of Indian Plate controlled the structures and sedimentology of the Southern Indus Basin. Northeast-Southwest rift systems are possibly produced by Jurassic-Early Cretaceous rifting. Parting of the Madagascar and Indian plates in the middle to Late Cretaceous may have caused sinistral strike-slip faulting, hotspot activity and thermal doming in the area. This separation in turn caused uplift, erosion,

extrusion of the Deccan flood basalts and probably the NNW-striking normal faults. Eocene passive margin conditions caused carbonate deposition. Sinistral transpression with fold-thrust structures overprinted by sinistral flower structures in the west are produced during the Oligocene to present-day Himalayan collision.

2.5 Basin Architecture of Pakistan

Pakistan has a large sedimentary area of 872,268 Sq. Kms. In terms of genesis and different geological histories, Pakistan comprises two main sedimentary basins namely

a) Indus Basin.
b) Baluchistan Basin.

Both the basins evolved through different geological episodes and were finally welded together during Cretaceous/Paleocene along Ornach Nal/Chaman strike slip faults. The geological history of the Indus Basin goes back to Precambrian age. The Paleo topographic features influenced, to a large extent, the depositional processes throughout the basin development. These features also marked the limit of the basin and its divisions (Kadri, 1995). Fig 2.2 is showing tectonic and sedimentary basin map of Pakistan.

Different Basins of Pakistan includes:

1. Indus Basin divided into
    a) Upper Indus Basin. (In north)
        i. Kohat Sub Basin
        ii. Potwar Sub Basin
    b) Lower Indus Basin. (In south)
        i. Central Indus Basin
        ii. Southern Indus Basin
2. Baluchistan Basin.
3. Kakar Khurasan Basin.
4. Pishin Basin.

2.5.1 Indus Basin

The Indus Basin is the largest sedimentary basin of Pakistan. Indus Basin includes the area of 25000 Km^2 of South-East of Pakistan. It includes the Thar-Cholistan desert and Indus Plain. The basin is oriented in NE-SW direction. Basement is exposed as outcrop at two places, one in NE as Sargodha High and second in SE as Nagger Parker High. It comprises of normal to

moderate and some steeply dipping structures. Tectonically it is much stable area as compared to other tectonic zones of Pakistan. It comprises of buried ridges, platform slop, zone of up warp and dawn warp.

2.5.2 Upper Indus Basin.

It is in the northern Pakistan and separated from the lower Indus Basin by the Sargodha High. In its north MBT runs through the Margala Hills, Kala Chitta and Kohat Ranges. Western boundary of the basin is marked by an uplift of Pre-Eocene sediments and eastward directed thrusting to the west of Bannu.The basin is further subdivided into Potwar, to the east and Kohat to the west, by river Indus. (Kadri, 1995). Kohat and Potwar sub basins are characterized by an unconformity between Cambrian and Permian.

In Kohat-Potwar, where mostly oil is found, the proven reservoirs are;

a) Murree formation (Miocene).
b) Sakesar limestone (Eocene).
c) Hangu and Lockhart (Paleocene).
d) Lumshiwal sandstone (Cretaceous).
e) Datta sandstone (Jurassic).
f) Wargal formation.
g) Tobra formation (Permian).
h) Khewra sandstone (Cambrian).

The source rock in Kohat area is probably Chichali formation (Lower Cretaceous) and in Potwar, Patala shale (Paleocene) is considered as the source rock.

2.5.3 Lower Indus Basin.

The Lower Indus Platform Basin is bounded to the north by the Central Indus Basin, Sulaiman Fold belt to the northwest and Kirthar Fold Belt in the south-west. The main tectonic events which have controlled the structures and sedimentology of the Lower Indus Basin are rifting of the Indian Plate from Gondwanaland (Jurassic or Early Cretaceous) which probably created NE-SW to N-S rift systems, isostatic uplift or ridge-push at the margins of the newly developed ocean probably caused uplift and eastwards tilting at the start of the Cretaceous. Separation of the Madgascan and Indian plates in the Mid to Late Cretaceous which may have caused some sinistral strike-slip faulting in the region, hotspot activity and thermal doming at the Cretaceous-Tertiary boundary. This in turn caused uplift, erosion, extrusion of the Deccan

flood basalts and probably the NW-striking normal faults. Paleocene- Eocene emplacement of the Bela Ophiolites may have caused gentle folding. Eocene passive margin conditions caused structural quiescence and carbonate deposition. Oligocene to present-day Himalayan collision caused sinistral transpression in the west of the Lower Indus Basin, with fold-thrust structures overprinted by sinistral flower structures. It comprises the following main units:

a) Thar Platform
b) Karachi Trough
c) Kirthar Foredeep
d) Kirthar Fold Belt
e) Offshore Indus

The Southern Indus Basin is bounded by the Indian Shield to the east and the marginal zone of Indian Plate to the west. Its southward extension is confined by offshore Murray Ridge-Oven fracture plate boundary. The oldest rocks encountered in the area are of Triassic age. Central and southern Indus basins were undivided until Khairpur-Jacobabad High became a prominent positive feature. This is indicated by homogeneous lithology of Chiltan Limestone (Jurassic) and Sembar Formation (Lower Cretaceous) across the High. Sand facies of Goru Formation (Lower Middle Cretaceous) are also extending up to Kandhkot and Giandari area. This is further substantiated by Khairpur and Jhatpat wells located on the High. In Khairpur-2 well, significant amount of Lower Cretaceous and Paleocene is missing while in Jhat Pat-4, the whole Cretaceous and Paleocene are absent with Eocene directly overlying Chiltan Limestone (Jurassic). Paleocene facies south of the High are quite different from that in north and are dominated by clastic sediments derived from the positive areas Khairpur- Jacobabad High and Nabisar Arc.

2.6 Structures of Lower Indus Basin.

The Sindh Monocline (SM) is the part of a Lower Indus Basin situated in the south eastern corner of the Pakistan. The slope of the sedimentary succession covering the SM generally dips westward bonded by the east by the Indian shield (Nagar Parker granite area, western limits are Kirthar fold and thrust belt and Karachi trough where it merges with a tectonically different entity, Sukkur Rift zone to the north. SM is also known for its several oil and gas fields located in the southern, central east and south eastern districts of Sindh province including Badin, Thatta, Mirpurkhas, Khairpur, Hyderabad, etc. These oil accumulations have been trapped in tilted fault blocks in the Early Cretaceous Lower Goru sandstone and sealed by overlying shale

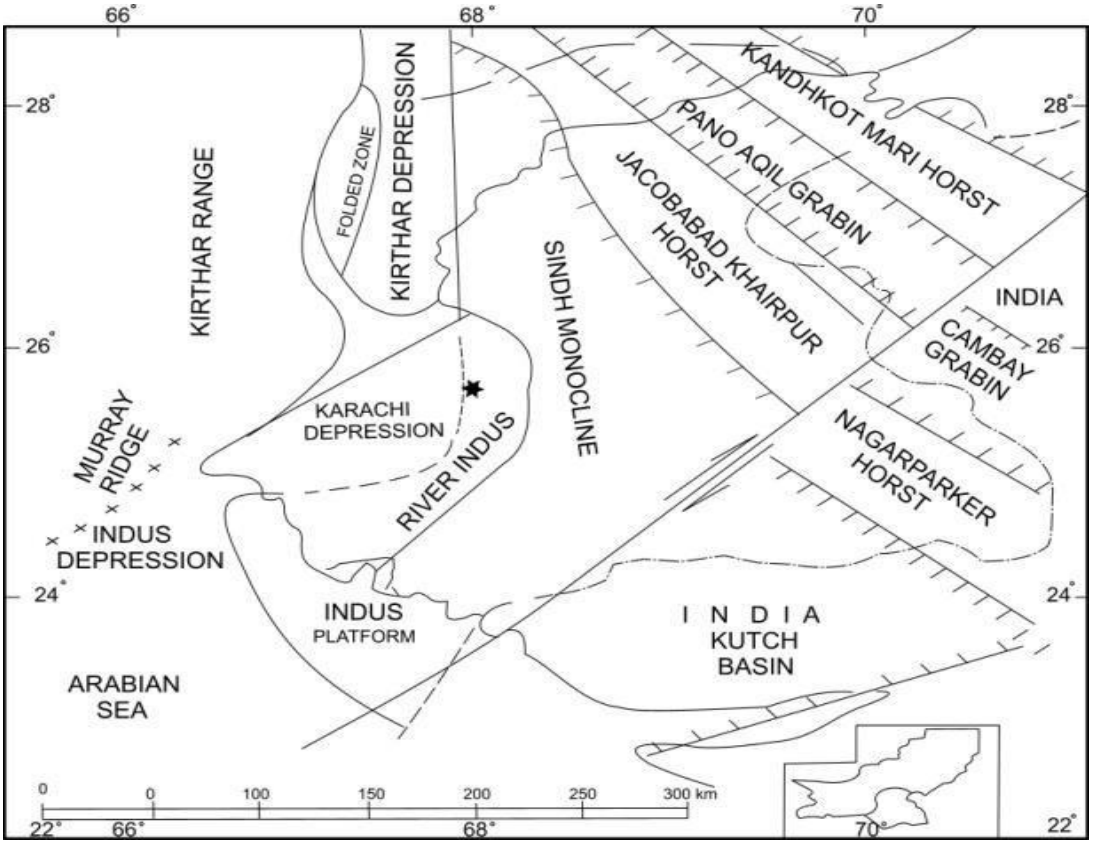

Fig 2.4 Tectonic map of Lower Indus Basin (Raza et al,1990)

and marl facies of Upper Goru Formation. The faulting took place during Early Jurassic to late Cretaceous and continued till early Paleocene time when the Indian plate was separated from larger southern Gondwana plate. This phase of tectonic is known as Mesozoic rifting. The Sukkur rifting (series of horst and grabens) was also resulted due to similar rift related activity during the same time as in the south but due to pre-existing basement induced positive area the Upper Cretaceous did not deposited and almost entirely missing on the crestal areas of the Khairpur Sukkur high and present in the flank areas only. After the rifting the area has undergone marine incursion which remained active during Paleocene through Oligocene and deposited Paleocene clastics, shales, Eocene carbonates and Oligocene successions. The outcropping Eocene limestone in the areas on Sukkur, Rohri and Khairpur areas subjected to the Tertiary compressional phase that helped to uplift and exhumed the Eocene carbonates on surface. The high where Eocene is present on surface is a paleo horst. The compressional phase was also associated with lateral strike slip movement (Kazmi et al., 1997).Fig 2.4 shows tectonic map of Lower Indus Basin.

2.7 Stratigraphy of Lower Indus Basin.

Suleiman Range and areas to the south constitute prolific gas producing habitat where Dhodak, Rodho, Sui, Pirkoh, Zin, Loti fields in the north, and in the plains Qadirpur, Kandhkot fields are gas producers. These fields produce from Sui Main Limestone (SML, Eocene), Ranikot sands, Dungan limestone (Paleocene) and the Pab sandstone (Late Cretaceous). In Kirthar

Range again Sui Main limestone and mostly Pab sandstone is the reservoir. Badin area and northern part of Sindh province also fall in Indus Basin where Lower Goru Sands (Lower Cretaceous) are the main reservoir for oil and gas. In all these areas, Sembar shales are considered as the source rock. Habib Rahi limestone (Eocene) is the gas reservoir in the giant Mari Field. Ghazij shale is the cap rock for SML while Ranikot shale provides cap rock for Pab. The intraformational shale within Lower Goru provides the seal (Shah et al., 1977).

2.8 Study Area

Study area Sinjhoro falls in Lower Indus basin of Pakistan which is extensional regime with normal faulting. Both stratigraphic and structural traps are present and most of the oil accumulations have been trapped in tilted fault blocks. Sinjhoro area is bounded in the east where the Indian shield merges into Kirthar and Karachi Trough and in the North by Marri Bughti folded zone. The Indus offshore platform in the South.

2.8.1 Geology of Study Area

Badin area of Lower Indus basin where Sinjhoro area exists, typically offers fault-block geometry having small to average size traps at Lower Goru level, below a basalt layer that marks the K/T boundary. The faults strike in a NNW-SSE orientation. The faults mostly stop at top Cretaceous, and only a few penetrate the Tertiary rocks due to the post-Tertiary re-activation. The Post-Cretaceous unconformity cuts deeper to the East where successively older rocks are truncated as one move from West to East. As the source of sediments was from the Indian shield located to the East the sand content in Lower Goru and even Sembar increases towards East. At the same time the shale percentage decreases and seal becomes a risk in the same direction.

2.8.2 Petroleum Geology of Study Area.

The oldest lithology penetrated in the study area is the Jurassic Chiltan Limestone. It is overlain by the Lower Cretaceous Sembar and Goru formations. The Goru Formation has conformable contact with overlying Parh limestone of Late Cretaceous age which is capped unconformably by the Ranikot Group. The Lower Goru is mostly composed of interbedded sandstone and shale in different proportions and is the main reservoir rock in the area. The Lower Goru horizon has been divided into five parts based on lithology;

a) Basal Sand unit.
b) lower Shale.

c) Massive Sand unit.
d) Upper Shale.
e) Upper Sand.

The Ranikot Group is capped unconformably by the Laki Formation of the Eocene age. During Oligocene the Proto-Indus River began to deposit Nari/Gaj sediments from the north into shallow embayment in the Karachi area. At the end of the Gaj depositional cycle, the eastward movement of the Afghan Plate along the Murray Ridge began, and the Indus course was shifted eastward by the compressional uplift in the Karachi area.

2.8.5 Stratigraphy of Study Area

The stratigraphic succession changes from east to west. Precambrian basement is elevated in the south-eastern corner of the basin. The thickness of the sediments increases westward. In the eastern part of the basin tertiary sequence has direct contact/ Interaction with Jurassic sequence. The stratigraphic chart of the study area is given in Fig 2.5.

2.8.5.1 Jurassic Stratigraphy

- **Chiltan Limestone**

  Age: Age of Chiltan limestone is middle to late Jurassic. .

  Lithology: This formation is mainly consists of limestone with traces of shale. The colour of limestone is light grey to dark grey and it is dense, compact and massive limestone.

  Thickness: Its thickness is estimated to be over 1,800 meters near Quetta (Shah, 2009).

2.8.5.2 Cretaceous Stratigraphy

- **Parh Limestone**

  Age: Parh limestone of Cretaceous age occurs widely throughout the Indus Basin from Karachi area to the Southern Waziristan.

  Lithology: It represents a light grey, white, cream to tan, thin bedded argillaceous Limestone.

  Thickness: The greatest accumulation of Parh Limestone, approximately 600 meters, is just west of the Kirthar Range deposited in a narrow elongate North-South area. The Parh is generally thin, though locally thick deposits in Bugti hills. The Parh is the most uniform formation in the Indus Basin.

- **Sember Formation**

Age: Age of Sember Formation is early Cretaceous.

Lithology: Sember Formation is mainly consisting of black shale with interbedded siltstone, Argillaceous limestone and sandy shale is present at basal part. **Thickness:** The thickness of this rock unit in type locality is 133 meters.

- **Goru Formation**

Age: Age of Goru Formation is early Cretaceous.

Lithology: Goru Formation is comprise of inter beds of sands, limestone, shale and siltstone. The limestone is fine grained and thin bedded. Sand beds have been also been in this rock unit. The Shales of Goru are the most widely distributed of post-Jurassic formations. It extends from Waziristan to as far South as Cutch in India. The Goru formation is dominantly Shale or Mudstone, frequently calcareous. **Thickness:** The thickness of Goru Formation is 536 meter in type locality. Goru Formation is divided into two members:

a) **Lower Goru**
b) **Upper Goru**

Fossils: Fossils found in Goru Formation are foraminifera and belemnites.

2.8.5.3 Paleocene Stratigraphy

- **Ranikot Group**

Ranikot Group was subdivided into

a) Lower Ranikot (Sandstone)
b) Upper Ranikot (Limestone) by Vredenburg (1909a).

Age: Age of Ranikot Formation is early Paleocene.

Lithology: Basal marine sequence of sandstone and shale with interbeds of limestone (Raza 2003). Ranikot Formation is mainly comprising grey limestone with some brown sandstone and shale in the upper part while sandstone with shale and limestone interbeds are found in lower part.

Thickness: The thickness ranges from 540 to 660 meters.

2.8.5.4 Eocene Stratigraphy

- **Laki Formation**

Age: Age of Laki formation is Eocene.

Lithology: Laki formation mainly consist of cream coloured to grey Limestone, Marl, calcareous Shale, Sandstone and lateritic Clay may become significant constituents of the formation locally.

Thickness: It is about 240 meters thick in the Bara Nai and type locality (Mari Nai), but attains more than 600 meters thickness at Tatti (Kirthar Province) and in Sui, it attains the thickness of 468 meters.

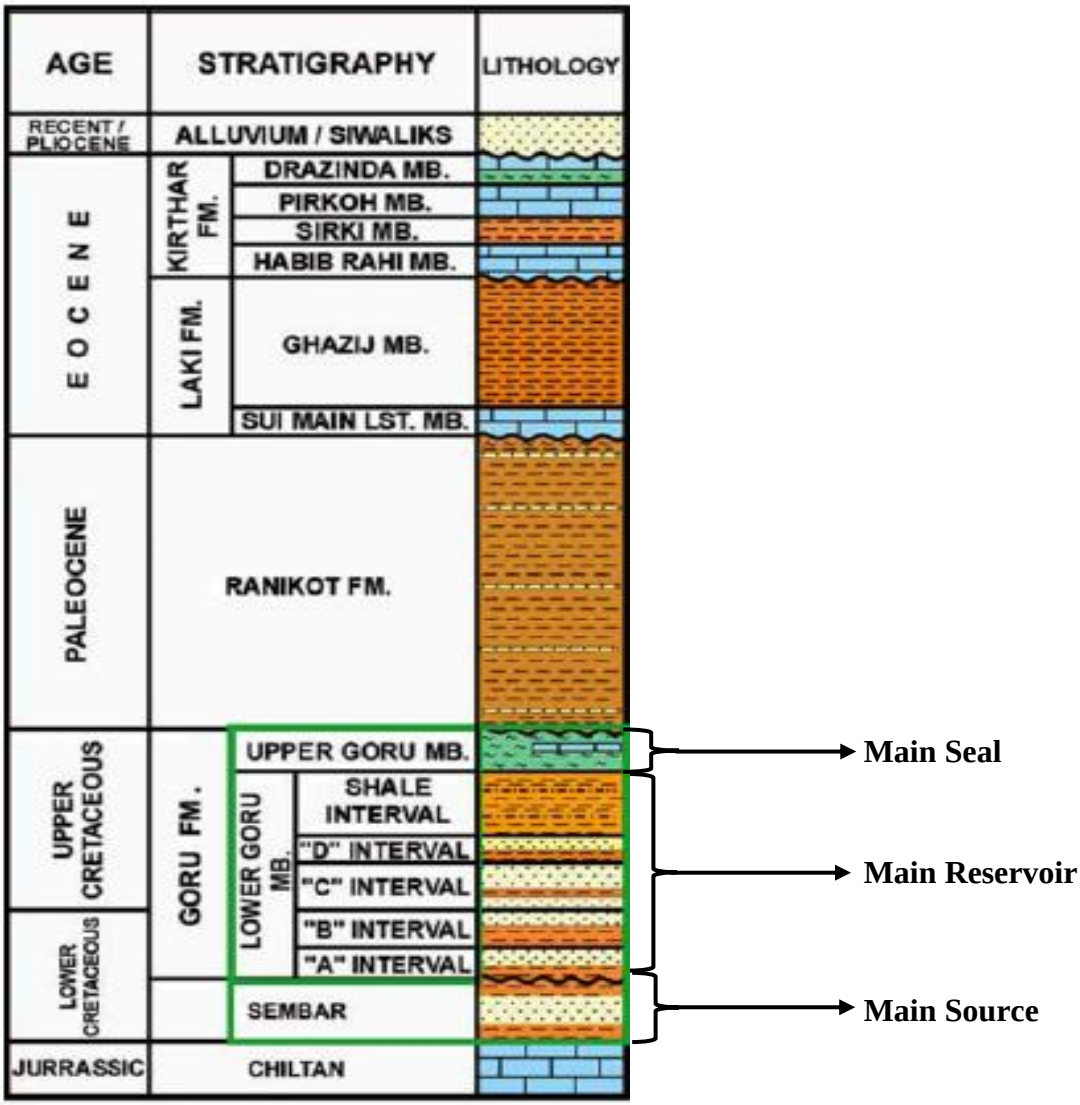

Fig 2.5 Stratigraphy of study area

2.9 Petroleum System of Study Area

The Petroleum System consists of a mature source rock, pathway, reservoir, trap and seal. Appropriate relative timing of formation of these elements and the processes of generation,

migration and accumulation are necessary for hydrocarbons to accumulate and be preserved. Exploration plays and prospects are typically developed in basins or regions in which a complete petroleum system has some likelihood of existing. (Kadri, 1995).

2.9.1 Traps

All production in the study area is from structural traps but stratigraphic traps are also found. The tilted fault traps in the Lower Indus Basin are a product of extension related to rifting and the formation of horst and graben structures. The temporal relationships among trap formation and hydrocarbon generation, expulsion, migration, and entrapment are variable- throughout the Indus Basin. These provide the significant trapping system along tilted fault blocks and negative flower structures.

2.9.2 Source Rocks

The Sembar Formation has been identified as the primary source rock for much of the Greater Indus Basin. There are other known and potential source rocks. Rock units containing known or potential source rocks include;

a) Salt Range Formation Precambrian shales.
b) Permian Dandot and Tredian Formations.
c) Triassic Wulgai Formation.
d) Jurassic Datta Formation.
e) Paleocene Patala Formation.
f) Eocene Ghazij formation.
g) Lower Miocene shales.

The Sembar Formation is the most likely source for the largest portion of the produced oil and gas in the Indus foreland. The Lower Cretaceous Sembar Formation consists mainly of shale with subordinate amounts of siltstone and sandstone. The Sembar was deposited over most of the Greater Indus Basin in marine environments and ranges in thickness from 0 to more than 260 m.

2.9.3 Reservoir Rocks

The principal reservoirs are deltaic and shallow-marine sandstones in the lower part of the Goru in the Lower Indus Basin and the Lumshiwal Formation in the Middle Indus Basin and limestone in the Eocene Ghazij and equivalent stratigraphic units. Potential reservoirs are as thick as 400 m. Sandstone porosities are as high as 30 percent, but more commonly range from

about 12 % to 16 % and limestone porosities range from 9 to 16 percent. The permeability of these reservoirs ranges from 1 to > 2,000 milli darcies. Reservoir quality generally diminishes in a westward direction but reservoir thickness increases. Because of the progressive eastward erosion and truncation of Cretaceous rocks, the Cretaceous reservoirs have all erosional up dip limits, whereas Tertiary reservoirs extend farther east overlying progressively older rocks.

2.9.4 Seal Rocks

The known seals in the system are composed of shales that are interbedded with and overlying the reservoirs. In producing fields, thin shale beds of variable thickness are effective seals. Additional seals that may be effective include impermeable seals above truncation traps, faults, and up dip facies changes. The thick sequence of shale and marl of upper Goru Formation serves as cap rock for underlying Lower Goru reservoir.

Chapter 3: Seismic Data Interpretation

3.1 Introduction

Seismic interpretation is the progression of determining information about the subsurface of the earth from seismic data. It may resolve general information about an area, locate prospects for drilling exploratory wells, or guide development of an already-discovered field (Coffeen, 1986).

Conventional seismic interpretation implies picking and tracking laterally consistent seismic reflectors for the purpose of mapping geologic structures, stratigraphy and reservoir architecture. The ultimate goal is to detect hydrocarbon accumulations, delineate their extent, and calculate their volumes. Conventional seismic interpretation is an art that requires skill and thorough experience in geology and geophysics. To meet the challenges of exploring ever increasingly complex targets, there have been tremendous advancements in data acquisition equipment, computer hardware and seismic processing algorithms in the last three decades (Khan, 1995).

3.2 Types of Seismic interpretation

Geologists ordinarily group the sequence of sedimentary rocks into units called Formations. These formations can be described in term of age, thickness, and lithology of the constituent layer. To distinguish different formations on the basis of seismic reflections is an important question in interpreting seismic data that may be structural, stratigraphic or lithological (Robinson & Coruh, 1988).

Final processed seismic lines are interpreted in order to construct a geological model of the subsurface that describes areas which are favourable for hydrocarbon accumulations. There are two main approaches for the interpretation, namely structural and stratigraphic interpretation etc (Al-Sadi, 1980; Badley, 1985).

3.2.1 Structural Interpretation

This type of analysis is very suitable in case of Pakistan, as most of the hydrocarbon is being extracted from the structural traps. It is study of reflector geometry on the basis of reflection time. The main application of the structural analysis on seismic data is to search structural traps containing hydrocarbon. Most structural interpretation uses two-way reflection time rather than depth and time structural maps are constructed to display the geometry of selected reflection

events. Discontinuity in reflections clearly indicate faults and undulating reflections reveal folded beds (Telford et al., 1990).

3.2.2 Stratigraphic Interpretation

Stratigraphic analysis greatly enhances the chances of successfully locating hydrocarbon traps in sedimentary basin environment. Seismic stratigraphy is used to find out the depositional processes and environmental settings, because genetically related sedimentary sequence normally consists of concordant strata that show discordance with sequence above and below it. Geologists ordinarily group the sequence of sedimentary rocks into units called Formations. These formations can be described in term of age, thickness, and lithology of the constituent layer. To distinguish different formations on the basis of seismic reflections is an important question in interpreting seismic data that may be structural, stratigraphic or lithological (Robinson & Coruh, 1988).

3.3 Work Procedure

The computer-based working (Processing & Interpretation) is more accurate, precise, efficient and satisfactory which provides more time for further analysis of data. This whole work is carried out using a combination of computer software products, which include all K-tron Software, SMT Kingdom suit and Golden software Surfer.

SMT Kingdom Suite was used for initial interpretation and further interpretation was carried out using K-tron X-Works which provides an interactive interface for marking horizons & faults, exporting horizon's time, velocity and depth data for contouring and for further analysis such as velocity smoothening, interpolation, Velocity Model building, crustal shortening, 2D seismic modelling and well columns correlation. The seismic velocities are processed (Converted, Interpolated and Smoothed) by using X-Works software. These velocities are then used in different applications like Time-to-Depth conversion, Modeling and Rock Physics. Contour maps and 3D Seismic model have been generated using SMT Kingdom Suite.

3.3.1 Seismic Horizons

The main task of interpretation is to identify various reflectors or horizons as interfaces between geological formations. For this good structural and stratigraphic knowledge of the area is required (McQuillin et al., 1984). Seismic horizons on seismic sections can be identified by creating synthetic seismogram from well logs, this whole process is called well to seismic tie.

3.3.2 Synthetic Seismogram

Synthetic seismogram is basically 1D modelling. It utilizes wireline logs like Sonic (DT) and Density (RHOB) to generate Acoustic impedance (AI) model and ultimately a series of Reflection Coefficient (RC). This RC is then convolved with source wavelet (Theoretical or Extracted) to generate synthetic seismogram.

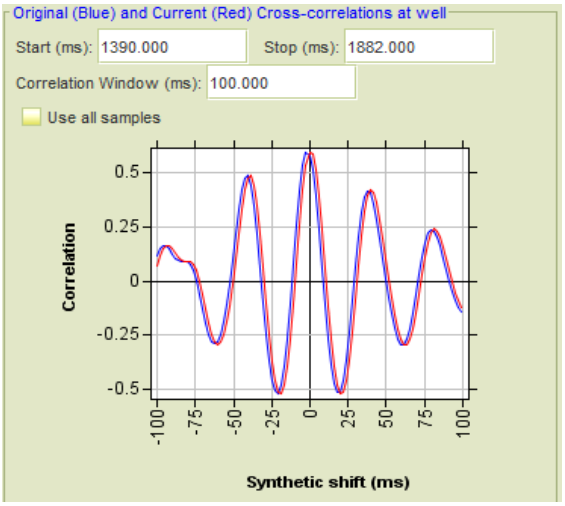

Fig:3.1: Correlation of Synthetic and Real Trace

A synthetic seismogram was generated using the wireline logs of well CHAK-5 DIM SOUTH_01. The well has been drilled near dip line 20017-SNJ-09. The final result produced a Synthetic Seismic trace with 58% correlation is shown in Fig 3.1. It is difficult to further improve this correlation because the well lies away from seismic line and another reason is presence of noise in seismic data. Final output of this process is shown in Fig 3.2.

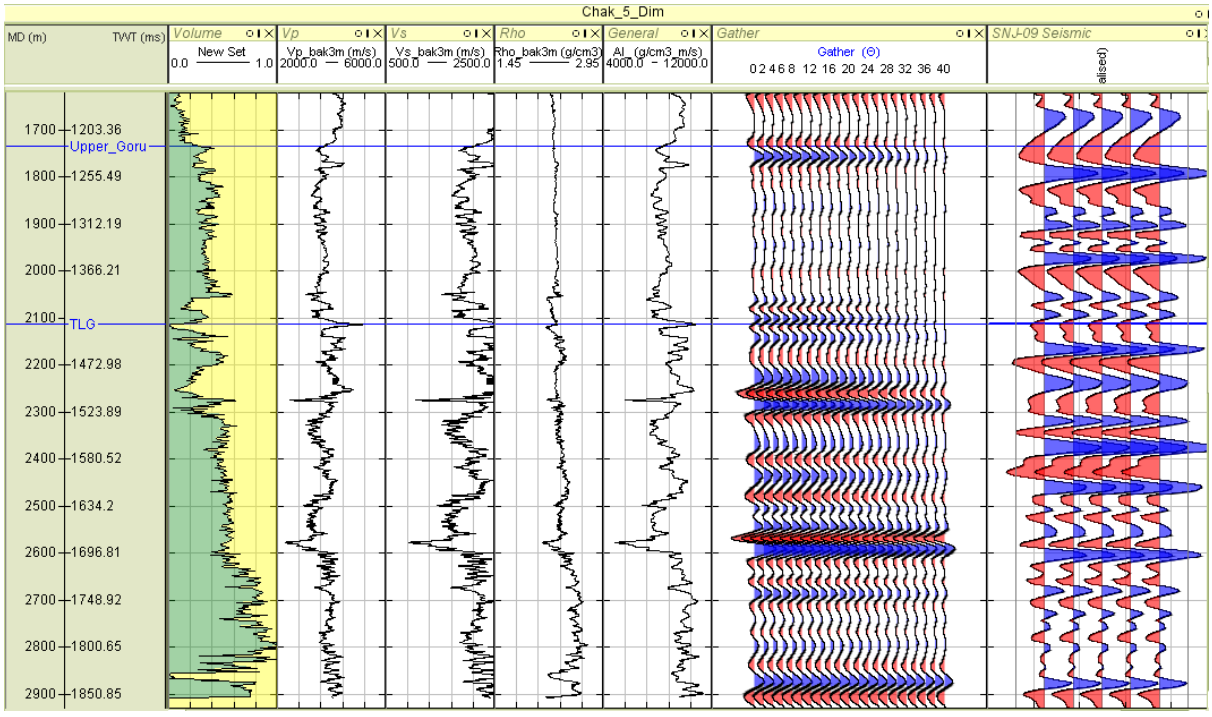

Fig 3.2: Synthetic Seismogram of CHAK-5 DIM SOUTH_01 drilled near Seismic dip line 20017-SNJ-09

3.3.3 Horizon Identification and Picking

Using the well-seismic tie information from synthetic seismogram the horizons identified on seismic are given in the Table 3.1 with their Depths and TWT.

Table 3.1 Horizons with their TWT and Depth in well CHAK-5 DIM SOUTH-01

Horizon Name	Two Way Time(ms)	TVDss (meters)
Laki	597.01	624.71
Ranikot	825.64	1154.6
Parh	1156.92	1600.82
Upper Goru	1220.51	1734.69
Lower Goru	1429.78	2113.98

The deepest horizon identified as Chiltan Limestone was marked on the basis of its strong reflection owing to prominent acoustic impedance contrast with overlying and underlying reflectors. Four horizons were marked on the dip line 20017-SNJ-09. These horizons were then transferred to the strike lines intersecting the marked dip line and then further on to the remaining lines. During the crosstie process, smaller misties were observed and were corrected instantly. Chiltan reflector helped in maintaining the continuity of Lower Goru reflector on available seismic lines.

3.3.4 Fault Identification

The area lies in an extensional regime dominated by normal faults thus, the associated structures are horsts and grabens. The identification of the faults was difficult to some extent due to poor data quality. Most of the marked faults have a NW-SE trend. On seismic sections, faults appear to originate from Chiltan and die out somewhere normally in Parh Limestone or above lying younger formations. The average throw of the faults is observed to be about 20 – 30 ms. Because of the more or less North-South (NS) trend of the faults, they are more obvious on dip lines as compared to the strike lines.

Fig 3.3 and 3.4 show interpreted Seismic dip line 20017-SNJ-09 and 20017-SNJ-03 respectively. Ranikot, Upper Goru, Lower Goru and Chiltan formations along with their associated faults are marked on these sections. These horizons are also marked on other given seismic lines.

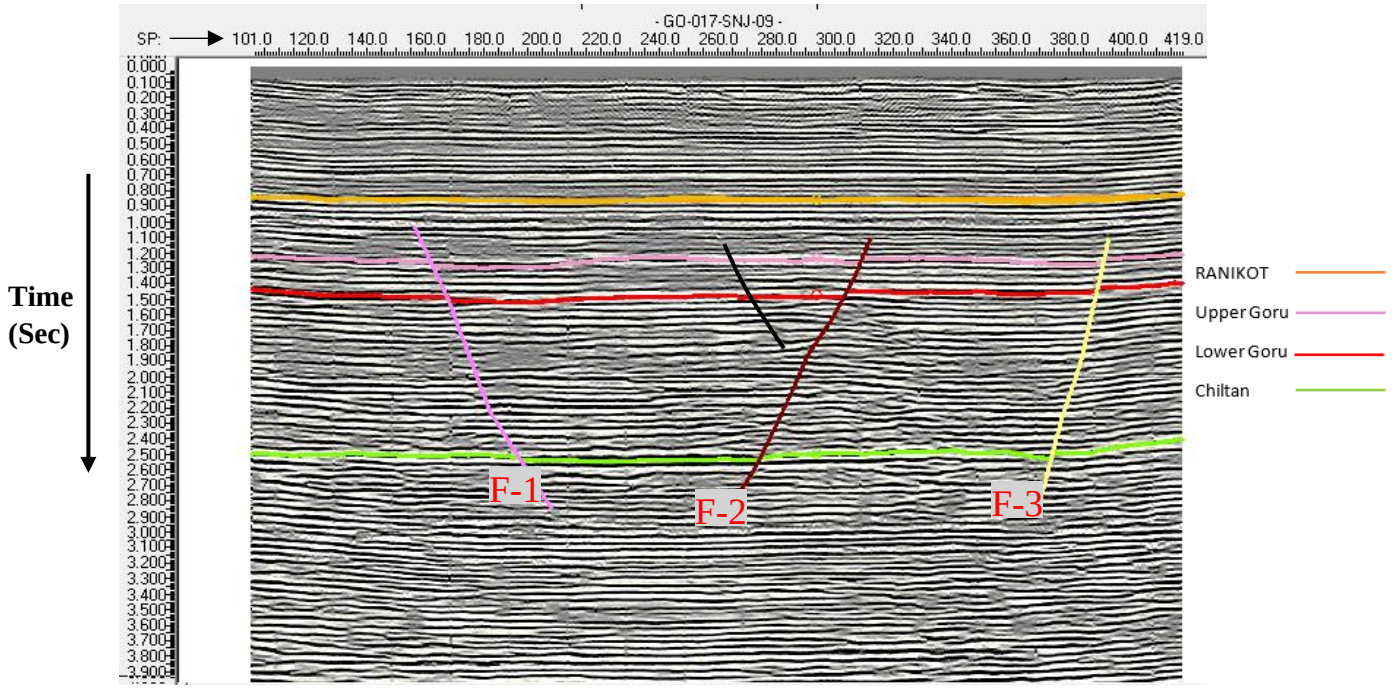

Fig 3.3: Interpreted Seismic dip line 20017-SNJ-09

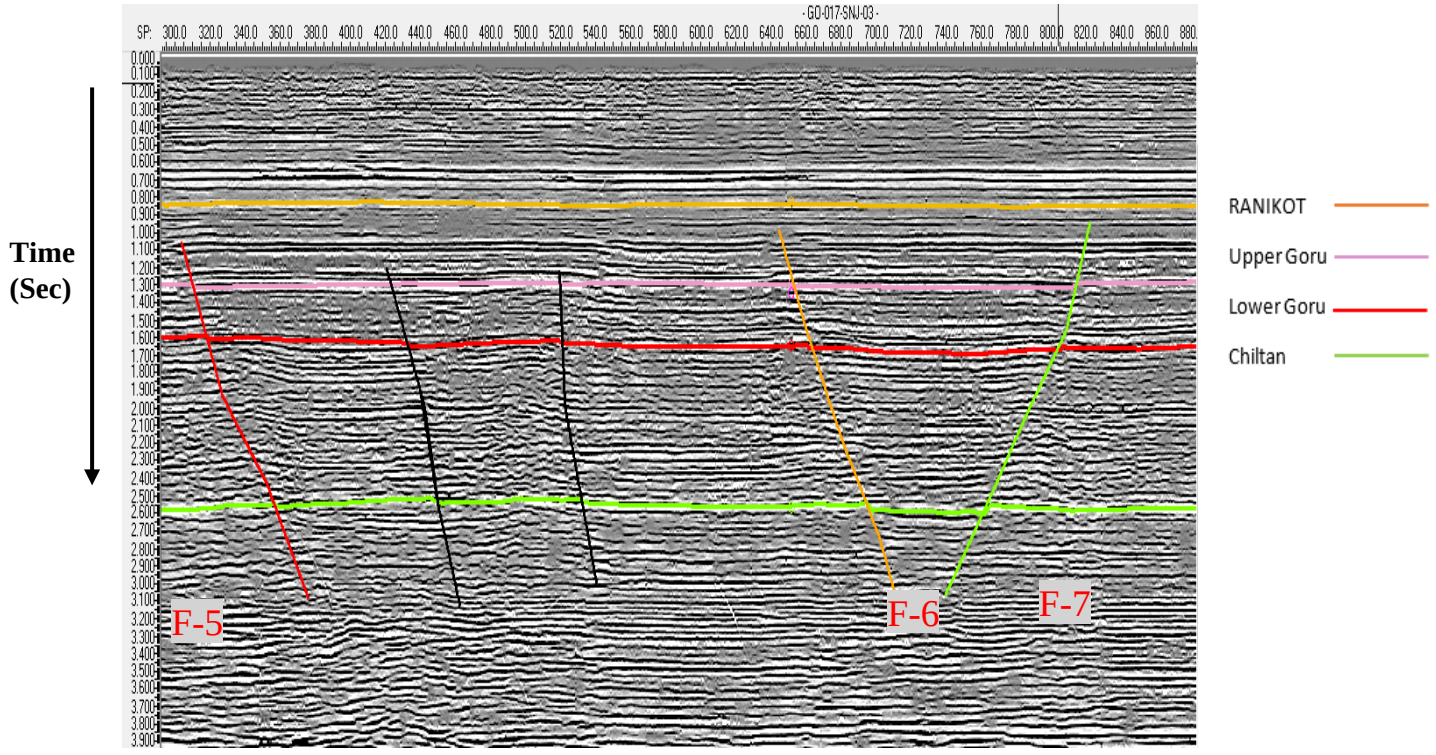

Fig 3.4: Interpreted Seismic dip line 20017-SNJ-03

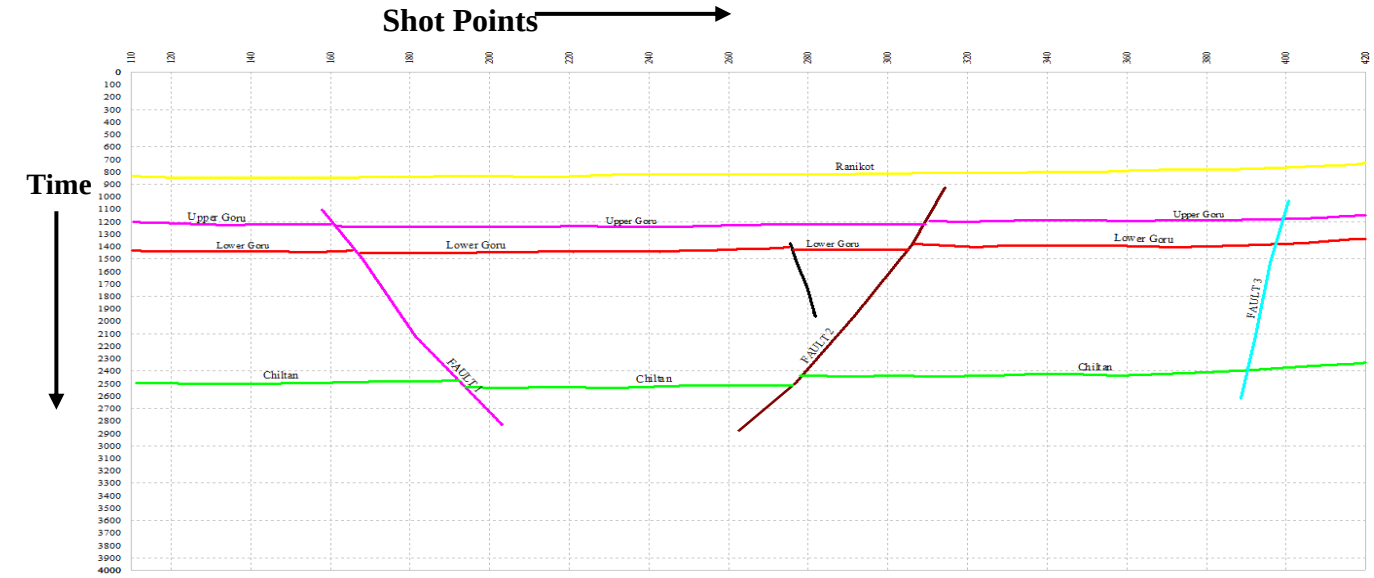

Fig 3.5: Time Section of seismic line 20017-SNJ-09

These horizons and faults were then transferred to all other lines in the given data. Fig 3.5 shows interpreted seismic time section in X-works.

3.3.5 Seismic Depth Section

Time-domain seismic imaging is a robust and efficient process routinely applied to seismic data (Yilmaz, 2001).

A good seismic image is not enough for an exploration or field development interpretation. Good well ties and reliable depth conversion are also required. Time to depth conversion is done by using Average velocities. The maps of two-way-time to various horizons and of the

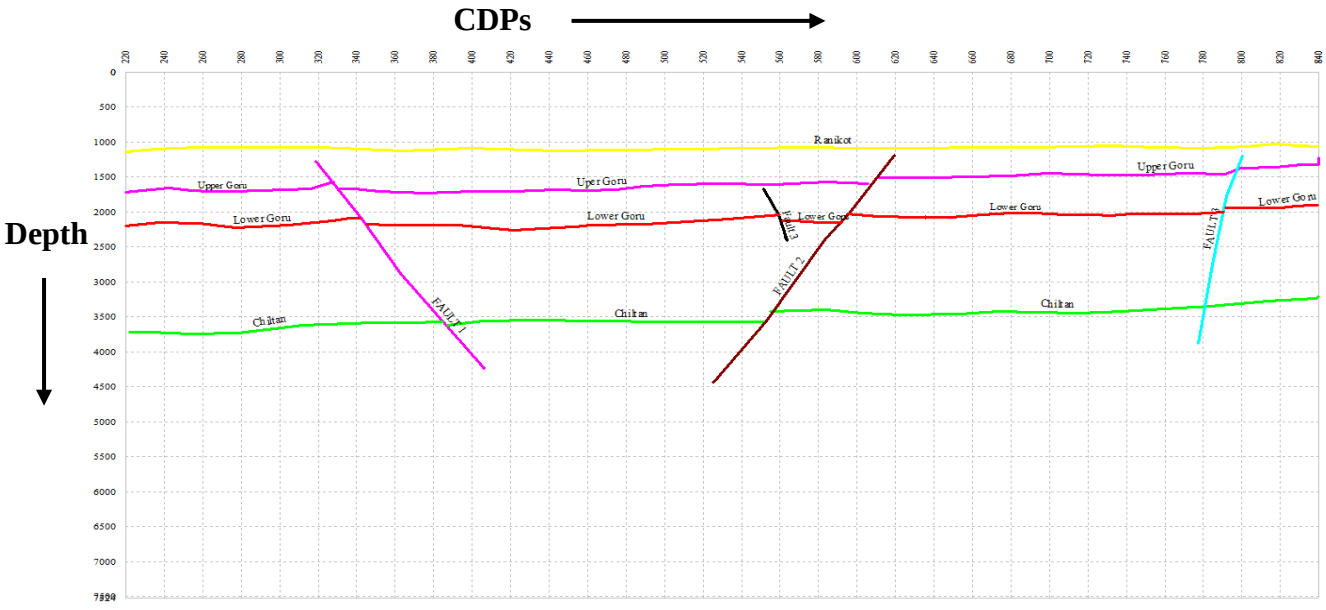

Fig 3.6: Depth Section of seismic line 20017-SNJ-09

average velocities between the formations are used to generate a depth contour map (Paturet, 1971). The input seismic Root Mean Square velocities were loaded in X-Works which uses a velocity processing engine to convert the input RMS velocities into interval and finally average velocities. It also provides spatio-temporal interpolation and smoothing of velocities. Velocity model building process is explained in chapter 5. These velocities are used to convert time of each reflector into depth to get the depth sections. The depth section of line 20017-SNJ-09 is shown in Fig 3.6. Ranikot, Upper Goru, Lower Goru and Chiltan formations were marked in time domain seismic section and then converted into depth section using average velocity functions in X-Works.

3.4 CONTOUR MAPS

The results of seismic interpretation are usually displayed in map form. Mapping is part of the interpretation of the data. The seismic map is usually the final product of seismic exploration, the one on which the entire operation depends for its usefulness. The contours are the lines of equal time or depth wandering around the map as dictated by the data (Coffeen, 1986).

In constructing a subsurface map from seismic data, a reference datum must first be selected. The datum may be sea level or any other depth above or below sea level. Frequently, another datum above sea level is selected in order to image a shallow marker on the seismic cross-section, which may have a great impact on the interpretation of the zone of interest (Gadallah & Fisher, 2009).

Contouring represents the three-dimensional Earth on a two-dimensional surface. The spacing of the contour lines is a measure of the steepness of the slope; the closer the spacing the steeper the slope. A subsurface structural map shows relief on a subsurface horizon with contour lines that represent equal depth below a reference datum or two-way time from the surface. These contour maps reveal the slope of the formation, structural relief of the formation, its dip and any faulting and folding.

Construction of fault polygons is very important as far as time and depth contouring of a particular horizon is concerned. Any mapping software needs all faults to be converted into polygons prior to contouring. This is due to the reason that if a fault is not converted into a polygon, the software doesn't recognize it as a barrier or a discontinuity in contours, thus masking any possible closures against faults and represent a false picture of the subsurface.

The interpreted seismic data is contoured for producing seismic maps which provide a

three-dimensional picture of the various layers within an area which is circumscribed by intersecting shooting lines. The Kingdom software is used to generate all the contour maps.

3.4.1 Time and Depth Contour maps of Upper Goru Formation.

3.4.1.1 Time Contour Map

A two-way time contour map is constructed on Upper Goru formation by using Kingdom Suite shown in Fig 3.7. The horizon is generally dipping from North-West to South-East. Fault polygons are constructed for this map. Each polygon is represented by different color. Contours are terminating at fault polygons. Contour interval is set at 0.004 sec. The time variation observed for Upper Goru Formation is 1.212 to 1.34 Sec. Upper Goru formation is composed of Shale, Sands and Marl. The thick sequence of shale and marl of upper Goru Formation serves as cap rock for underlying Lower Goru reservoir.

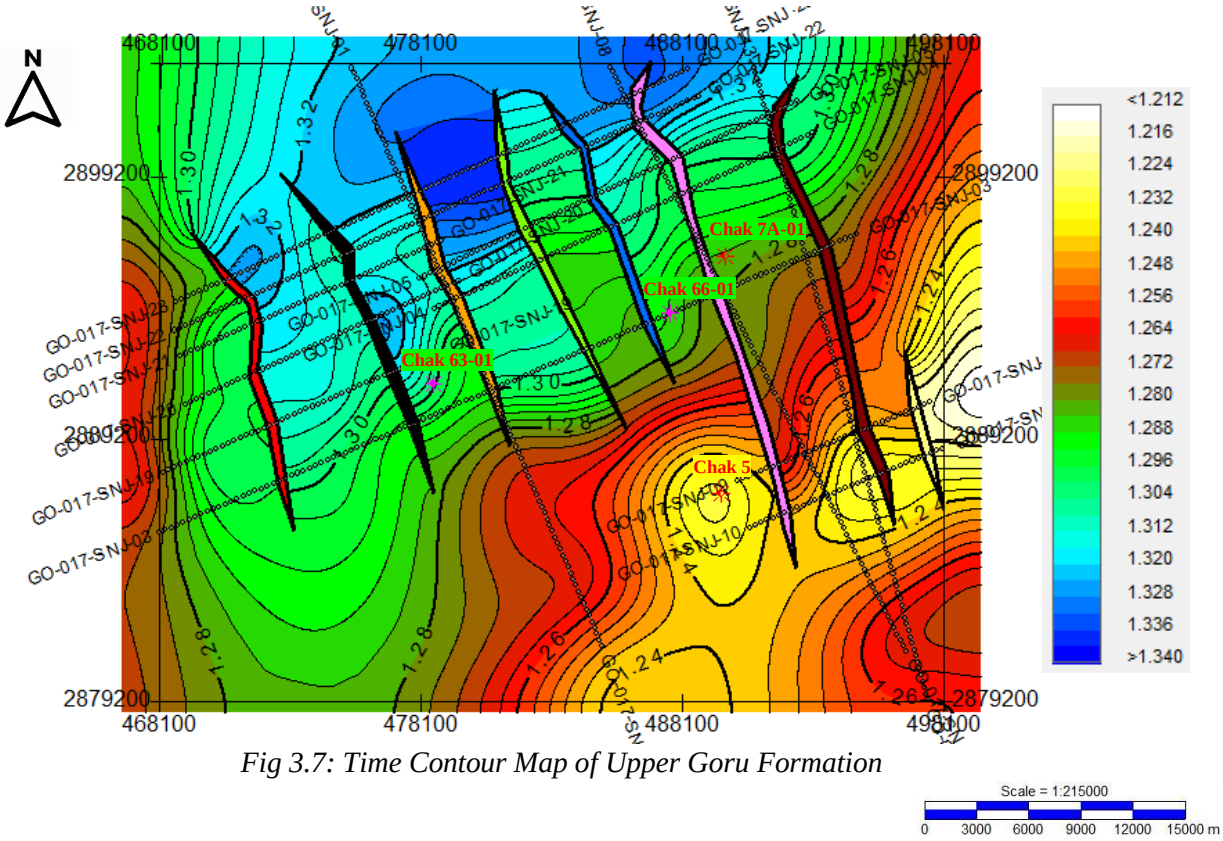

Fig 3.7: Time Contour Map of Upper Goru Formation

3.4.1.2 Depth Contour Map

A Depth contour map is constructed on Upper Goru formation by using Kingdom Suite as shown in Fig 3.8. Horizon depth is computed from horizon two-way time by using average velocity functions. The horizon is generally dipping from North-West to South-East. Fault polygons are constructed for this map. Each polygon is represented by different color. Contours

are terminating at fault polygons. Contour interval is set at 5 meters. The depth variation observed for Upper Goru Formation is 1690 to 1850 meter. Depth Variation in Upper Goru formation is less than Lower Goru and Chiltan. Almost every major fault terminates into Parh

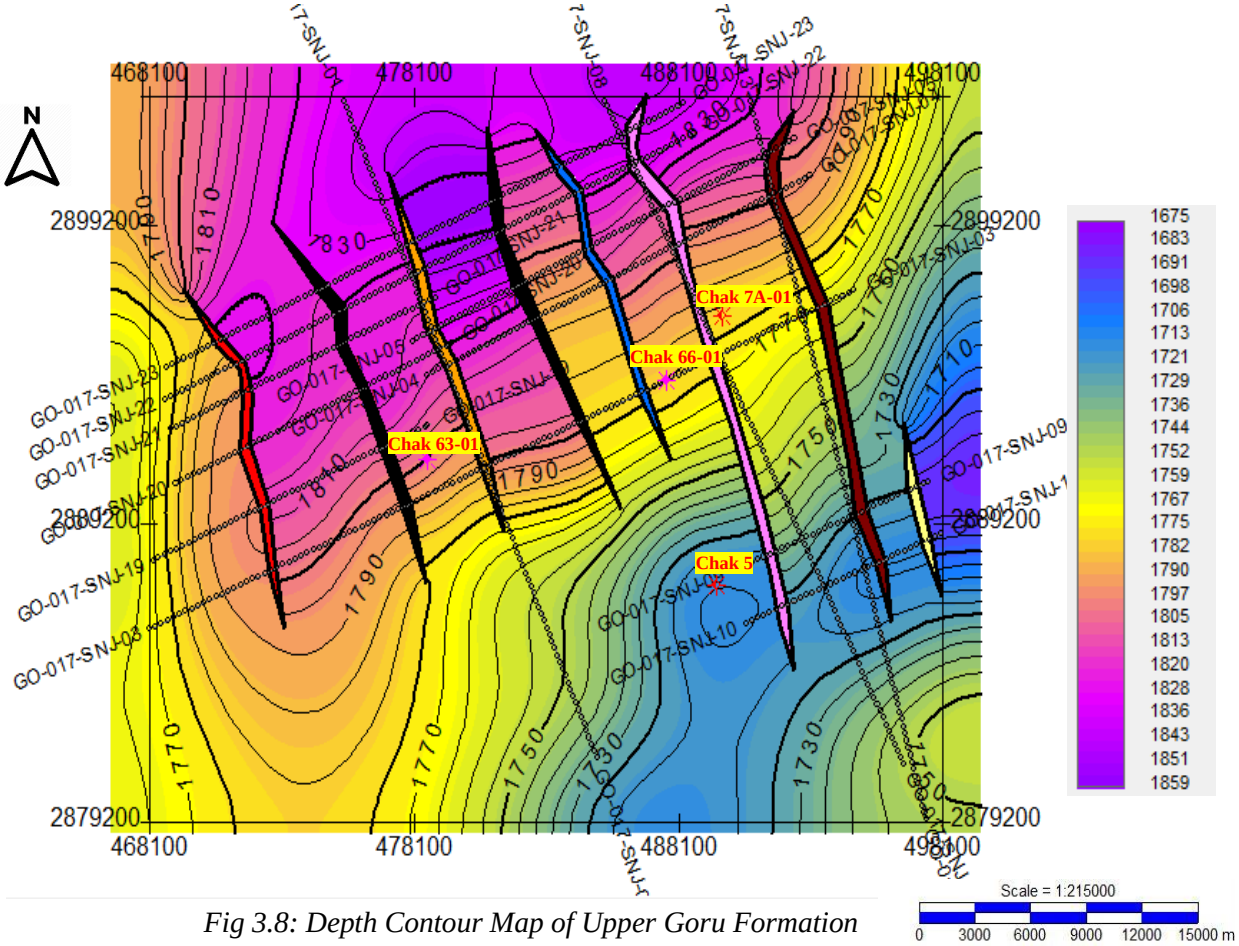

Fig 3.8: Depth Contour Map of Upper Goru Formation

formation which lies above Upper Goru.

3.4.2 Time and Depth Contour maps of Lower Goru Formation.

3.4.2.1 Time Contour Map

A two-way time contour map is constructed on Upper Goru formation by using Kingdom Suite shown in Fig 3.9 The horizon is generally dipping from North-West to South-East. Fault polygons are constructed for this map. Each polygon is represented by different color. Contours are terminating at fault polygons. Contour interval is set at 0.0065 sec. The time variation observed for Lower Formation is 1.387 to 1.79 Sec. Lower formation is composed of Shale and Sands. The thick sequence of Basal sands in Lower Goru Formation serves as reservoir in this area.

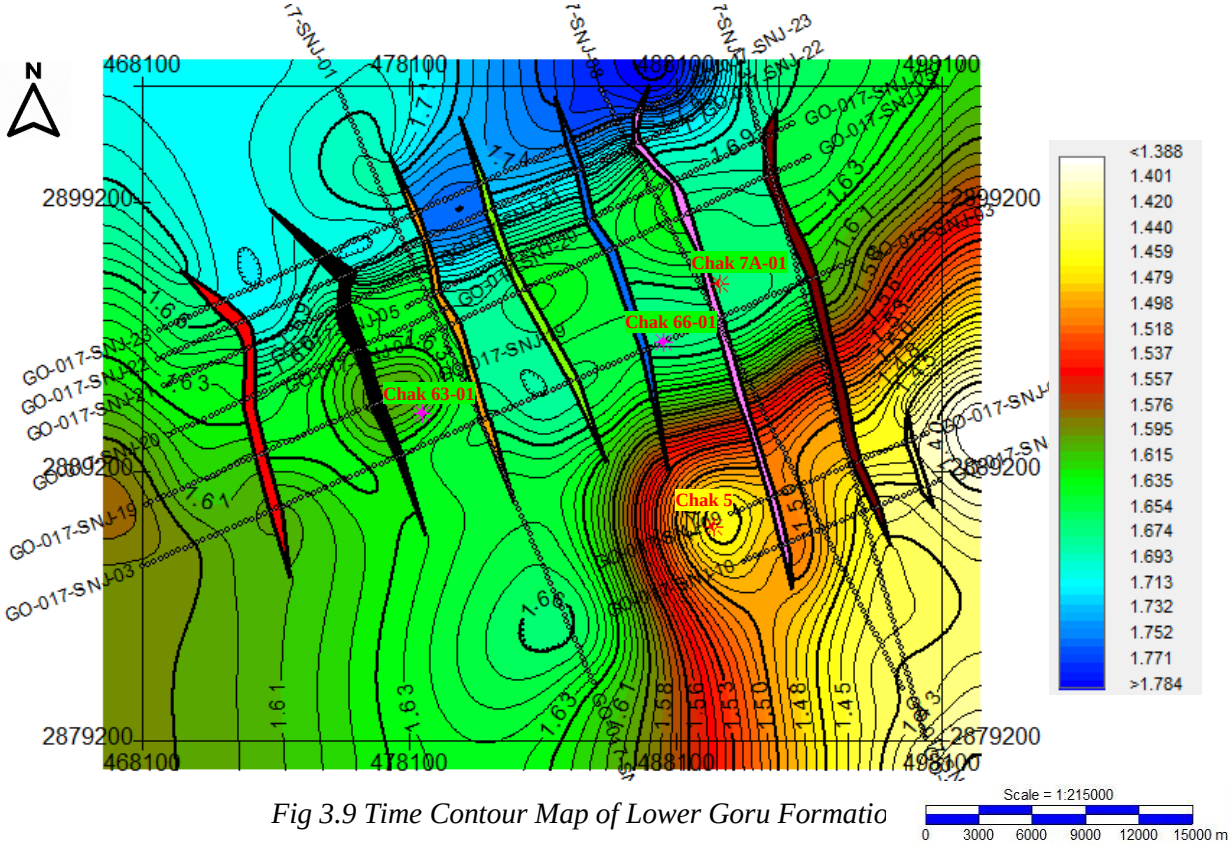

Fig 3.9 Time Contour Map of Lower Goru Formatio

3.4.2.2 Depth Contour Map

A Depth contour map is constructed on Lower Goru formation by using Kingdom Suite shown in Fig 3.10. Horizon depth is computed from horizon two-way time by using average velocity functions. The horizon is generally dipping from North-West to South-East. Fault polygons are constructed for this map. Each polygon is represented by different color. Contours are

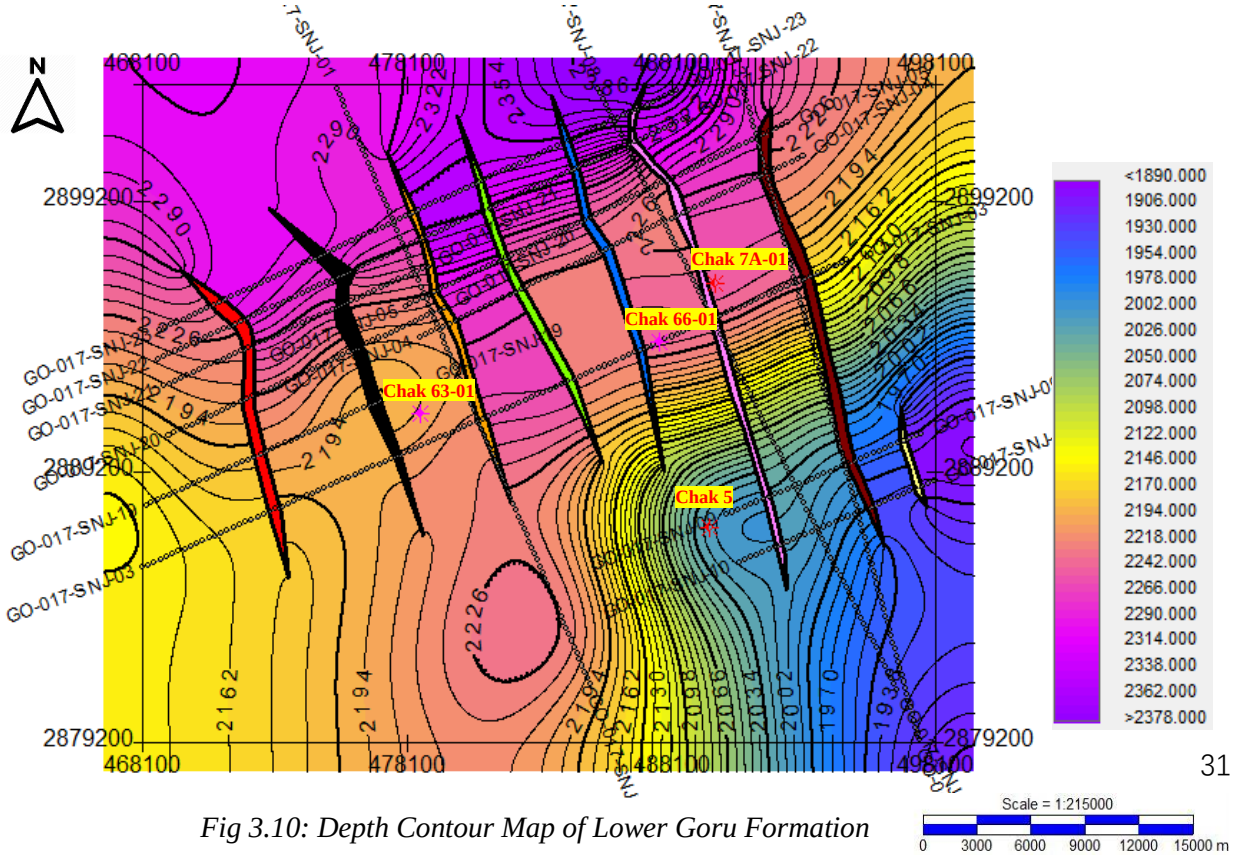

Fig 3.10: Depth Contour Map of Lower Goru Formation

terminating at fault polygons. Contour interval is set at 8 meters. The depth variation observed for Lower Goru Formation is 1890 to 2386 meter.

3.4.3 Time and Depth Contour maps of Chiltan Formation.

3.4.3.1 Time Contour Map

A two-way time contour map is constructed on Chiltan formation by using Kingdom Suite shown in Fig 3.11. The horizon is generally dipping from North-West to South-East. Contours are terminating at fault polygons. Contour interval is set at 0.006 sec. The time variation observed for Lower Formation is 2.4 to 2.69 Sec. This formation is mainly consisting of dense, compact and massive limestone with traces of shale. Major Faults show maximum throw at this formation

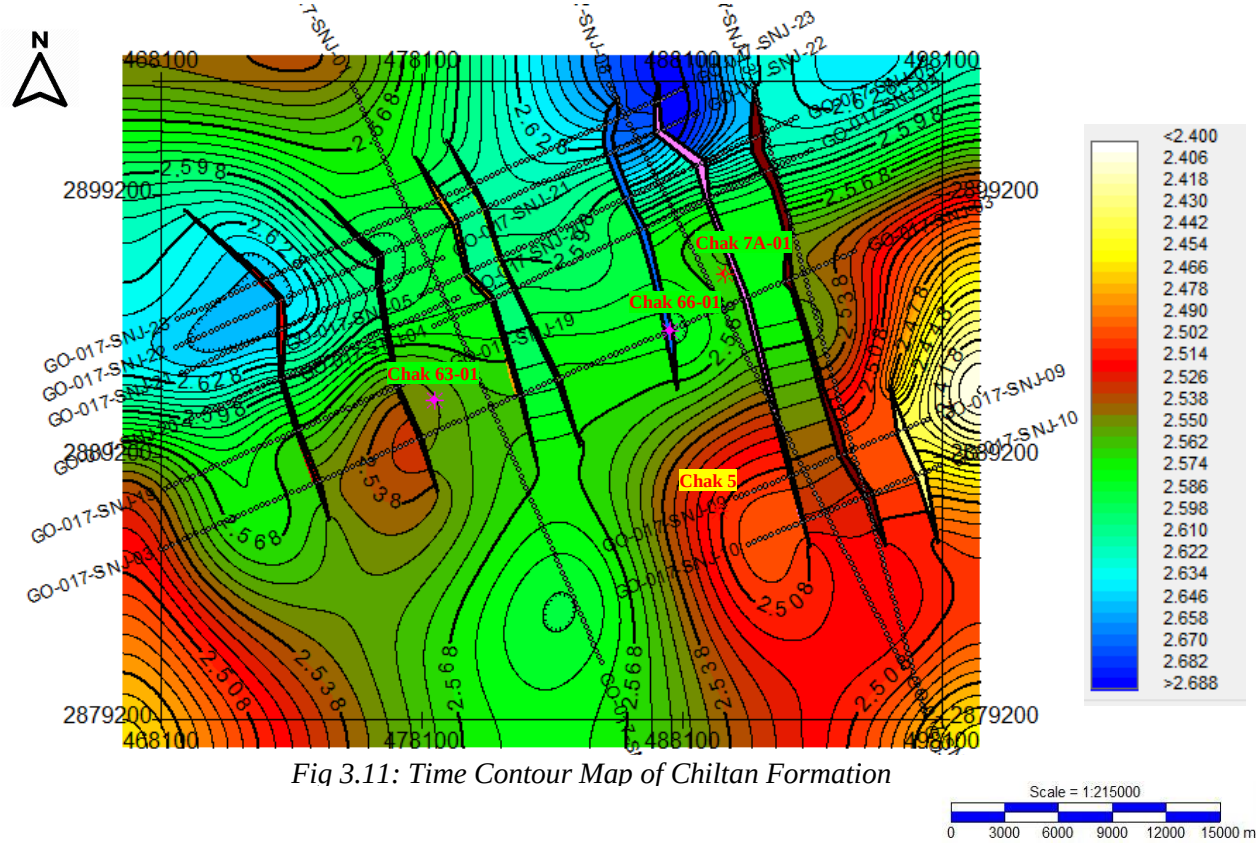

Fig 3.11: Time Contour Map of Chiltan Formation

3.4.3.2 Depth Contour Map

A Depth contour map is constructed on Chiltan formation by using Kingdom Suite shown in Fig 3.12. Horizon depth is computed from horizon two-way time by using average velocity functions. The horizon is generally dipping from North-West to South-East. Fault polygons are constructed for this map. Each polygon is represented by different color. Contours are

terminating at fault polygons. Contour interval is set at 6 meters. The depth variation observed for Chiltan Formation is 3887 to 4287 meters.

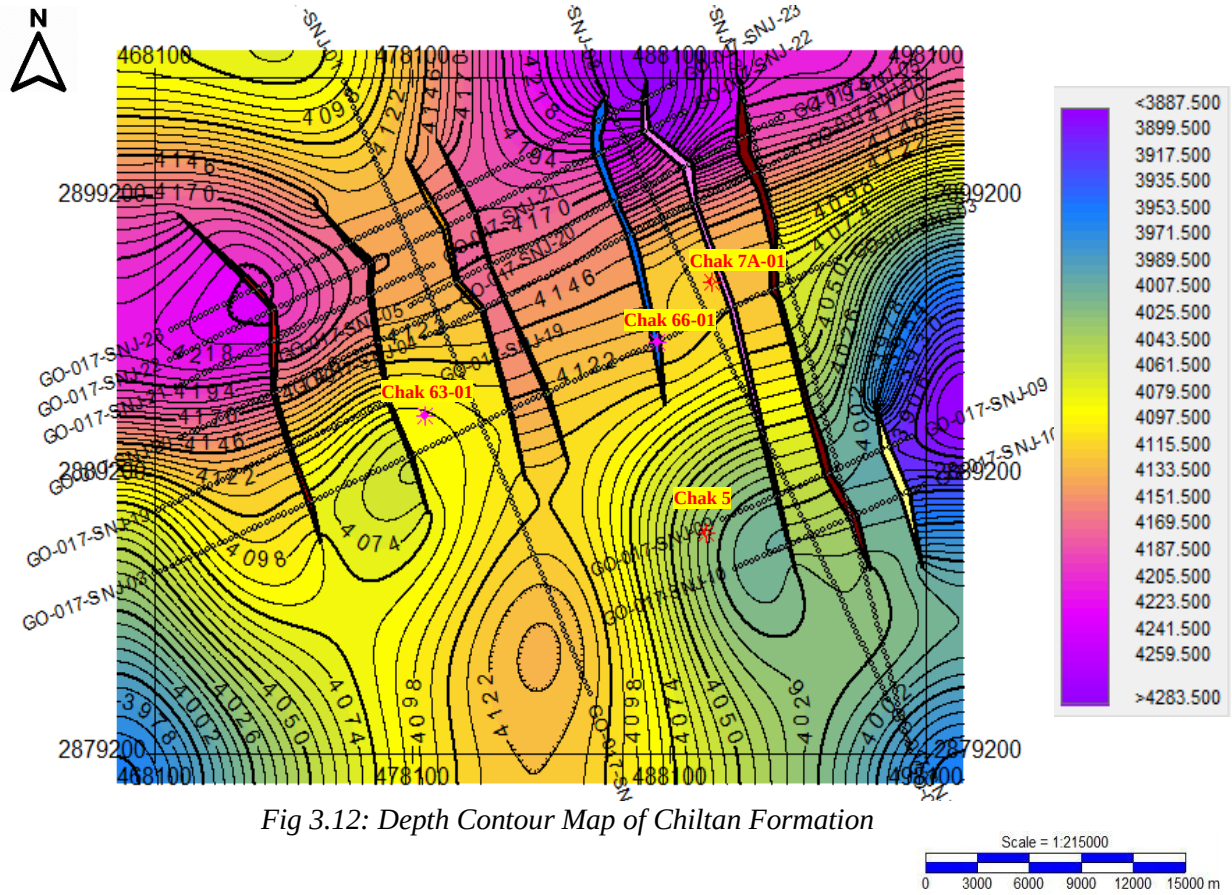

Fig 3.12: Depth Contour Map of Chiltan Formation

3.5 3D Surface Visualization

Today geophysicists display their datasets in a number of innovative ways to combine and correlate a variety of information. Advances in computer graphics have made it possible to display seismic data as true 3D surfaces complete with complex lighting effects. (Khan et al, 2011).

Lower Goru has primary importance in a sense that it is a reservoir in study area. The depth surfaces are generated for Upper Goru, Lower Goru and Chiltan Formation as shown in Fig 3.13. by multiplying time grids with average velocity functions. These Formations especially Lower Goru is dipping from an E to W direction. The Lower Cretaceous age succession was subjected to a long period of extension forces that severely deformed the strata of the study region. Subsequently, horst and graben structures were formed and are signature features of the study area. Very deep-seated regional level normal faults have been identified (discordant with the reservoir) within, above, and below the reservoir level. Since the formation of structures

pre-dates the gen- eration of hydrocarbon (Wandrey et al., 2004), these latterly extended conjugate normal faults are significant for the exploration prospects in two main ways.

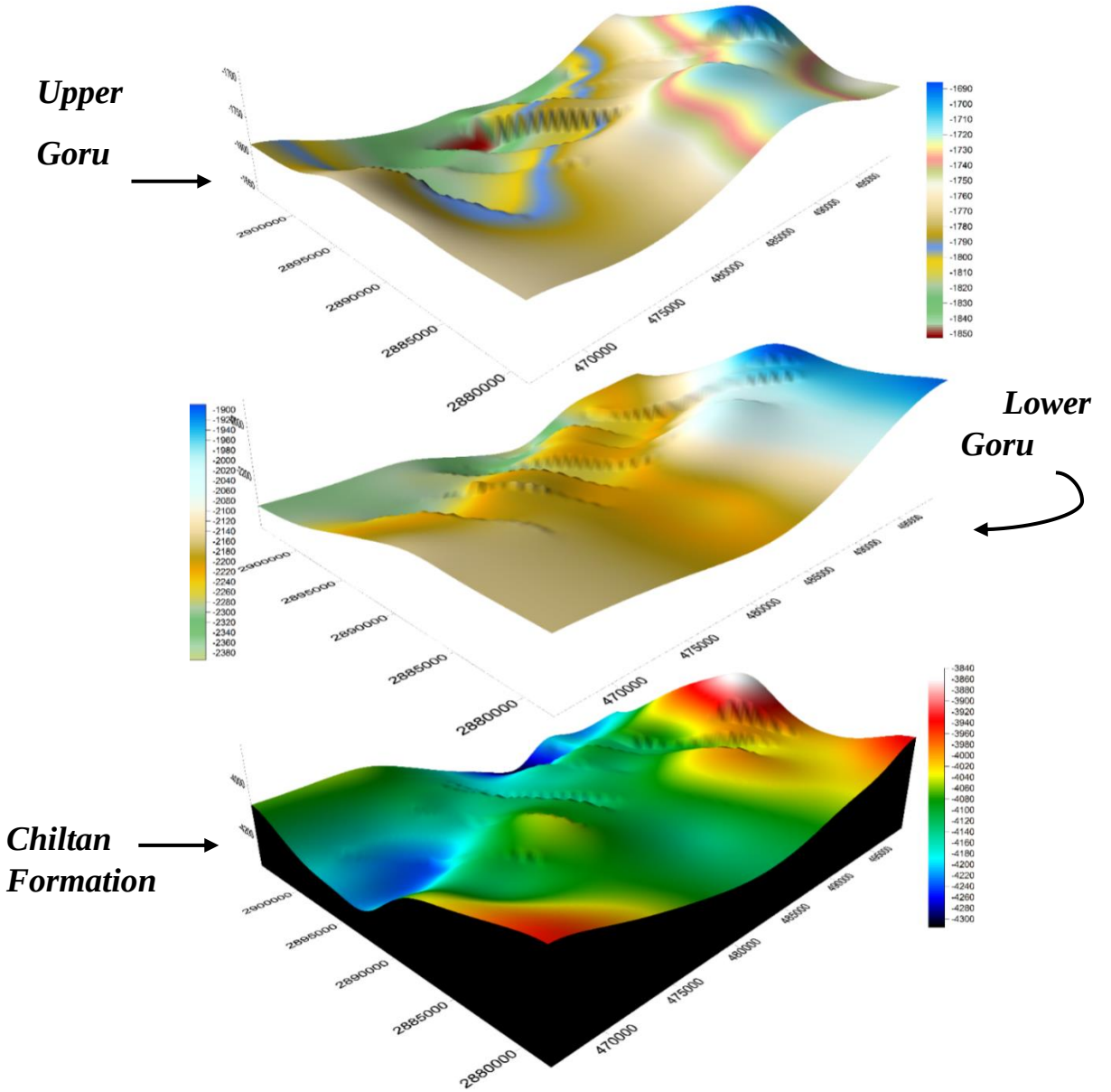

Fig 3.13: 3D surface maps of Upper Goru, Lower Goru and Chiltan formations.

Firstly, these faults are deep-rooted into the Sembar source shales (lies between Chiltan and Lower Goru), and therefore they can act as conduits to primary hydrocarbon migration. Secondly, these faults can act as a barrier and thus provide a lateral seal to trap the hydrocarbons within the structure.

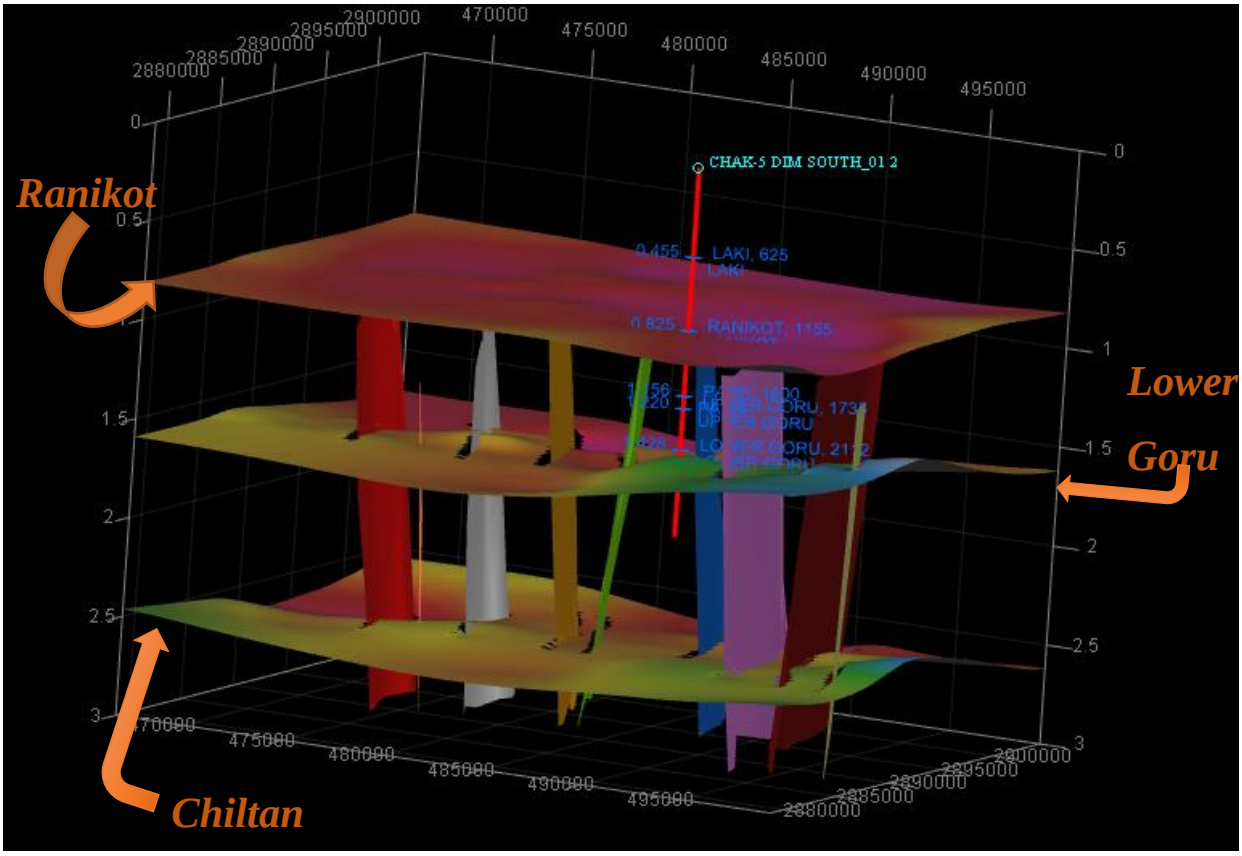

Fig 3.14: 3D model of formations, faults and well in VuPAK

A Seismic model was generated using *VuPak* application of *Kingdom Suite* is shown in Fig 3.14. It generates a 3D model of the subsurface at desired level and helps in visualizing the actual geological image with Fault Surfaces and Wells. This Model shows surfaces of Chiltan, Lower Goru and Ranikot Formation. Ranikot formation is almost stable with no major fault penetration. Almost every major fault in this area end into Parh Limestone. Well CHAK-5 DIM SOUTH-01 is also visible in this 3D view.

3.6 Crustal Extension

Crustal extension is the process of stretching the earth's crust, usually normal faulting and linear folding take place in such case. Pakistan geographically lies between 60°E to78°E and 24°N to 37°N. It has high density of active faults and is seismically one of the most active area

of the Asia. Tectonically it is located in the region of intersection of three plates, Indian, Eurasian and Arabian sea plate. The study area lies in the extensional regime where normal faults are present. To quantify the effect of the tectonic regime in the study area crustal extension of seismic line 20017-SNJ-09 has been computed using X-Works software.

3.6.1 Procedure

The interpreted seismic line 20017-SNJ-09, after time to depth conversion is basically a geological cross-section which shows the deformation in the horizons (formations) due to normal faulting. The length of the section (Lo) is calculated by the multiplication the number of CDP with the CDP interval. Similarly, the length (L) of the horizon is calculated by adding the lengths of its faulted segments. The crustal extension (CE) is then given by;

$$\mathbf{CE = L - Lo}$$

3.6.2 Crustal Extension of Rocks.

The crustal extension is computed for Upper Goru, Lower Goru and Chiltan formations. The current length of 20017-SNJ-09 is 6200 meters. After deformation the formations are divided into different parts due to normal faulting. The length of each faulted part is given in Fig 3.15. The total horizon lengths and their crustal extension are given in Table 3.2. It can be observed that an average 86 meters crustal extension has taken place along the three horizons, indicating an extensional regime.

Table 3.2 Horizons with their Length, Section Length and Crustal Extension

Horizon Name	**Horizon Length L (m)**	**Section Length Lo (m)**	**Crustal Extension L – Lo (m)**
Upper Goru	6122	6200	78
Lower Goru	6114	6200	86
Chiltan	6105	6200	95

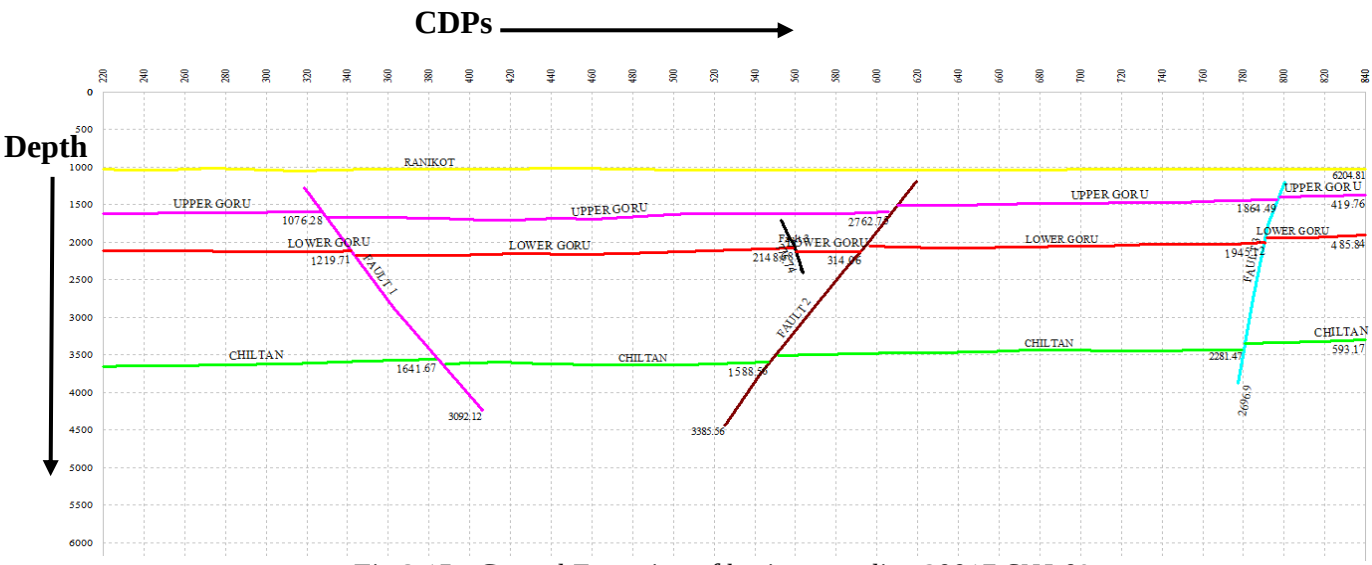

Fig 3.15: Crustal Extension of horizons on line 20017-SNJ-09

3.7 Seismic Attributes

Seismic attributes are related to any information related to seismic data. They can be considered as any information that can be mathematical computed from seismic data. This information can then be interpreted into useful geological information such as lithology, porosity, fluid content and other rock physics and reservoir properties (Khan, 2010). Seismic attributes are set of properties computed from input seismic data which consists of amplitude as a basic attribute.

3.7.1 Importance of Seismic Attributes

Seismic amplitude is basic attribute of seismic which is governed by reflection coefficient. Thus amplitude is composite information and we need to break it into various instantaneous attributes. Each of these instantaneous attributes is affected by different geologic conditions. Thus seismic attributes are important as each of them are able to highlight different geologic feature.

3.7.2Instantaneous Amplitude

Envelop of a trace, also called as reflection strength, represents the total instantaneous energy of the complex trace which is independent of the phase and is computed as the modulus of the complex trace.

The envelope relates directly to the acoustic impedance contrasts. It may represent the individual interface contrast or, more likely, the combined response of several interfaces, depending on the seismic bandwidth. The Hilbert Transform of the real seismic trace is generates an imaginary trace and using both these traces the envelope trace is computed. Fig 3.16. shows the real, imaginary and envelope trace. It can be observed that the envelope trace always remains positive.

The envelope relates directly to the acoustic impedance contrasts. It can be used as an effective tool of distinction for the following characteristics:

- ✓ Bright spots, possibly gas accumulation.
- ✓ Sequence boundaries.
- ✓ Thin bed tuning effects.
- ✓ Major changes in depositional environment.
- ✓ Spatial correlation to porosity and other lithological variations

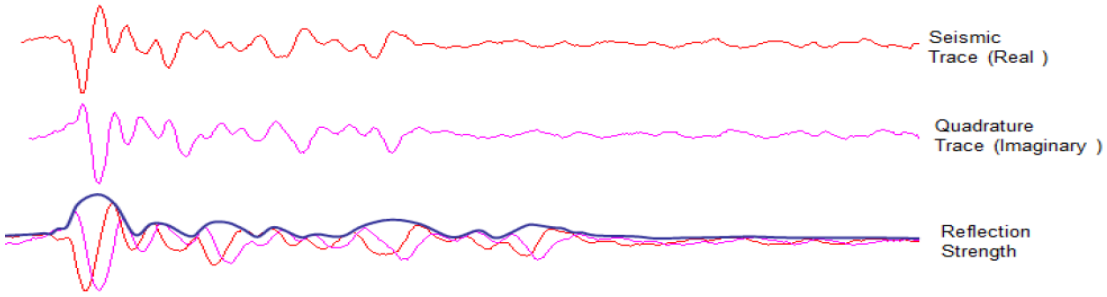

Fig 3.16: An envelope trace attribute is calculated for real seismic trace (Khan et al., 2006; Khan & Akhter 2015)

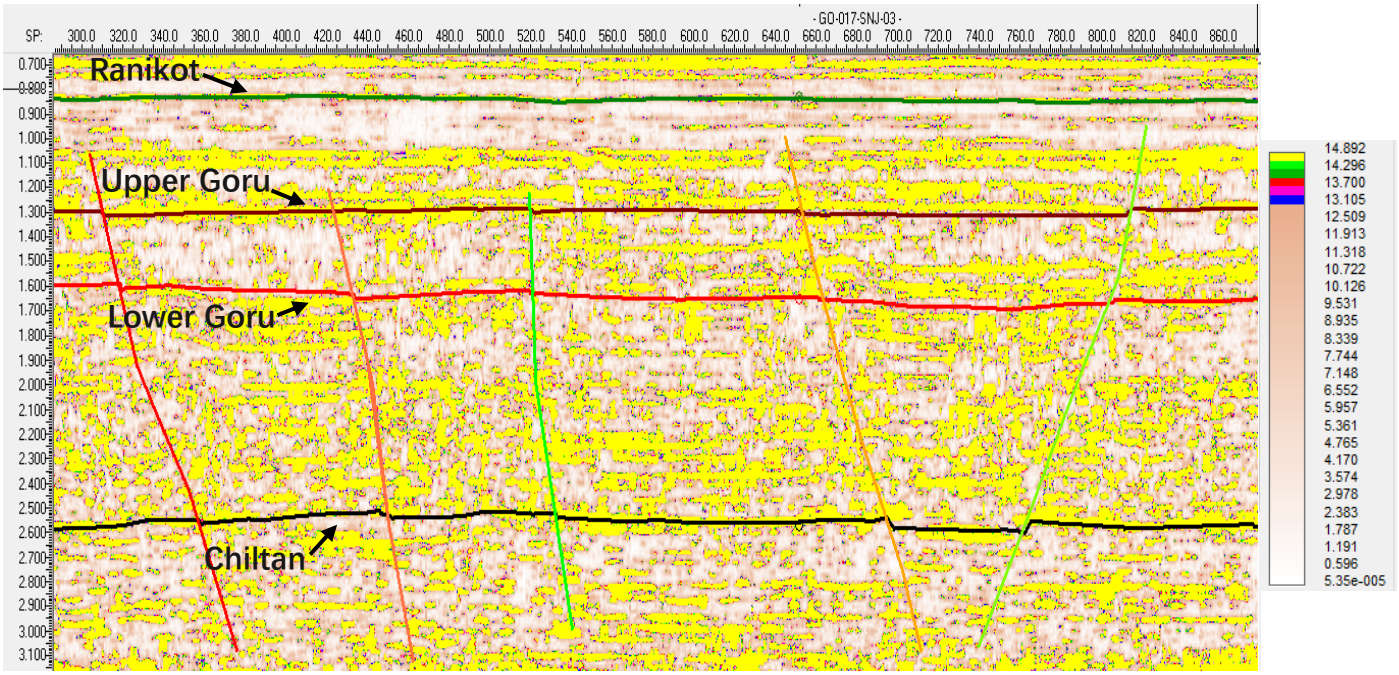

Fig 3.17: Envelope attribute map of seismic line 20017-SNJ-03

The attribute is computed for seismic line 20017-SNJ-03 to see the major changes in lithologies. A positive response is generated by Chiltan Limestone which has confirmed its presence. Chiltan Limestone formation was marked based on Strong amplitude during horizon interpretation. Fig 3.17 shows the envelope attribute map of 20017-SNJ-03. The thick (yellow) packages indicate the maximum reflection strength corresponding to the source, reservoir and seal rocks. It also shows spatial patterns representing changes in the limestone thickness and breakage due to the faults. In this case not every patch is scattered due to fault these weak reflections may because of interbedded sands or shale. Well CHAK 63-01 is located at SP 576. This area is bounded by normal faults. Envelop attribute clearly separated the source rock (Sembar formation lies between Lower

Goru and Chiltan Limestone) Reservoir rock (Lower Goru formation of interbedded sands and shales) and Seal rock (Upper Goru).

3.7.3 Average Energy Attribute

Average energy is a post-stack wavelet attribute, in which, within a specified window the square root of the sum of squared amplitudes is calculated and divided by their number of samples. The wavelet attributes are computed at the peak of the envelope, which represent the attributes of the wavelets within a zone defined by the trace envelope minima. These attributes

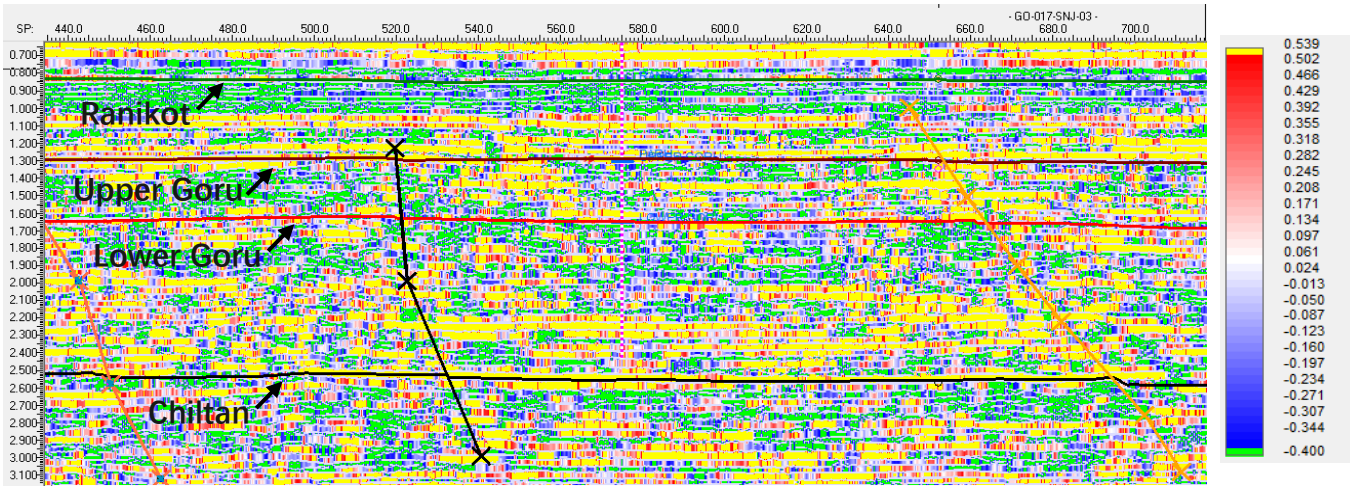

Fig 3.18: Average Energy attribute map of seismic line 20017-SNJ-03

indicate spatial variation of the wavelets and therefore relate to the response of the composite group of individual interfaces below the seismic resolution. The attribute has a blocky response and individually highlights the seal, reservoir and source rocks as shown in Fig 3.18 attribute map of 20017-SNJ-03.

3.7.4 Instantaneous Phase Attribute

The phase information is independent of trace amplitudes and relates to the propagation of phase of the seismic wave front. Since, most of the time, wave fronts are defined as lines of constant phase, the phase attribute is also a physical attribute and can be effectively used as a discriminator for geometrical shape classifications. It is computed from real and imaginary traces as given below;

$$\Theta\,(t) = \tan^{-1}\,[h\,(t) / f\,(t)]$$

h(t) = Quadrature (Imaginary) trace.

f(t) = Recorded (Real) trace.

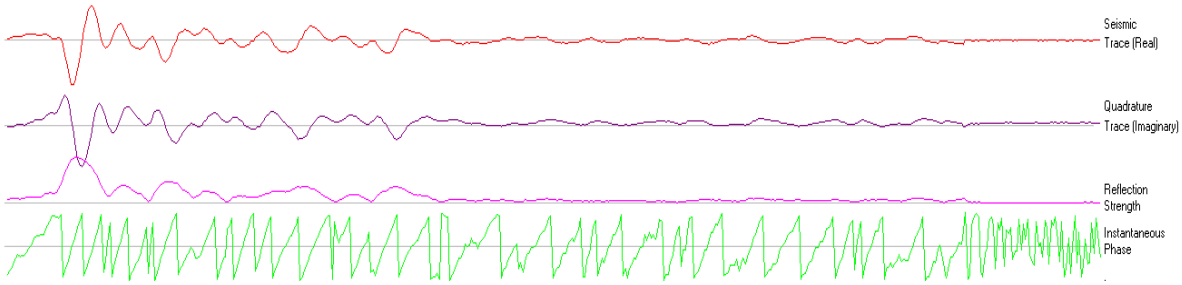

Fig 3.19: Instantaneous Phase trace when normalized maximum amplitude is 1

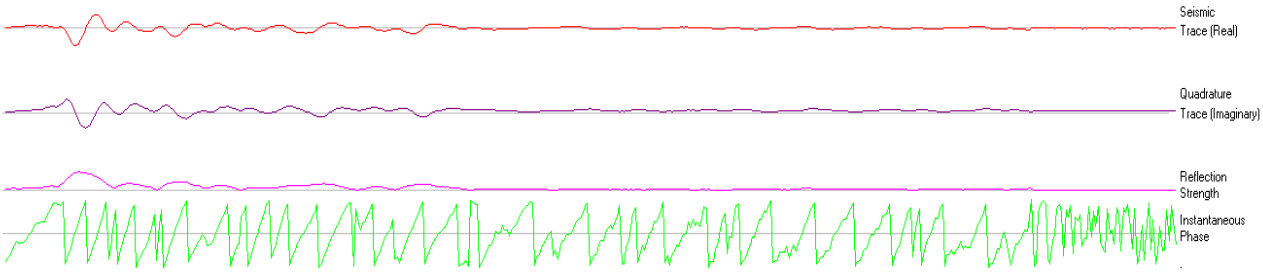

Fig 3.20: Instantaneous Phase trace when normalized maximum amplitude is 0.4.

Instantaneous phase is the best indicator of lateral continuity, relates to the phase component of the wave propagation and has no amplitude information, hence all events are represented. It can be used to highlight interface in sections with high decay of amplitudes and even highlight deeper horizons which are not visible in the normal Fig 3.19 & 3.20 shows instantaneous phase computed for two version of seismic trace one with normalize maximum amplitude 1 and other by 0.4 respectively. The 2nd trace is showing weak events. It shows that by decreasing the amplitude to 40%, it is observed that the amplitude is decaying but resulting instantaneous phase shows no change. Thus, this attribute is useful for marking the reflector where amplitude is weak. Fig 3.21 shows the instantaneous phase attribute for seismic line 20017-SNJ-03 which changes from -180° to +180°. The interpreted horizons lie over the zero phase regions. This attribute further confirms the interpretation as the input data is zero phase. It can be observed in comparison to amplitude-based sections that the instantaneous phase shows much deeper horizons.

3.7.5 Geological Importance of Seismic Attributes

Seismic attributes form an integral part of qualitative interpretative tool that facilitates structural and stratigraphic (channels, pinch out, meanders, etc) interpretation as well as offer clues to lithology type and fluid content estimation with a potential benefit of detailed reservoir characterization.

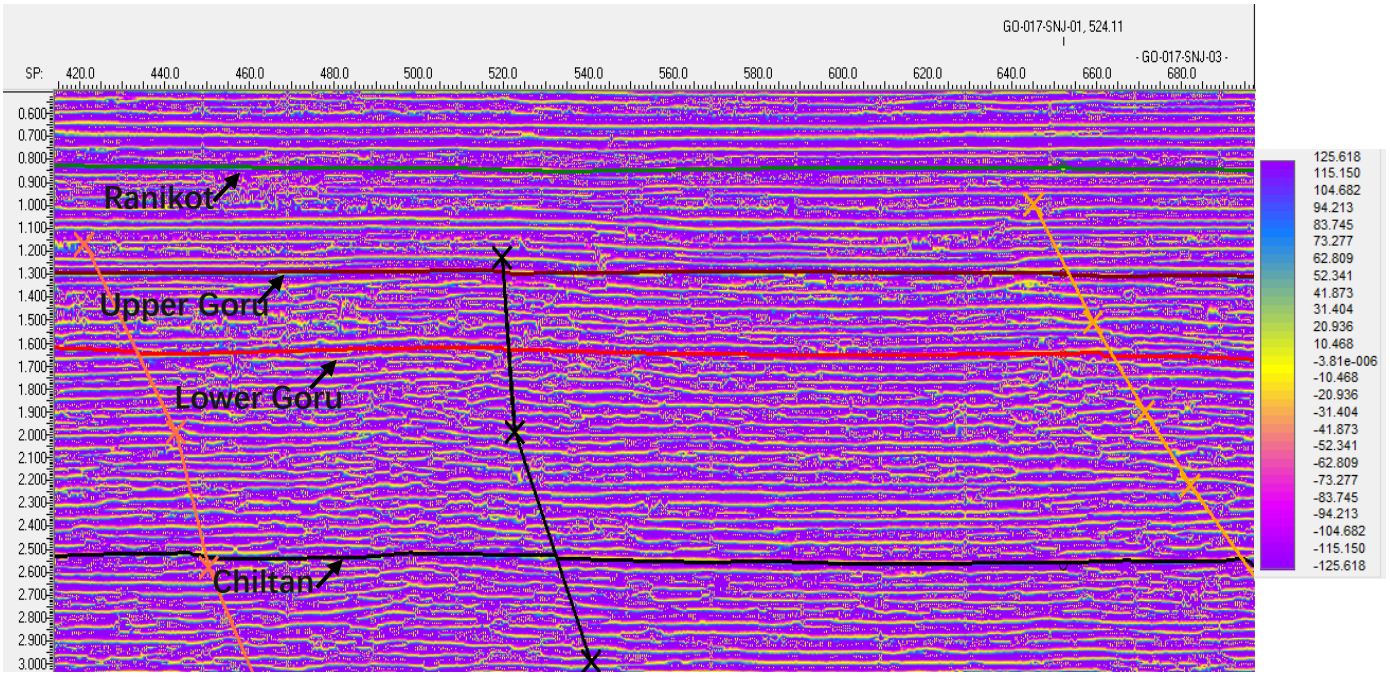

Fig 3.21: Instantaneous Phase attribute map of seismic line 20017-SNJ-03

Attribute analysis of seismic data with several types of seismic attribute may reveal geologic factors that control spatial distribution of subsurface energy reserves. Table 3.3 shows some seismic attributes and the geologic information they provide.

Table 3.3 Seismic Attributes and Their Geological Significance

Attribute	Geological Information
Instantaneous Frequency	Lithological contrasts, Bed thickness, Fluid content
Reflection strength	Lithological contrasts, Bedding continuity, Bed spacing, Gross porosity
Instantaneous phase	Bedding continuity
Polarity	Polarity of seismic, Lithological contrasts
Amplitude	Lithological contrast, Bedding continuity, Bed spacing, Gross porosity, Fluid content.

Chapter 4: Petrophysics, Rockphysics and Facies Analysis

4.1 Petrophysics

In reservoir characterization lithology and pore fluid prediction are vital. Lithology and pore fluid prediction are very important aspects of exploration and production such as geological studies, reservoir modeling, formation evaluation, enhanced oil recovery processes, and well planning including drilling and well completion management.

Lithology basically refers to the type of rock in the Earth crust. Different kinds of rocks exist in the subsurface but not all are conducive for hydrocarbon accumulation. For a subsurface rock to be a good hydrocarbon storage, the rock should be sedimentary with pore spaces. These pore spaces can be filled with hydrocarbons (Schlumberger, 1989).

Lithology and pore fluid can be unambiguously determined using core samples obtained from underground formation. Core sample analysis for lithology and pore fluid prediction is expensive and usually involves vast amount of time and effort to obtain reliable information (Chang et al., 2002).

Electrical well logging was introduced to the oil and gas industry over half a century ago and since then, many improved and additional logging tools and devices have been developed and have been put in general use. The art of interpretation of the data advanced along with the advancements in well logging science. Today, the detailed analysis of a carefully chosen suite of wire-line services provide a method of inferring or deriving accurate values for the hydrocarbons and water saturations, the permeability index, the porosity, and the lithology of the reservoir rock (Schlumberger, 1998).

Petrophysics, which refers to the study of both chemical and physical properties of rocks and their communication with pore fluid, is used to determine the hydrocarbon bearing reservoir of a well. In the hydrocarbon industry, petrophysics is primarily used for the study of reservoir. Petrophysical analysis employ methods that emphasize on the estimation of a single property at a time.

A detailed Petrophysics, Rock physics, and facies analysis has been done in this research work for Well CHAK 5 DIM SOUTH 01. Lithology and Fluid properties of reservoir have been

estimated carefully using wireline log data analysis. Identifying type of lithology, pore fluid and their saturations in Lower Goru formation led to mark zone of interest in this well.

4.2 Log Curves

The log data of CHAK 5 DIM SOUTH 01 was available in Logging ASCII Standard (LAS) format. The log curves along with some parameters given in the LAS file header are used to calculate all basic and advance parameters. The available logs that were run through the well are SP, Caliper, GR, Resistivity (complete suite), Sonic, Neutron, Density and PEF The methodology adopted for this work is given in Fig 4.1 and each analysis step is discussed in the proceeding sub-sections.

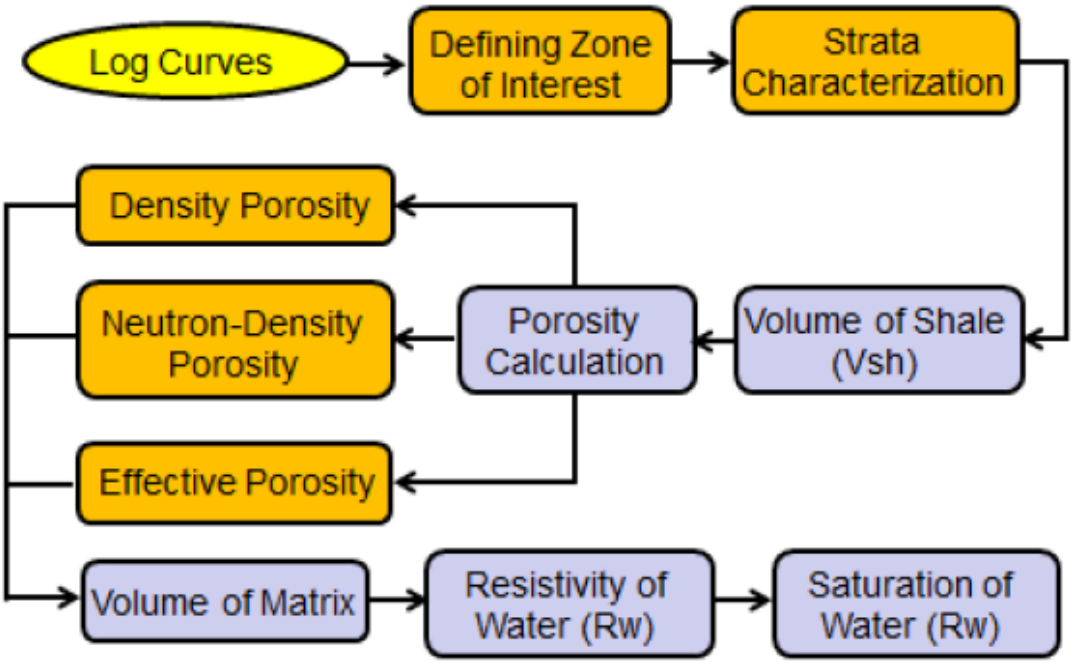

Fig 4.1: Workflow for petrophysical analysis

4.2.1 Quality Check

In practice, Well Logs contain several intrinsic problems particularly problems of noise, gaps and spikes. A quality check was conducted for the logs at different depth levels to confirm the data reliability of log data. Diameter of borehole was confirmed through calliper log to check reliability of all other logs (since value of any log is not reliable in washout zone and we have to go for some alternate method in that case).

4.2.2 Zone of Interest

The zones of interest were defined on the basis of source, reservoir and seal rock formations given in well tops of CHAK 5 DIM SOUTH 01 well. The zones of interest in this well is Lower Goru formation which is the main reservoir in this area. Lower Goru formation starts from depth 2112.0 m. This formation is composed of shale and sands packages commonly divided as Basal Sands, Talahr Shale and Massive Sands. Sands of Lower Goru formation act as good reservoir. Formation tops of these sands and shales were not give in the provided data.GR log then used to identify them.

4.2.3 Strata Characterization

The lithologies are marked by Gamma Ray log deflections; it is a good indicator of shale. The shale and sand formations are identified by this log, but sometimes caliper and SP log information is also very important for strata characterization. It can also be calculated using SP log in case GR is absent. Sand and shale lines are marked at the minimum and maximum values of Gamma Ray in the selected zone of interest, A cut off line is marked in the middle of the two lines which is used to demarcate sand and shale formations.

4.2.4 Volume of Shale

Gamma ray log was used to calculate the volume of shale. In the quantitative evaluation of shale content, it is assumed that radioactive minerals are absent in clean rocks and are compared to shaly rocks. The source formations are commonly shaly with higher radioactive content and are therefore indicated by a higher Gamma Ray value. On the other hand, it is also assumed that the radioactive material is not present in other formations which are termed as clean formations. This creates a contrast between shale and other formations.

The following mathematical equation was used for computation of Volume of Shale.

$$V_{sh} = \frac{GR_{log} - GR_{min}}{GR_{max} - GR_{min}}$$

Where

V_{sh} = Volume of Shale.

GR_{log} = Value of GR in the Zone of Interest.

GR_{min}= Minimum Value of the GR in Clean Beds.

GR_{max}= Maximum value of the GR in Shaly beds.

A constant cut-off value of 45% (0.45) was applied on Vsh curve in order to identify the clean intervals within the zone.

4.2.5 Porosity Calculation

Net interval was defined on the basis of Effective Porosity (PHIE) curve. However, prior to that, values of porosity were determined using density and neutron logs

4.2.5.1 Density derived Porosity

Formation density is a function of both porosity and rock type. Porosity is denoted by "Φ". and expressed either by percentage or in decimals. So if the rock type is known then porosity can be calculated. In this research, rock type in zone of interest is known from gamma ray which is sandstone. Therefore, porosity was calculated by using following relation (Asquith and Gibson, 1982).

$$\Phi_{density} = (\rho_{ma}-\rho_b) / (\rho_{ma}-\rho_f)$$

Where

$\Phi_{density}$ = Density derived porosity.

ρ_{ma} = Matrix Density.

ρ_b = Formation Bulk Density. (Value from Log)

ρ_f = Fluid Density.

Values used for density of matrix (sandstone) and fluid (mud) are 2.65 g/cm3 and 1.0 g/cm3 respectively (Schlumberger, 1972).

4.2.5.2 Sonic derived Porosity

Porosity can also be calculated using the sonic log. However, the basic principle is same as applied in the above case. To evaluate porosity of consolidated rocks from sonic log, a mathematical relation given by Wyllie et al., (1958) was used. For unconsolidated sandstone, a compaction factor Cp=(Δtsh*C)/100 (Wyllie et al., 1958) should be added to this equation. Moreover, for calculation of vuggy or secondary porosity in carbonates, sonic porosity subtracted from total porosity (i.e. derived from density or neutron log).

$$\Phi_{sonic} = (\Delta t_{log}-\Delta t_{ma}) / (\Delta t_f-\Delta t_{ma})$$

Where,

Φ_{sonic} = Sonic derived porosity (PHIS)

Δt_{log} = Transient time of formation

Δt_{ma} = Transient time of matrix

Δt_{f} = Transient time for fluid

Values used for transient time of matrix (sandstone) and fluid (fresh mud) are 55μsec/ft and 189μsec/ft respectively (Schlumberger, 1972).

4.2.5.6 Neutron Porosity

Neutron Porosity is directly obtained from Neutron log values.

4.2.5.7 Average Porosity

Porosity values, either density derived or sonic derived, were averaged out with Neutron Porosity.

$$\Phi_{avg} = (\Phi_{den} + \Phi_{neutron}) / 2$$

OR

$$\Phi_{avg} = (\Phi_{sonic} + \Phi_{neutron}) / 2$$

Where

Φ_{avg} = Average Porosity. (PHIA)

Φ_{den} = Density Porosity.

Φ_{sonic}= Sonic Porosity.

4.2.5.8 Effective Porosity

Finally, the effective porosity was calculated using the following equation:

$$\Phi_{effective} = \Phi_{avg} * V_{matrix}$$

Where,

$\Phi_{effective}$ = Effective porosity (PHIE)

V_{matrix} = (1 - Vsh)

4.2.6 Calculation of Water Saturation

The fraction of pore spaces containing water is termed as Water Saturation (Sw). A normal practice to calculate Sw is applying Archie's Equation mentioned as under;

$$S_w = \sqrt[n]{\frac{a * R_w}{LLD * \Phi_{avg}{}^{m}}}$$

Where,

S_w = Saturation of water (Apparent).

n = Water saturation factor.

a = Tortuosity factor = 1

m= Cementation factor = 0.81

R_w = Resistivity of water (Typically 0.06 is used for this area).

LLD = Log reading of resistivity (deep) tool.

4.2.7 Calculation of Hydrocarbon Saturation

The fraction of pore spaces containing Hydrocarbons is known as Hydrocarbon Saturation and mathematically given by the following equation;

$$S_{hc} = 1 - S_w$$

S_{hc} = Saturation of Hydrocarbons.

S_w = Saturation of Water.

As the S_{hc} is the remaining percentage of the Pore volume occupied by Water, hence this method is indirect quantitative estimation of the hydrocarbons.

4.2.8 Hydrocarbon Bearing Zone

Lower Goru sands are good reservoir in this area. Petrophysical analysis of well CHAK 5 DIM SOUTH 01 clearly indicate the zone of interest in this well which lies from depth 2854 to 2868 m. This reservoir lies in 14m thick massive sand package marked by red color in
Fig 2. Logs behavior in this reservoir confirmed the presence of hydrocarbons. Separation of NPHI and RHOB indicated gas effects in the reservoir. Values of average porosity, effective porosity, hydrocarbon saturation, and water saturation calculated for this reservoir are given in table 4.1.

Table 4.1: Results of Petrophysical analysis of Hydrocarbon bearing zone.

Interval	V_{sh}	V_{sand}	$\Phi_{effective}$	Φ_{avg}	S_{water}	S_{HC}
2854-2868m	27.2%	72.8%	6.5%	17.3	33.9%	66.1%

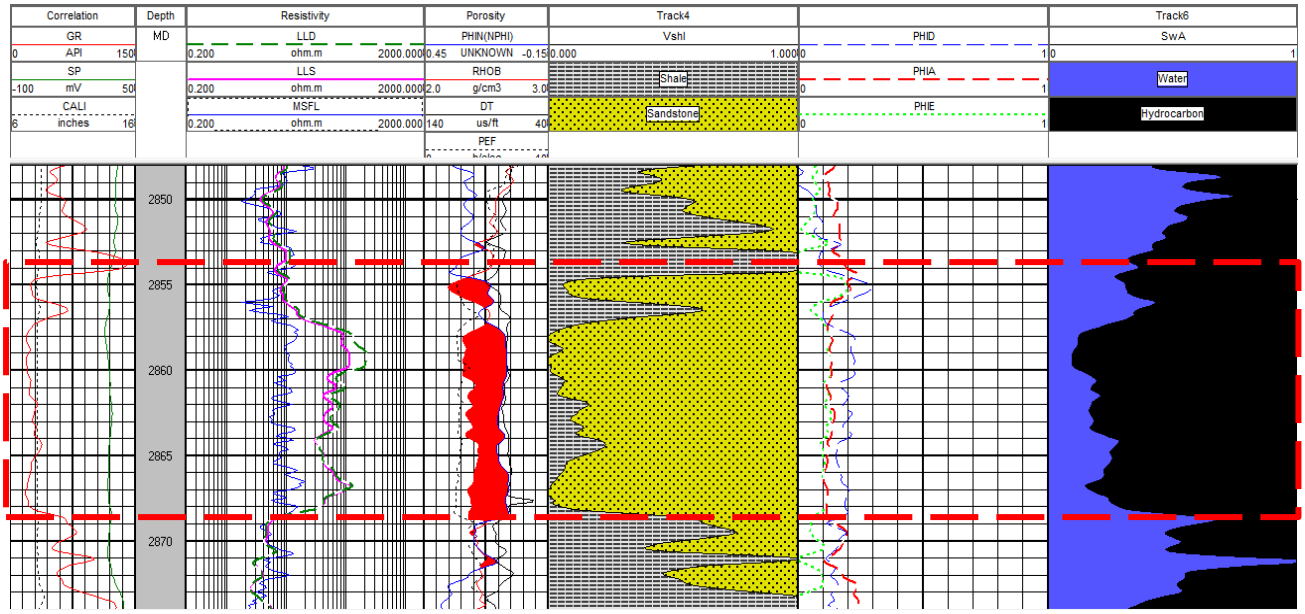

Fig 4.2 : Results of Petrophysical analysis of Well Chak 5 Dim South 01 at the level of Lower Goru.

4.3 Rockphysics and Facies Modeling

Rock Physics is an integration science linking seismic data, its derived attributes, Petrophysical data, as well as lab measured elastic parameters and core data. It consists of a wide range of empirical relations that have been established through best-fit least square regression. Correlations can be established between any two or more rock properties that can be used to compute one rock parameter from another. Rock physics templates have been developed to visualize lithological and mineralogical variations in terms of Petrophysical logs; derived rock physics, derived seismic attributes and can be applied for the quantitative interpretation of well

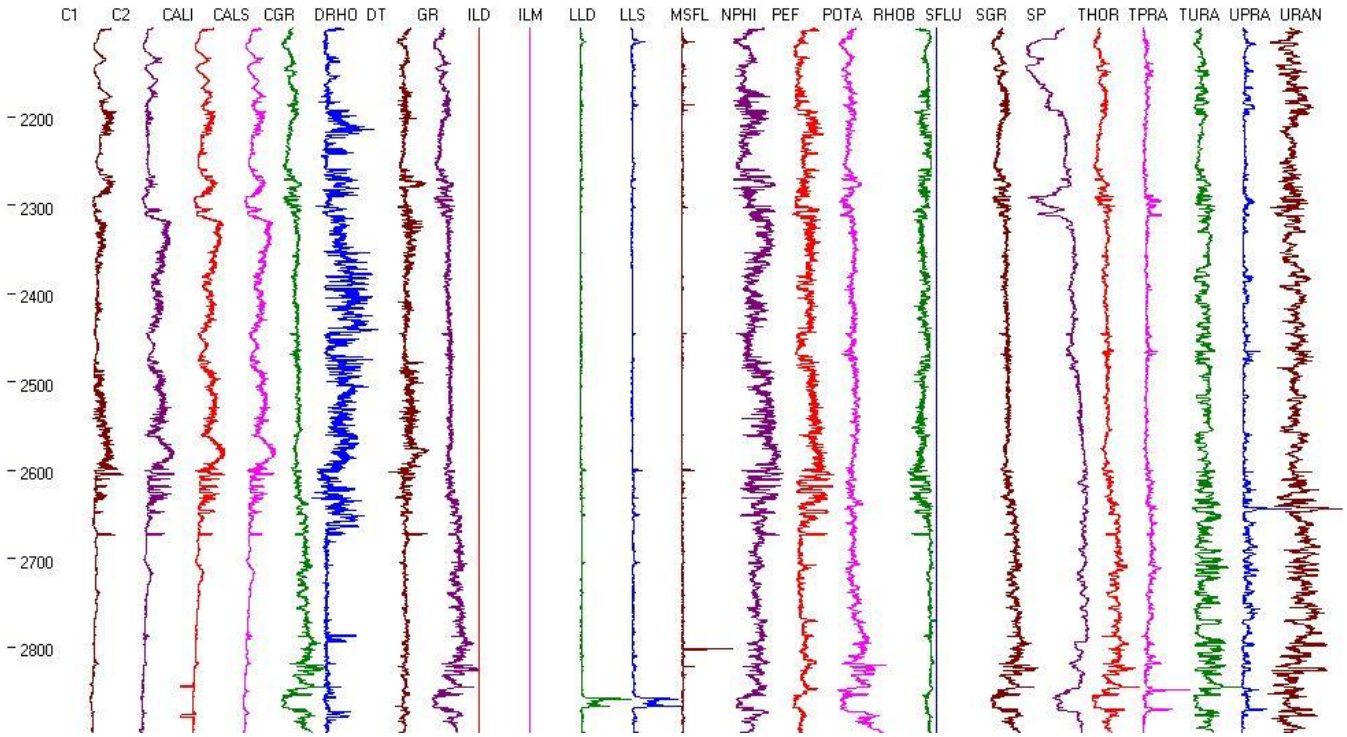

Fig 4.3: Petrophysical logs of Well Chak 5 Dim South 01 for the depth interval 2100 to 2900 m.

log and seismic data. (Perez et al, 2011) constructed rock physics templates using a combination of Hertz–Mindlin contact theory and the lower modified Hashin–Shtrikman bounds to guide interpretations of estimated ultimate recovery in shales.

Fig 4.3 shows the Petrophysical logs of well Chak 5 Dim South-01 for the depth range 2100 to 2900 meter. To compute the elastic logs we need sonic, shear sonic and density logs. However, it can be observed from Fig 4.3 that shear log is not available for this well. Thus, the Castagna et al., (1993) empirical relationship is used to compute the shear velocity from the P-wave velocity (sonic) log.

4.3.1 Computation of Elastic Logs

The P-wave velocity (sonic) log, S-wave velocity (computed shear sonic) log and density log are used to compute the elastic logs of various moduli along with acoustic impedance and shear acoustic impedance logs as shown in Fig 4.4.

The Petrophysical logs along with the computed Acoustic Impedance and Elastic Logs are used in various types of cross plot for classification or facies modeling. Before we go into the details of each facies modeling cross plots a brief description of each elastic parameter is given below.

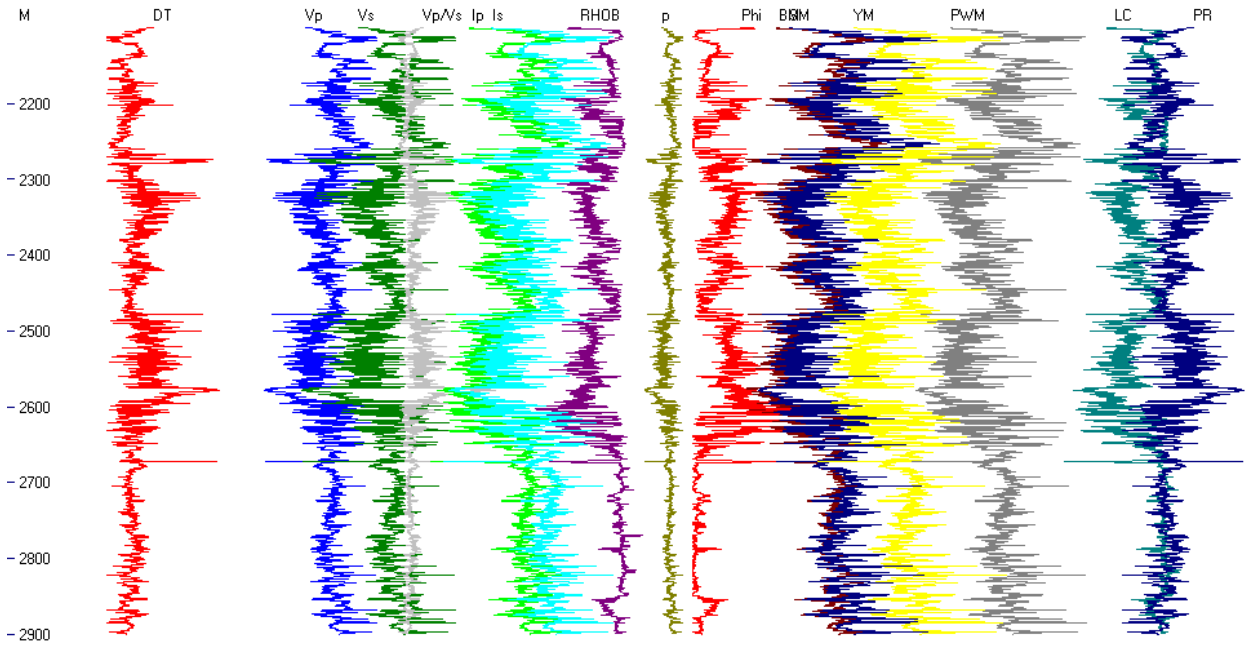

Fig 4.4: Impedance and Elastic logs computed for Well Chak 5 Dim South 01 for the depth interval 2100 to 2900 m.

4.3.1.2 Acoustic Impedance (AI)

Acoustic impedance is a layer property of a rock and is equal to the product of compressional velocity and density (Onajite et al., 2014). The density log and the compressional wave velocity log generated from the DT log are used to compute the acoustic impedance log by using equation:

$$\boldsymbol{AI = V_P \times \rho_b}$$

Where, ρb is the density of the formation and Vp is he compressional wave velocity.

4.3.1.3 Shear Impedance (SI)

Shear impedance is a layer property of a rock and is equal to the product of shear velocity and density also known as elastic impedance (Connolly, 1998, 1999). Similarly, as acoustic impedance the density log and the shear wave velocity derived from the Castagna et al., (1993) empirical relation was used to generate the shear impedance log using equation:

$$\boldsymbol{SI = V_S \times \rho_b}$$

Where, $\boldsymbol{\rho_b}$ is the density of the formation and **Vs** is the shear wave velocity.

4.3.1.4 Young's Modulus (E)

This modulus is obtained to measure the stiffness of the material. The relation between the density, compressional wave velocity, young's modulus, and shear wave velocity is given in equation (Mavko et al., 2009).

$$\boldsymbol{E = \frac{\rho V_s^2\left(3V_P^2 - 4V_S^2\right)}{V_p^2 - V_p^2}}$$

Where, $\boldsymbol{\rho}$ is the density that is obtained from the density (RHOB) log, **Vs** and **Vp** are the shear wave and compressional wave velocity that is obtained from the sonic log (DT).

4.3.1.5 Poisson's Ratio (σ)

The Poisson's ratio is used to indicate the maturity of the shale oil/gas zone. The low value of poisson's ratio will indicate the mature oil/gas shale zone. The relation between the poisson's ratio, compressional wave velocity, and shear wave velocity is given in equation (Mavko et al., 2009).

$$\sigma = \frac{\left(\frac{V_P}{V_S}\right)^2 - 2}{2\left(\frac{V_P}{V_S}\right)^2 - 2}$$

4.4 Facies Modeling

Cross plot-based facies analysis is an important methodology accepted worldwide to properly characterize a hydrocarbon reservoir and exploit the remaining volumes in development phase. In this study, shale, shaly sand and clean sands are characterized using various cross plots. Common methods for cross plot-based facies modeling are polygon bounds and cluster analysis. In this study the polygon method is used for facies modeling. With the help of well Log data of Chak 5 Dim South -01, different cross plots are compared with the standard cross plots to identify the lithologies, and the prospect zone to be marked.

4.4.1 $\mu\rho$ versus $\lambda\rho$

Fig 4.5 shows the $\lambda\rho$-$\mu\rho$ crossplot, also referred as LMR, by Goodway et al., (2007) for improved fluid detection and lithology discrimination. The parameters of $\lambda\rho$ and $\mu\rho$ are measures of the incompressibility and rigidity of rocks, respectively, of which μ and λ were calculated from the petrophysical logs. It can be observed from the Fig 4.5 that $\mu\rho$ decreases

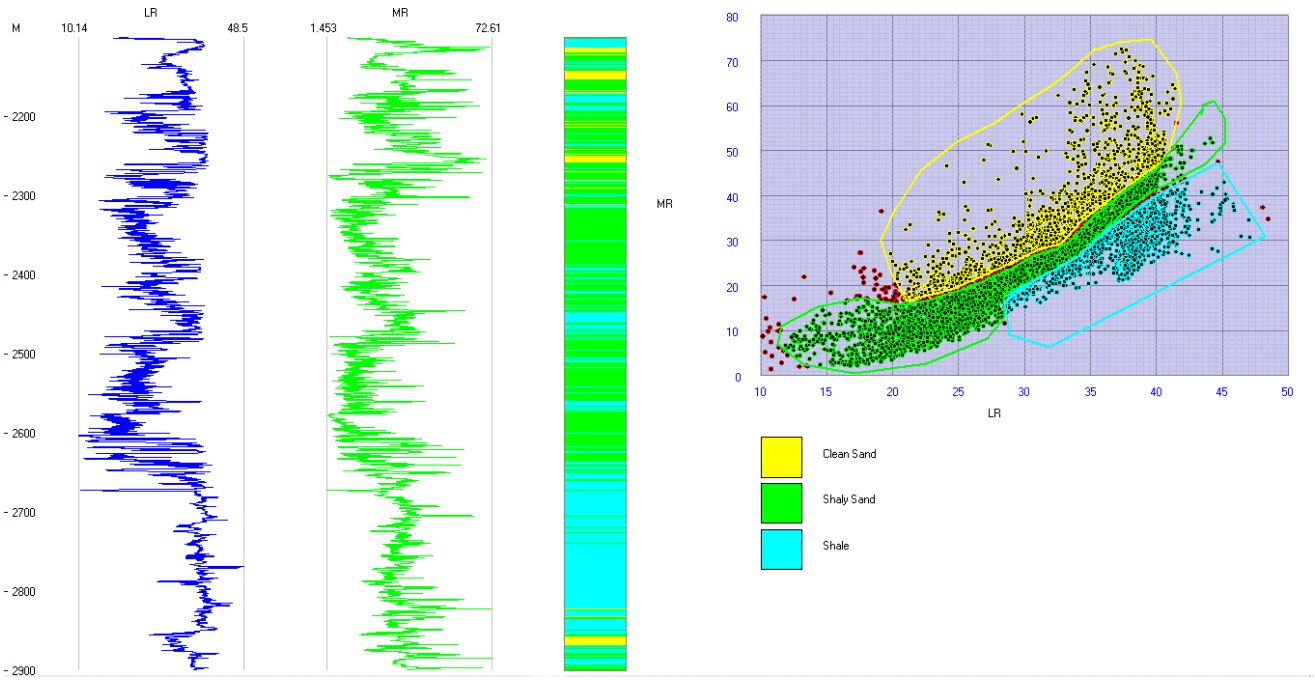

Fig 4.5: Lambda-Meu-Rho Cross-plot used for characterizing Sand, Shaly Sand and Shale.

as clay content increases for increase in the porosity, but $\lambda\rho$ may represent opposite trends. This proves $\lambda\rho$ to be a good indicator for lithology.

4.4.2 Porosity versus Density

Porosity versus density is a standard cross plot template for classification of facies as shown in Fig 4.6. The GR log is used for lithology classification. It can be observed that the facies modeling results of this log are comparable with the interpretation of previous cross plot. In this study Density-NPHI cross plot template was used. In this standard template density of fluid kept to 1.0 (CP-1c, 1997).

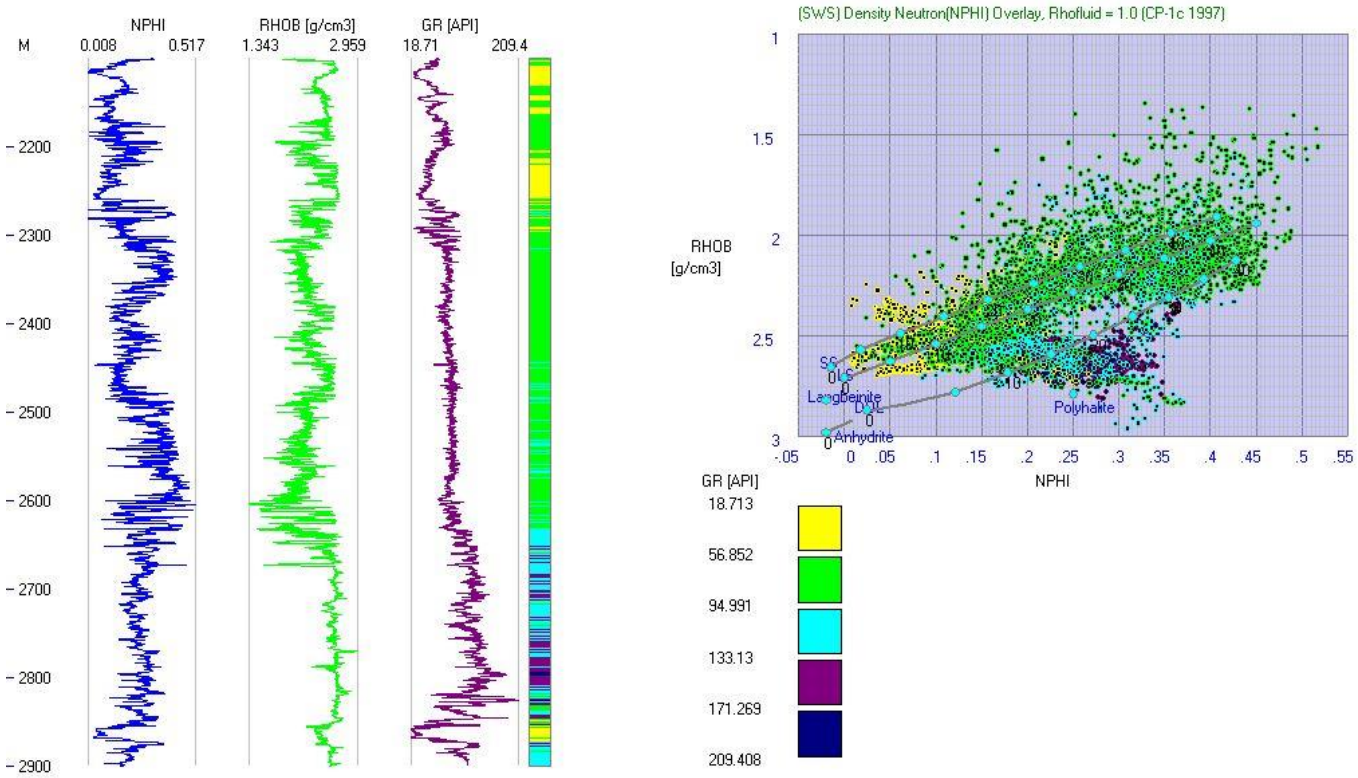

Fig 4.6: Porosity Vs Density Standard Cross-plot used for characterizing facies in the zone.

4.4.3 P-Wave Velocity (Vp) Versus Neutron Porosity (NPHI)

Fig 4.7 shows P-Wave velocity Vs Neutron Porosity cross plot. It also shows almost same interpretation as the previous cross plots. The clean sands in reservoir zone provide space for

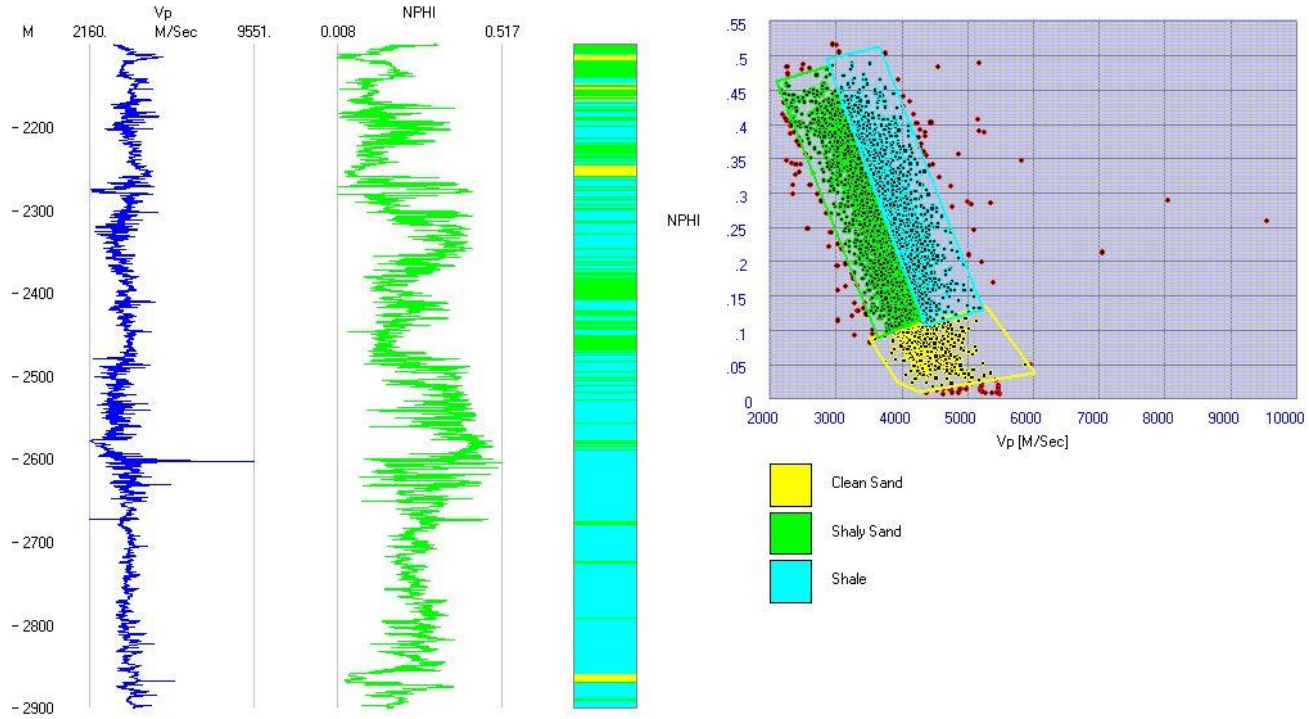

Fig 4.7: P-wave velocity vs Neutron Density Cross plot.

hydrocarbons to accumulate. Facies modeling confirms that using different cross plots we are getting the same classification of facies.

4.5 Rock Physics Empirical Relations

Another important work in Rock Physics is to establish correlations between various petrophysical, elastic and seismic parameters. The empirical relation that have a good

Log-X	Log-Y	L.Corr.Coef	Equation
Vp	RHOB	.52206	RHOB = 1.248 + 0.0003 Vp
Vp	NPHI	-.74003	NPHI = 0.851 - 0.0002 Vp
Vp	GR	-.21379	GR = 144.100 - 0.0143 Vp
Vp	SP	-.29173	SP = 67.310 - 0.0091 Vp
Vp	LLD	.2054	LLD = -15.963 + 0.0055 Vp
Vp	LLS	.2894	LLS = -15.105 + 0.0052 Vp
Vp	MSFL	.31586	MSFL = -24.098 + 0.0076 Vp
RHOB	Vp	.52206	Vp = 1624.170 + 918.5652 RHOB
RHOB	NPHI	-.52051	NPHI = 0.711 - 0.1999 RHOB
RHOB	GR	.24538	GR = 21.154 + 28.8378 RHOB
RHOB	SP	-.0569	SP = 39.971 - 3.1357 RHOB
RHOB	LLD	.08988	LLD = -5.144 + 4.2122 RHOB
RHOB	LLS	.14958	LLS = -6.562 + 4.7202 RHOB
RHOB	MSFL	.28352	MSFL = -23.697 + 11.9306 RHOB
NPHI	Vp	-.74003	Vp = 4609.167 - 3390.8074 NPHI
NPHI	RHOB	-.52051	RHOB = 2.698 - 1.3555 NPHI
NPHI	GR	.44989	GR = 57.198 + 137.6841 NPHI
NPHI	SP	.56044	SP = 13.517 + 80.4245 NPHI
NPHI	LLD	-.23197	LLD = 11.558 - 28.3098 NPHI
NPHI	LLS	-.28722	LLS = 10.236 - 23.6025 NPHI
NPHI	MSFL	-.19769	MSFL = 9.787 - 21.6639 NPHI
GR	Vp	-.21379	Vp = 4095.385 - 3.2008 GR
GR	RHOB	.24538	RHOB = 2.190 + 0.0021 GR
GR	NPHI	.44989	NPHI = 0.104 + 0.0015 GR
GR	SP	.66797	SP = 4.413 + 0.3132 GR
GR	LLD	-.16391	LLD = 10.735 - 0.0654 GR
GR	LLS	-.16033	LLS = 8.524 - 0.0431 GR
GR	MSFL	.02745	MSFL = 3.788 + 0.0098 GR
SP	Vp	-.29173	Vp = 4111.079 - 9.3148 SP
SP	RHOB	-.0569	RHOB = 2.411 - 0.0010 SP
SP	NPHI	.56044	NPHI = 0.109 + 0.0039 SP
SP	GR	.66797	GR = 43.402 + 1.4245 SP
SP	LLD	-.05406	LLD = 6.366 - 0.0460 SP
SP	LLS	-.05956	LLS = 5.770 - 0.0341 SP
SP	MSFL	-.04677	MSFL = 5.831 - 0.0357 SP
LLD	Vp	.2054	Vp = 3770.645 + 7.7119 LLD
LLD	RHOB	.08988	RHOB = 2.368 + 0.0019 LLD
LLD	NPHI	-.23197	NPHI = 0.245 - 0.0019 LLD
LLD	GR	-.16391	GR = 91.723 - 0.4110 LLD
LLD	SP	-.05406	SP = 32.825 - 0.0636 LLD
LLD	LLS	.96298	LLS = 1.503 + 0.6484 LLD
LLD	MSFL	.14066	MSFL = 4.055 + 0.1263 LLD
LLS	Vp	.2894	Vp = 3732.995 + 16.1363 LLS
LLS	RHOB	.14958	RHOB = 2.356 + 0.0047 LLS
LLS	NPHI	-.28722	NPHI = 0.253 - 0.0035 LLS
LLS	GR	-.16033	GR = 92.504 - 0.5971 LLS
LLS	SP	-.05956	SP = 33.000 - 0.1040 LLS
LLS	LLD	.96298	LLD = -1.795 + 1.4301 LLS
LLS	MSFL	.19742	MSFL = 3.443 + 0.2633 LLS
MSFL	Vp	.31586	Vp = 3746.533 + 13.2067 MSFL
MSFL	RHOB	.28352	RHOB = 2.346 + 0.0067 MSFL
MSFL	NPHI	-.19769	NPHI = 0.245 - 0.0018 MSFL
MSFL	GR	.02745	GR = 89.363 + 0.0767 MSFL
MSFL	SP	-.04677	SP = 32.801 - 0.0612 MSFL
MSFL	LLD	.14066	LLD = 4.139 + 0.1566 MSFL
MSFL	LLS	.19742	LLS = 3.970 + 0.1480 MSFL

Fig 4.8: Results of Correlation analysis with their empirical relation

correlation coefficient are very useful in reservoir characterization. They can be used to computeother parameters for the datasets in the area.

Correlation analysis has been performed for all logs of well Chak 5 Dim South 01 to view the relationship between different parameters. The correlation results along with their empirical relations are given in Fig 4.8. It can be seen that most of the parameters don't have good correlation while Vp and NPHI have high correlation. GR and Sp has Average correlation. Therefore, in next steps regression analysis has been performed between these logs.

4.5.1 GR vs SP

A regression trend has been fitted between GR and SP using 1st order least squares regression using data of well Chak 5 Dim South 01 as shown in Fig 4.9. The following empirical relation

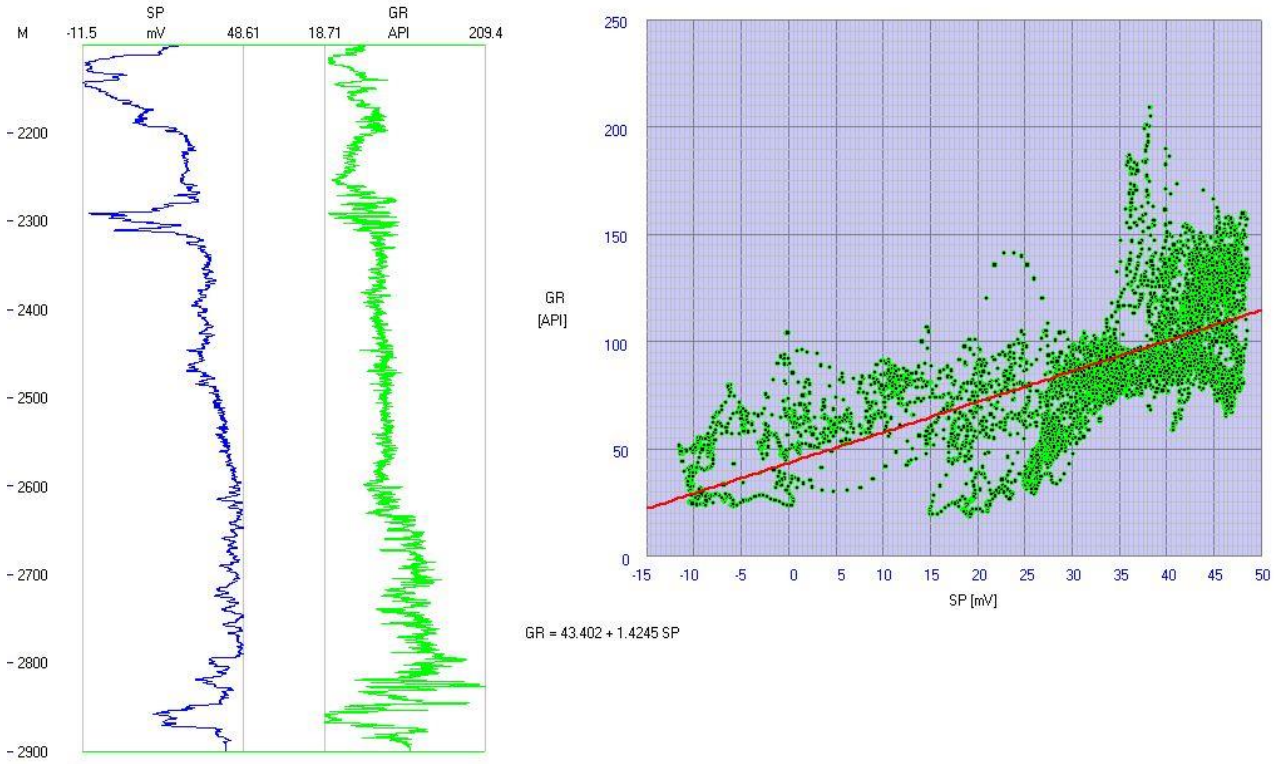

Fig 4.9: Best fit regression trend between GR and SP log

has been established with a correlation coefficient of 0.712. Sp log is used to identify lithology in the absence of GR log. This good correlation coefficient indicates that in this data SP log can also give good lithology indications.

GR= 43.402+1.4245 SP

4.5.2 Vp vs NPHI

A regression trend has been fitted between P-Wave Velocity and Porosity using 1st order least squares regression using data of well Chak 5 Dim South 01 as shown in Fig 4.10. The following empirical relation has been established with a correlation coefficient of 0.794. It can be used to compute porosity volumes for any seismic inversion-based datasets in the area.

NPHI = 0.851- 0.0002 Vp

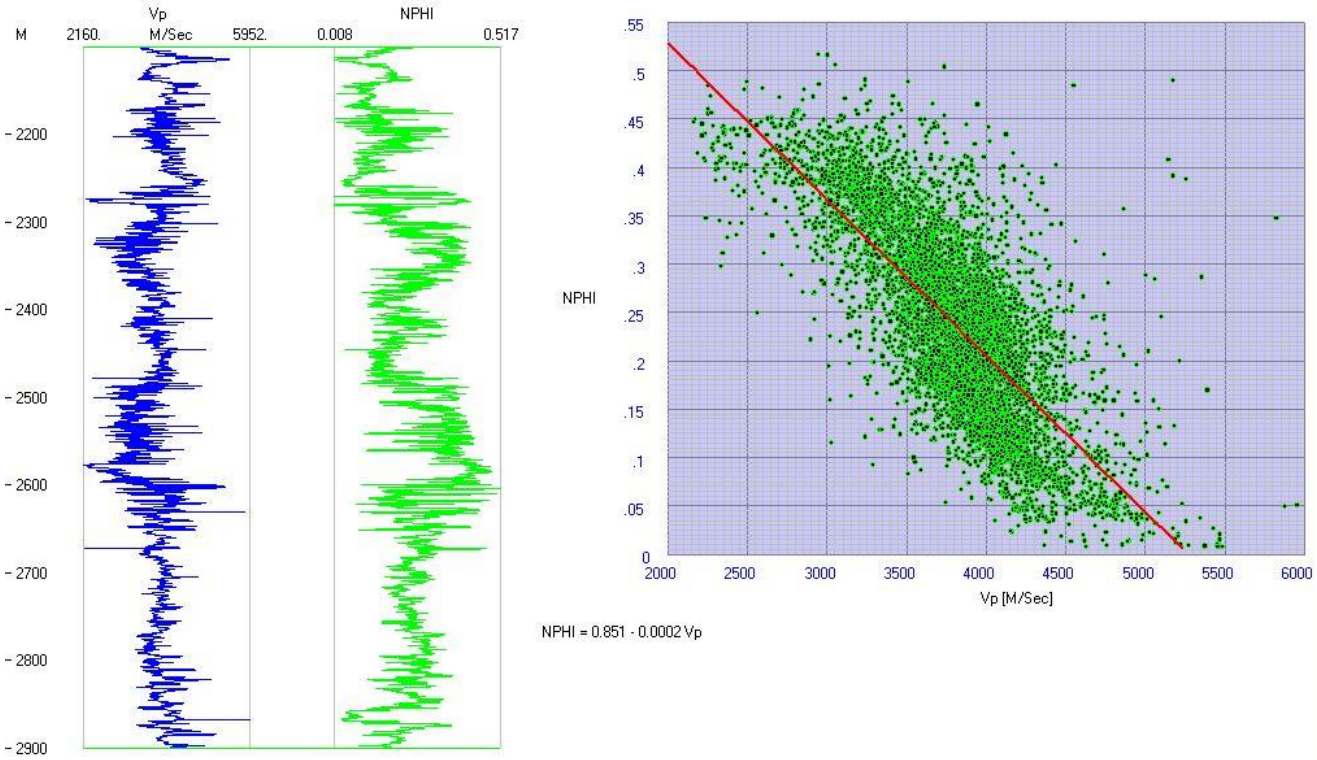

Fig 4.10: Best fit regression trend between VP and NPHI log

Chapter 5: Seismic Velocities, 2D Synthetic Modeling & Full Wave Inversion.

5.1 Introduction

The seismic method is governed by velocities, which in turn depend on density and elastic moduli of rocks. Velocity data contains enormous amount of rock information, which can be extracted by handling the velocity data with extreme care and understanding. Many explorationists consider velocity as the most underutilized and over-abused of all the geophysical parameters in petroleum exploration. Yet, velocity is the bridge between time and depth, between milliseconds and feet, between timing lines and drill stem.

Velocity is a complex parameter due to its various types and sources. It is measured directly using borehole techniques such as check shots, vertical seismic profiling (VSP) (Yilmaz, 2001) and sonic logs. On the other hand it is derived indirectly from seismic data. The velocities determined from any source are ultimately converted into interval velocities which in turn are correlated with particular lithologies. A velocity model is derived when interval velocities are properly correlated with their corresponding lithologies. This model can then be used for different applications.

Seismic modeling is reverse process of seismic interpretation. In seismic interpretation we mark geological horizons whereas in seismic modeling we generate the synthetic seismic section. As this modeling is completely based on the structural data the derived synthetic section completely matches the structures. This type of modeling is commonly used to get seismic response of stratigraphic models as well as confirmation of seismic interpretation.

The velocity data is usually available in the form of functions (velocity as a function of time or depth) consisting of velocity time (VT) pairs. X-Works reads velocity data in IGS format. X-Works provide Spatio-Temporal interpolation of Velocity data at given intervals of CDP and Time respectively. This Velocity interpolation tool also smooths the velocity data for desired smoothing operator.

2D synthetic seismic model generation is done by using X-Works. In this research work Velocity and 2D synthetic model was built for interpreted seismic line 20017-SNJ-09.

5.2 Workflow of Velocity Model building using Seismic velocities

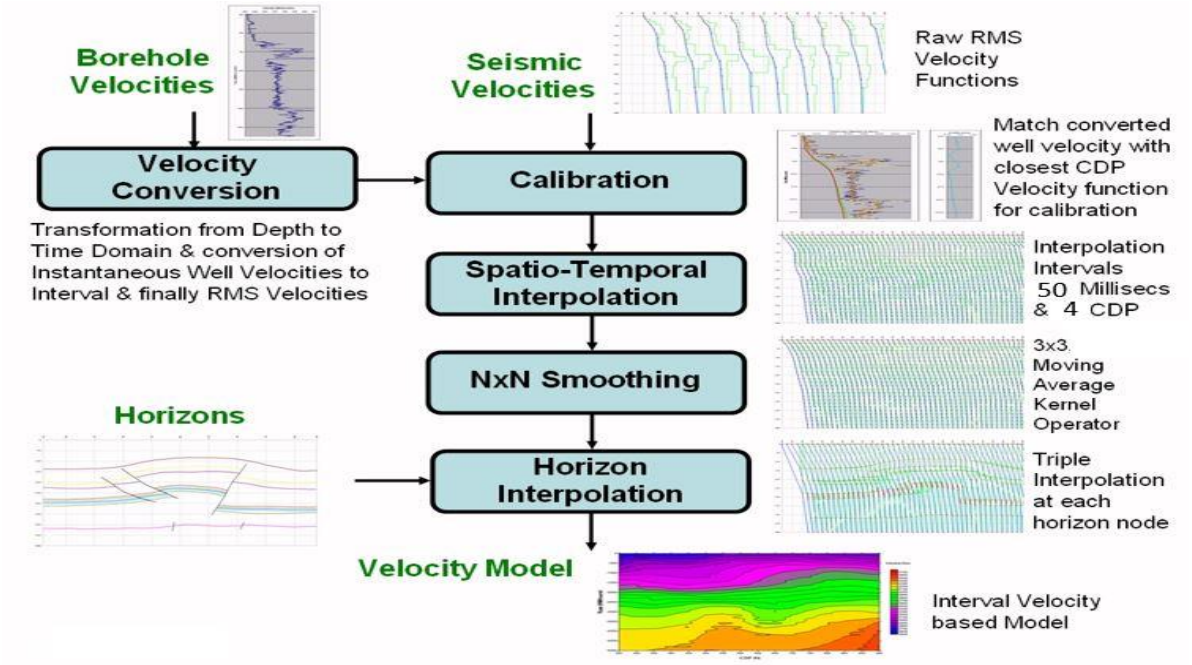

Fig 5.1: Complete Workflow of Velocity Model building using Seismic velocities (Khan & Akhter, 2011)

5.3 Velocity Conversion

The Root Mean Square Velocity functions are given on seismic section. Velocity analysis is carried out in X-Works in which RMS velocities are converted into interval and average velocities. Dix equation is used to convert RMS velocity into interval velocity. Dix equation (1955).

$$V_{int,n}^2 = \frac{V_{rms,n}^2 T_n - V^2{}_{rms,n-1} T_{n-1}}{T_n - T_{n-1}}$$

Where

V_{int} = Interval velocity (m/s)

V_{rms} = Root mean square velocity (m/s)

T = Zero Offset travel time (s)

X-Works uses a velocity processing engine which automatically converts the input RMS velocities into interval velocity and average velocity. Average velocities are then used for time

to depth conversion. Interval velocities are converted into average velocities using following formula

$$V_{avg,n} = \frac{V_{int,n}(T_n - T_{n-1}) + V_{avg,n-1}\,T_{n-1}}{T_n}$$

Where

$V_{avg,n}$= Average Velocity.

V_{int}= Interval Velocity

T = Travel Time (Zero Offset)

The Interpreted geologic section of seismic line 20017-SNJ-09 containing faults and horizon was used to construct the velocity model. The horizons are used to compute the interval velocity layer by layer as shown in Fig 5.2. The velocity data functions along with the interpreted horizons are shown without seismic data in Fig 5.3

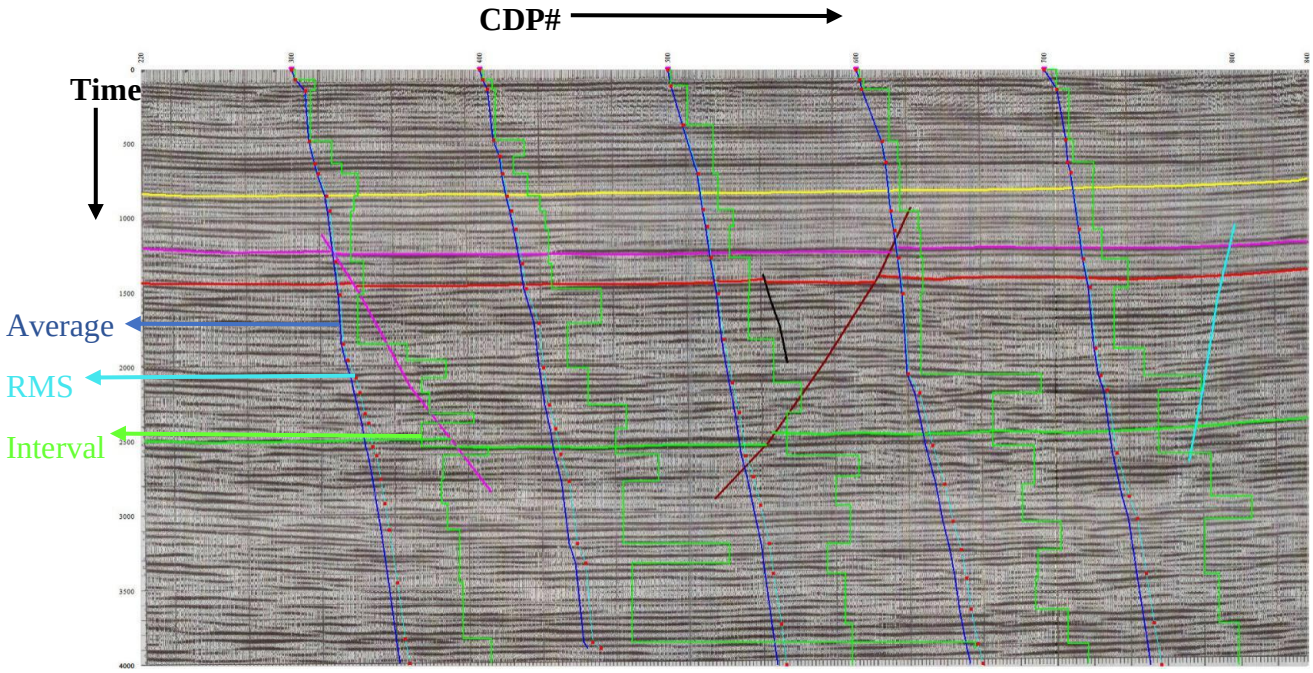

Fig 5.2: Interpreted seismic section (20017-SNJ-09) with RMS, Interval and Average Velocities.

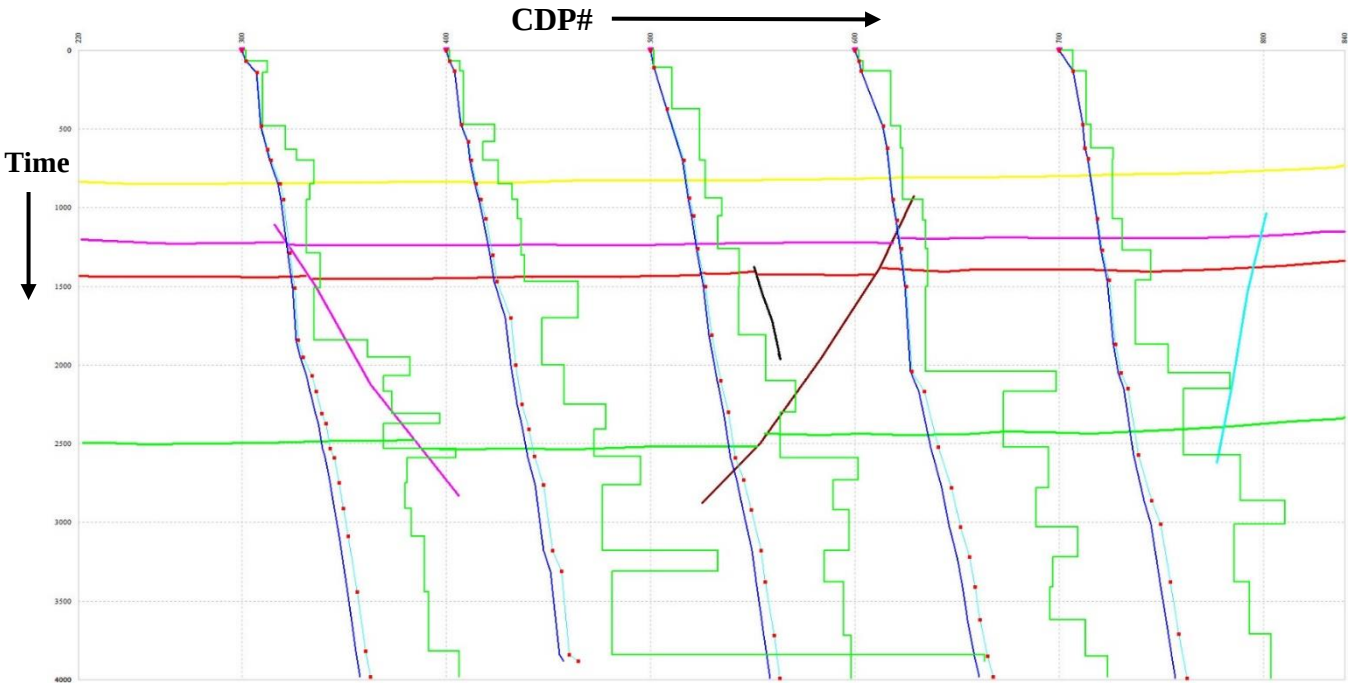

Fig 5.3: Interpreted Geological section (20017-SNJ-09) with RMS, Interval and Average Velocities.

5.4 Spatio-Temporal Interpolation

The input velocity functions are basically velocity-time pairs (VT-Pairs) without fixed time intervals. In this technique, first temporal (vertical) interpolation of 100 milliseconds is applied to get velocity functions with VT-Pairs after regular time intervals. After interpolation 3x3 point moving average operator is applied along each function to get vertical and horizontal smoothing of velocities. Next spatial interpolation at every 2 CDP is applied to generate velocity functions at the specified CDP interval. The 3x3 point moving average operator across the velocity functions or along the time slice provide smoothing of velocities. This generates the spatio-temporal interpolated velocity model. Fig 5.4, 5.5 and 5.6 shows Spatio-Temporal Interpolated RMS Velocities, Spatio-Temporal Interpolated Interval Velocities and Spatio-Temporal Interpolated Average Velocities respectively.

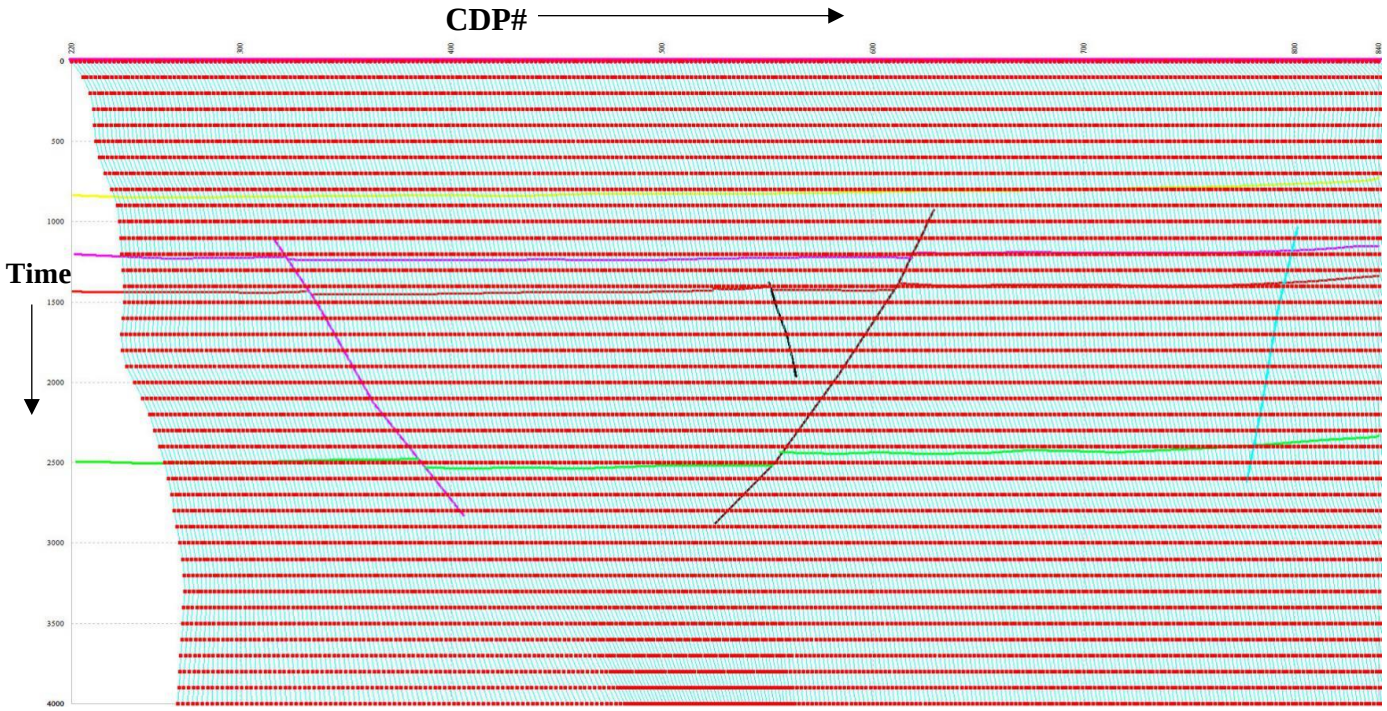

Fig 5.4: Spatio-Temporal Interpolated RMS Velocities for Line 20017-SNJ-09.

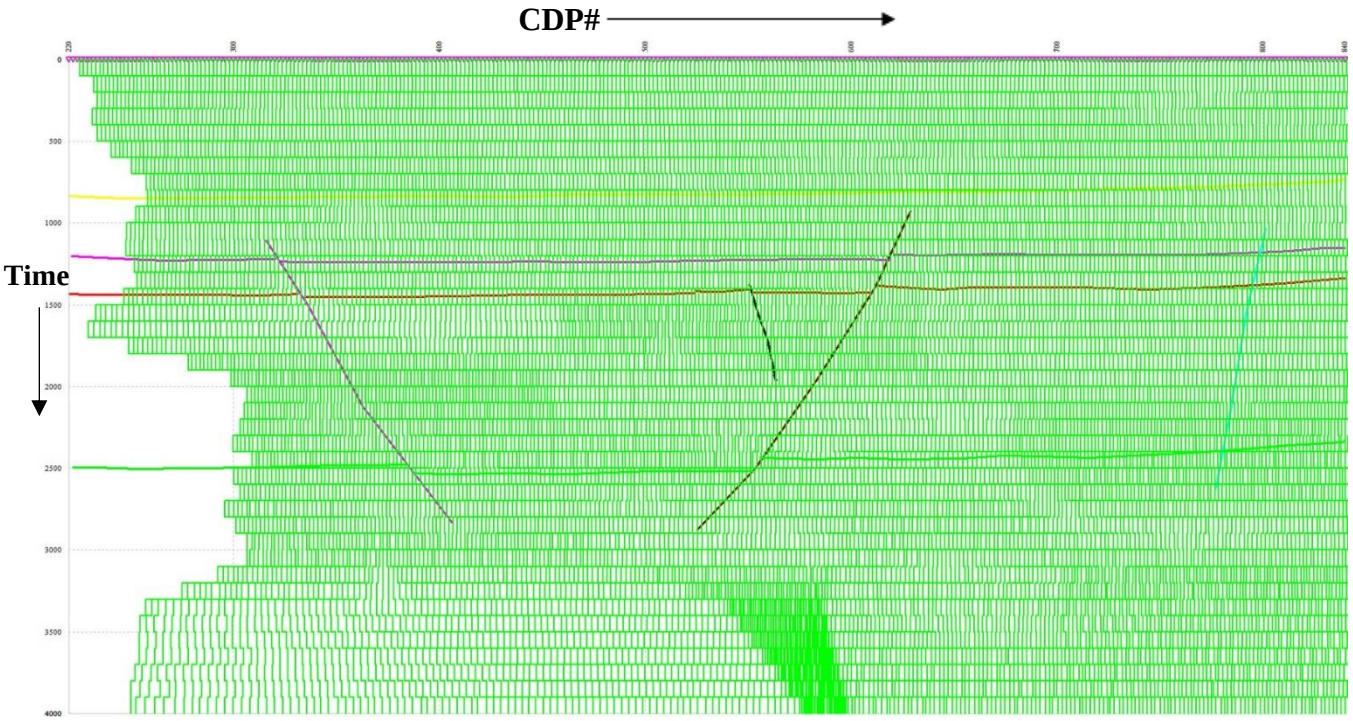

Fig 5.5: Spatio-Temporal Interpolated Interval Velocities for Line 20017-SNJ-09.

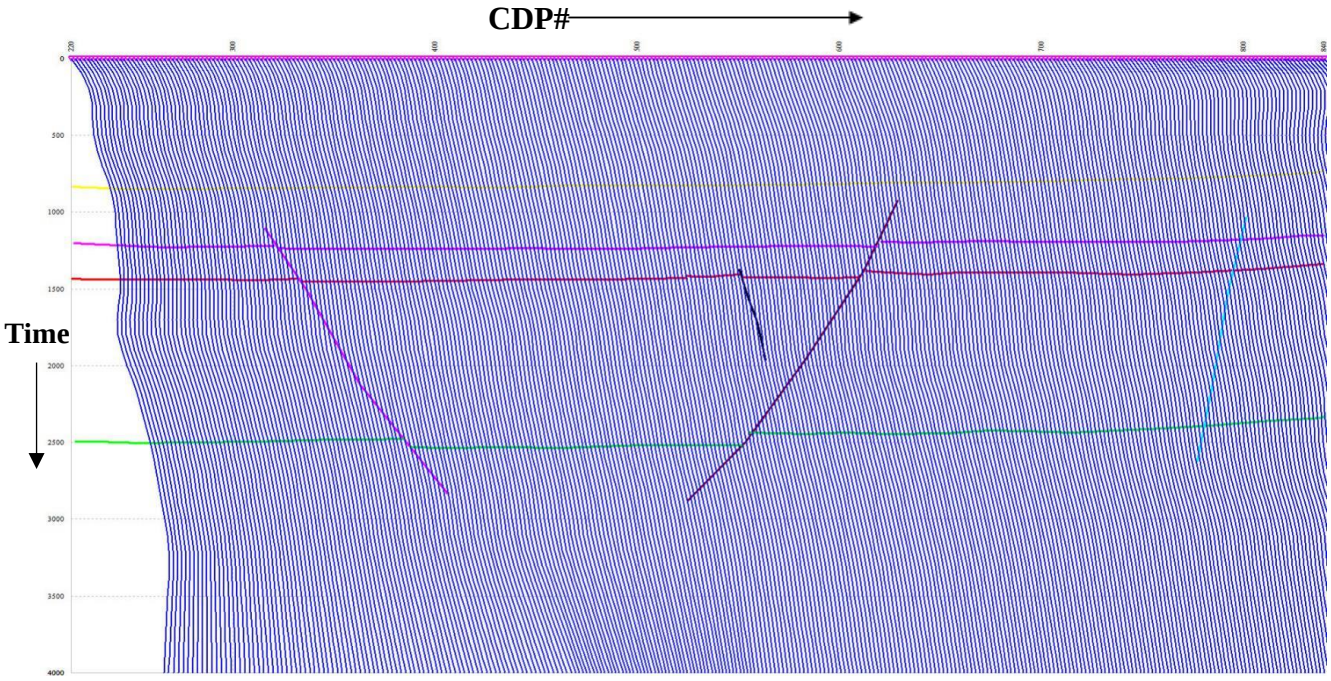

Fig 5.6: Spatio-Temporal Interpolated Average Velocities for Line 20017-SNJ-09.

5.5 Horizon Based Velocity Interpolation

This is a more complex interpolation technique which requires input of interpreted horizons, in addition to the velocity data. The velocity is interpolated along these horizons, instead of interpolation along the time slice. It requires computation of nodes for each horizon at the specified CDP interval. VT-Pairs are then interpolated at these nodes to generate velocity functions. Horizon velocity analysis provides velocities at ever CDP location along the profile (Yilmaz,2001). The velocity model generated by horizon interpolation technique closely matches the subsurface structures as shown in Fig 5.7 on the right side horizon nodes are represented by red dots.

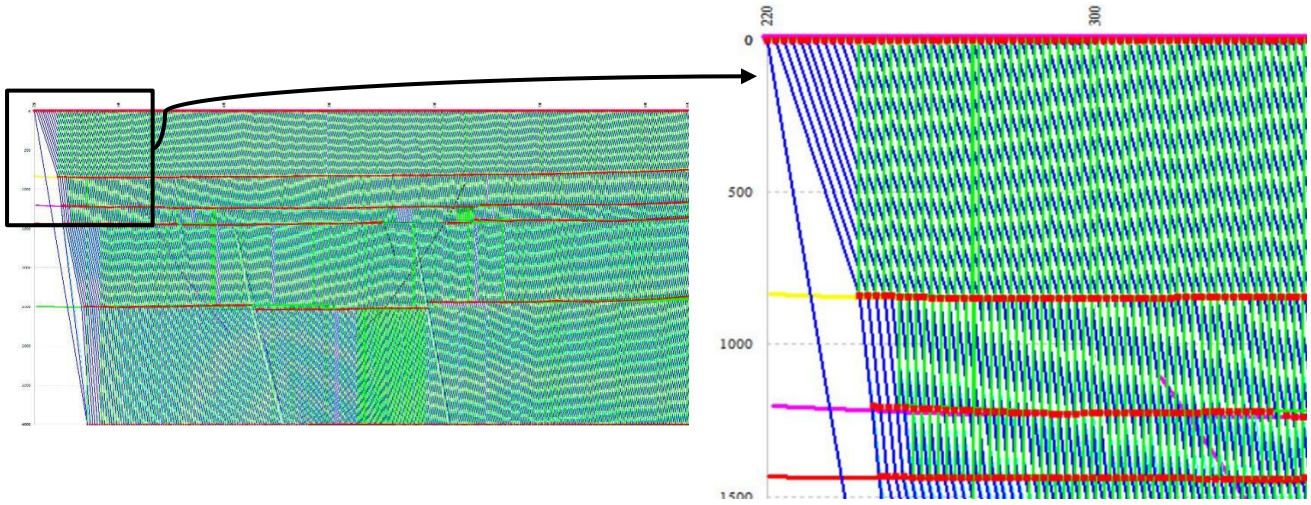

Fig 5.7: Horizon Based Interpolated Velocities for Line 20017-SNJ-09 at left. Close view of the section is at right side

5.6 2-D Seismic Modelling

A 2D seismic model was generated for seismic line 20017-SNJ-09. It is generated from the horizon interpolated velocity model discussed in the previous section. A Ricker Wavelet of 35 Hz is convolved with horizon based interpolated velocity model. Signa/Noise component was also added to final synthetic seismic section. The interface for generating a Ricker wavelet along with its amplitude and phase spectrum is shown in Fig 5.8. Final 2-D seismic model is shown in Fig 5.9.

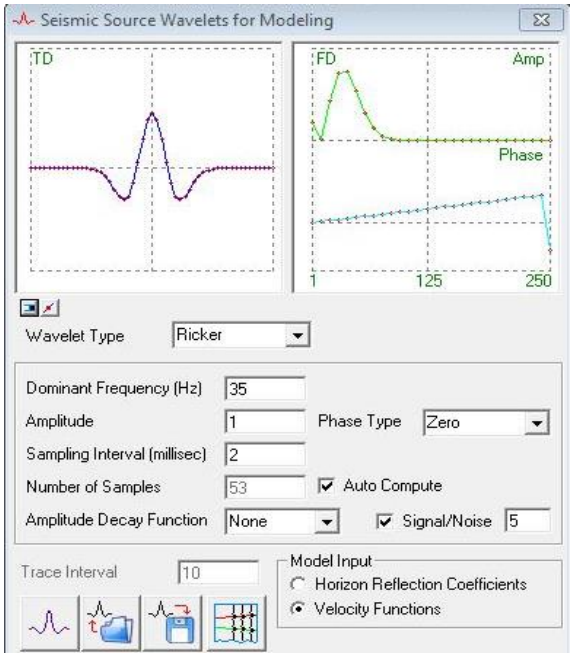

Fig 5.8: Seismic Source Wavelet for modeling

This 2D seismic model is a Zero Offset 2D synthetic seismic section. This section is similar to a migrated seismic section. It shows the interpreted layers. It can be seen that this seismic model clearly shows sub-surface image with horizons and Faults so it confirms the interpretation.The interpreted geological cross-section has been modelled using X-Works, a geological cross-sections software application, (Khan et al., 2006). This 2D synthetic model can be refined by minimizing the difference between observed and modeled synthetic data by using Full Wave Inversion.

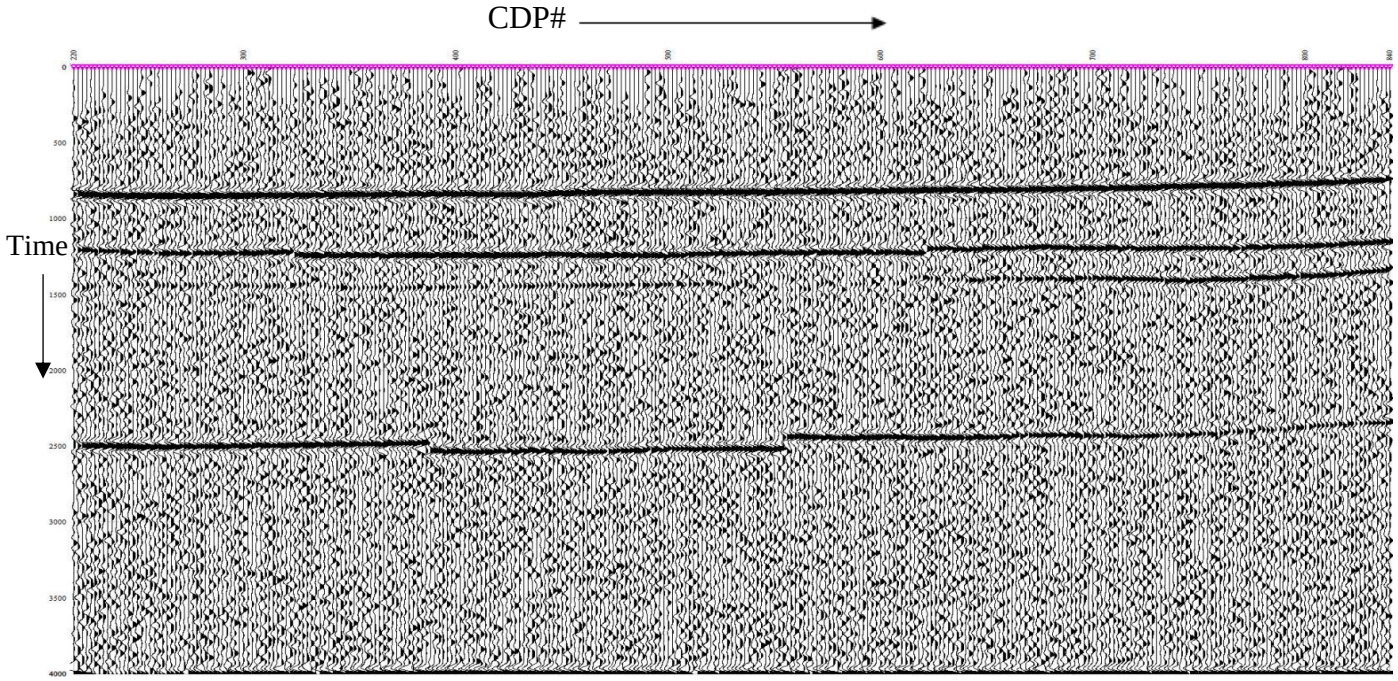

Fig 5.9: 2D seismic model for Line 20017-SNJ-09

5.7 Full Wave Inversion

Full-waveform inversion (FWI), proposed by Lailly and Tarantola in the 1980s, is considered to be the most promising data-driven tool for automatically building velocity models. Many successful examples have been reported using FWI to update shallow sediments, gas pockets, and mud volcanoes.

FWI derives high-resolution velocity models by minimizing the difference between observed and modeled synthetic data. It goes beyond refraction and reflection tomography techniques, which use only the travel time kinematics of the seismic data, by using additional information provided by the amplitude and phase of the seismic waveform. (Lailly, *1983; Tarantola, 1984; Pratt, 1999; Sirgue and Pratt, 2004).

The highly detailed models provided by FWI can be used to resolve complex geological features, as well as aid in identifying potential geohazards. These high-definition models can also be input directly to pore pressure prediction flows, time-lapse monitoring, and reservoir characterization analysis. Subsurface images produced using these highly accurate models provide interpreters with a much higher degree of confidence with respect to reservoir delineation and subsequent well planning.

5.7.1 Methodology for FWI

FWI uses both the amplitude as well as the phase information from all the waves produced. In this method it is not necessary to determine the single wave type such as P,S or surface waves. Instead, on the basis of three-dimensional equations of motion the complete seismogram is analyzed and the entire wave field in the subsurface is calculated.

The equation of motion relates temporal and spatial oscillations with each other.

$$\frac{\partial u}{\partial t^2} + \frac{\partial}{\partial x}$$

Here spatial and temporal derivative must be calculated at many locations in the subsurface and at many points in time which need high performance computer processing.

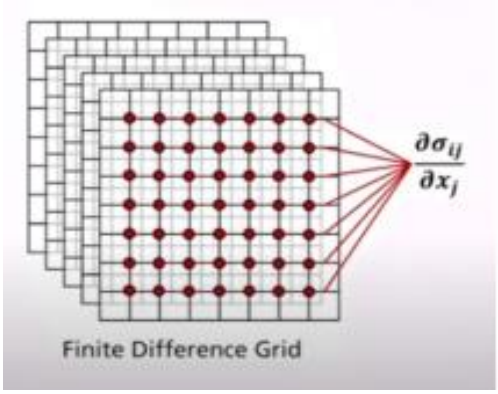

Fig 5.10: Finite Difference Grid

One way to implement this task is to use finite difference method. In order to calculate the wave field in the subsurface,

the subsurface is divided into an equidistant grid. The Finite Difference method approximates the derivatives of the equation of motion using differential quotients at the equidistant grid points as shown in fig 5.10 Both the spatial and temporal derivatives are then calculated in equidistant time steps.

5.7.2 Framework of Calculation

The objective of inversion in geophysics is always to deduce the material properties of the subsurface from the observed measurement data. Several different methods can be used to seek out a subsurface model that can satisfactorily explain the measured data. One approach is to try out as many models as possible and to see which one is the best. This approach needs more computational power and time. Another approach is to systematically refine an existing starting model of the subsurface. This will ensure at the end that a realistic subsurface model can be calculated. Fig 5.11 shows the workflow of FWI.

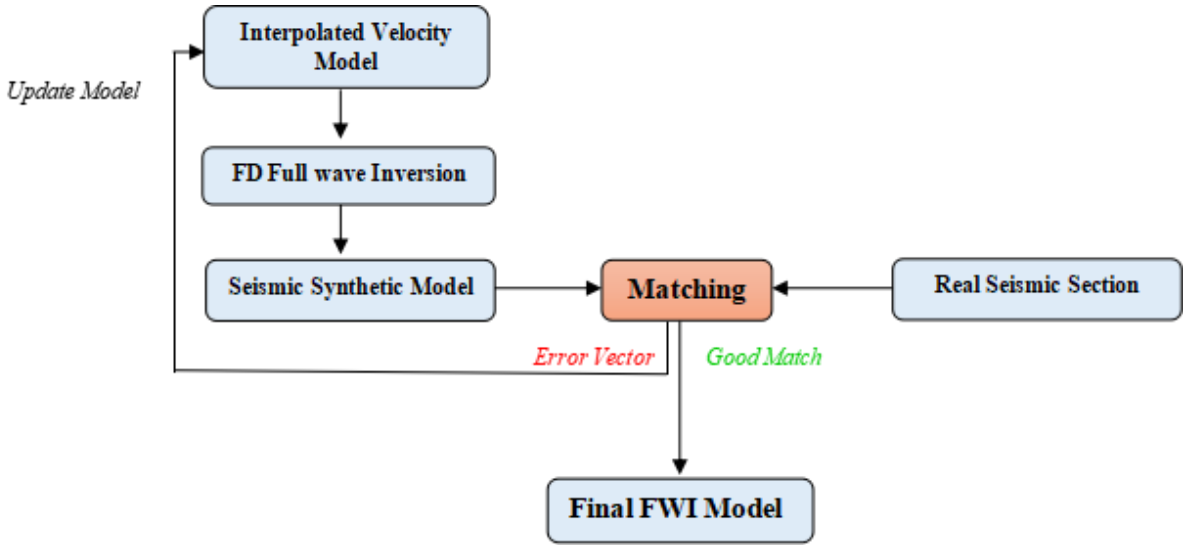

Fig 5.11: Workflow for Full Wave inversion

Zero Offset 2D synthetic model was generated for seismic line 20017-SNJ-09. It was generated from the horizon interpolated velocity model. This section is similar to a migrated seismic section. This section can be further refined by applying Full wave Inversion to the interpolated velocity model. In this process Seismic synthetic model generated using Interpolated velocity model will be refined by applying finite difference Full Wave Inversion algorithm. Software calculates Error vector by matching it with real seismic section. In order to minimize the error, interpolated velocity model then updated and again matched. This process is repeated iteratively until the error is minimized. Horizon based interpolated model and inverted velocity model for line 20017-SNJ-09 are shown in Fig 5.12, and 5.13 respectively.

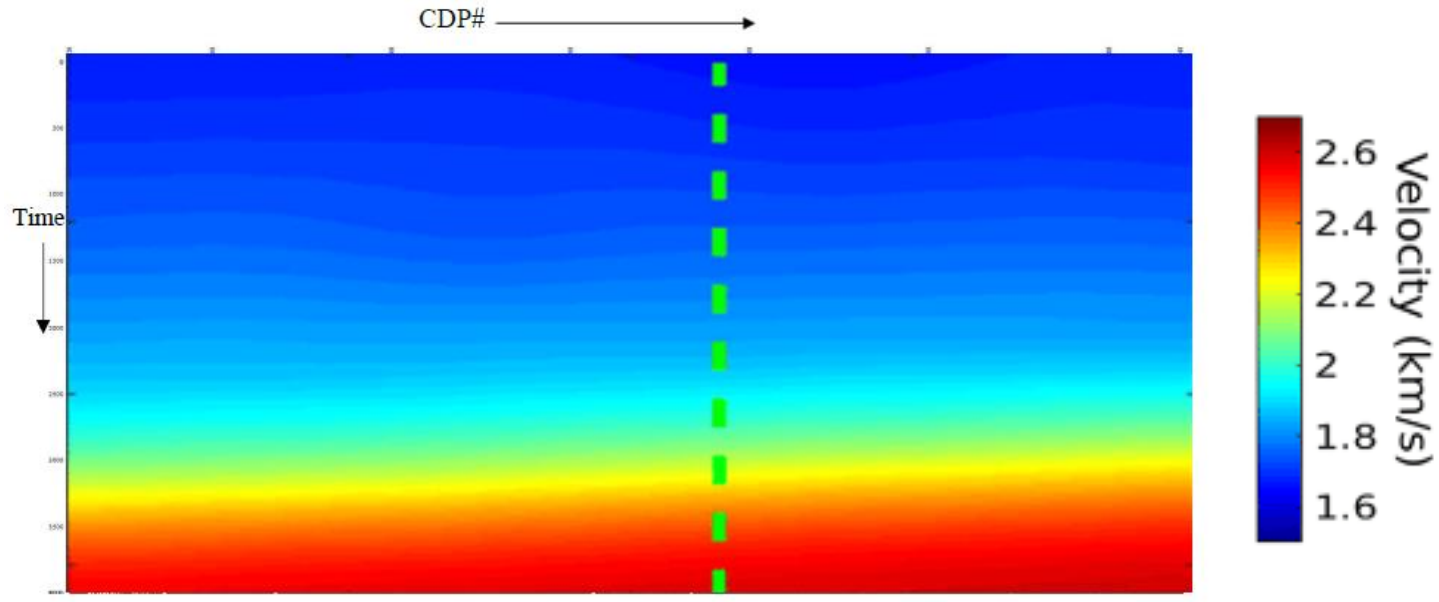

Fig 5.12: Horizon based Interpolated velocity model for Full Wave inversion of Line 20017-SNJ-09

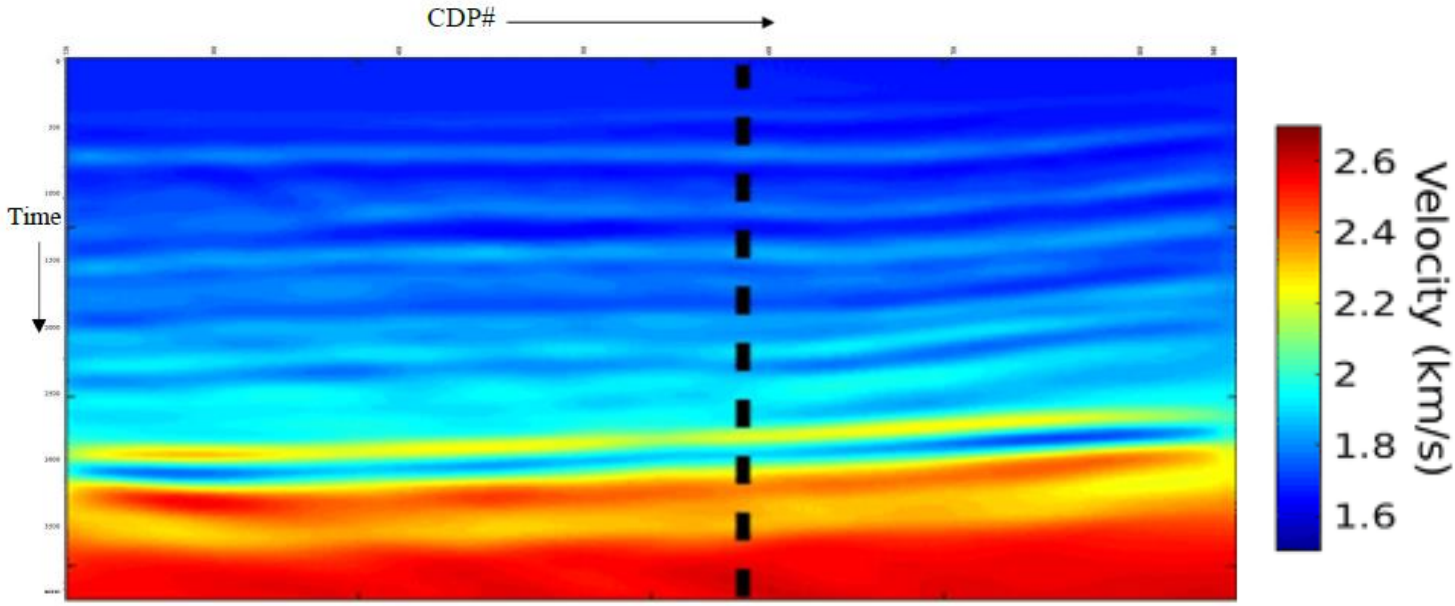

Fig 5.13: Inverted Velocity model after applying Full Wave inversion at Line 20017-SNJ-09

Chapter 6: Seismic Inversion

6.1 Introduction

Reservoir characterization plays an essential role in the prediction of the reservoir properties as well into the economic potential of the field. Perception of reservoir characterization requires integrated analysis and understanding of the available data, such as seismic data and well log data (Torres, C. Sen, M., 2004).

In seismic reservoir characterization studies, the first step towards a successful hydrocarbon discovery is the mastering of a good subsurface image of seismic data. The reflected seismic wave amplitudes are function of acoustic/elastic impedances, which project a contrast (reflection coefficient) between the lithology above and below a reflecting boundary (Yilmaz, 2001). Seismic data is produced by forward modelling. Seismic data is the output of a convolution operation between earth reflectivity and source wavelet. The convolution operation produces a band-limited trace, the bandwidth of which is determined by the seismic wavelet. Due to the band-limited nature of seismic data, lack of low frequencies prevent the transformed impedance trace from gaining the basic impedance or velocity structure which is crucial to making a geological interpretation. (Nawaz, 2003). An attempt to recover this resolution is usually made by obtaining the reflectivity through a deconvolution operation which is an inverse problem. (Robinson, E.A., Silvia, M.T., 1978).

Seismic inversion is the process of extracting information about elastic properties from seismic data based on travel-time, amplitude, and phase information contained within a seismogram (Sheriff, Society of Exploration Geophysicists 2002). It is an optimal way to get a better subsurface image. Seismic inversion is the result of Inverse modelling. Commercially different seismic inversion methods are used to map the detailed reservoir properties (Russell, B., Hampson, 1991). In this research work model based seismic post stack inversion analysis and AVA synthetic gather generation is carried out to identify the hydrocarbon bearing potential zones. This research work also concludes the different types inversion methods are being used in the industry.

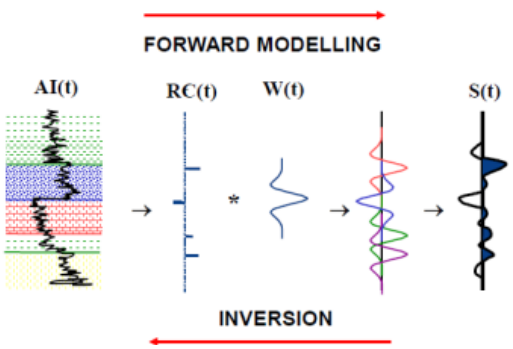

Fig 6.1: Forward and Inverse modelling

6.2 Classification of Seismic Inversion

Seismic inversion has two broad classifications in industry and academia:

6.2.1 Pre-stack inversion

The interpretation of seismic amplitude variations with offset, i.e. AVO analysis, can be performed on pre-stack data - in which angular information is preserved - to predict lithological and fluid properties (Margrave et al., 1998; Leite and Vidal, 2011).

The utilization of inversion before the stacking provide effective mechanism for the extraction of multiple attributes form impedance. Changes within the impedance of seismic due to P and S waves along with integration of density based on seismic data and well data.

The key part in seismic forward modelling is the understanding of various seismic wave energy partitioning equations. The earliest among such works is the Knott–Zoeppritz equations, that describe the various reflection and transmission coefficients, for plane waves as a function of angle of incidence, at the interface between two homogeneous isotropic elastic half spaces. These equations are useful in forward modelling to determine the seismic response that would be recorded for the given subsurface configuration which is defined in terms of compressional and shear velocities along with densities.These equations form the basis of amplitude versus offset analysis, a useful technique in the detection of petroleum reservoirs. (Khan, K.A., 2017).

Zoeppritz equations express the partition of energy when a plane wave hits an interface with an acoustic-impedance contrast. For a non-zero angle of incidence four waves are generated: reflected P-wave and S-wave and transmitted P-wave and S-wave as shown in Fig 6.2

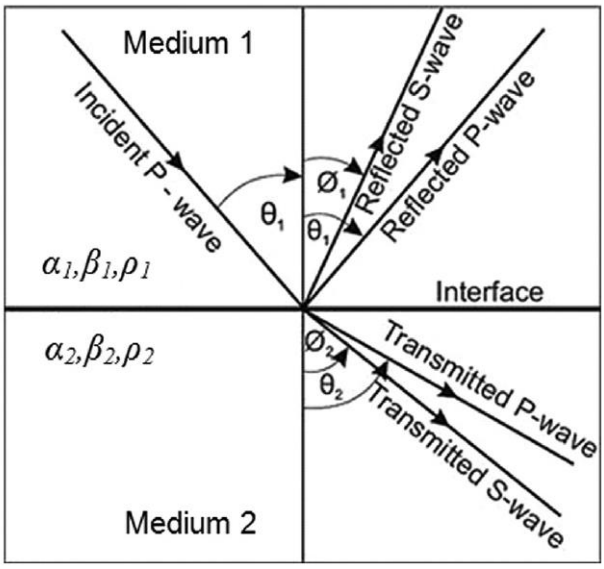

α_1, α_2	*S-Wave velocities in medium 1 and 2*
β_1, β_2	*P-Wave velocities in medium 1 and 2*
ρ_1, ρ_2	*SDensities in Medium 1 and 2*

Fig 6.2: Reflection and transmission angles involved in energy partitioning at the interface between two mediums

The Zoeppritz equations (Sheriff and Geldart, 1995) give the amplitudes (reflection coefficients) R_{PP}, R_{SS}, T_{PP}, and T_{SS} of the reflected P- and S-waves and the transmitted P- and S-waves respectively.

$$\begin{bmatrix} R_{PP} \\ R_{PS} \\ T_{PP} \\ T_{PS} \end{bmatrix} = \begin{bmatrix} -\sin\theta_1 & -\cos\phi_1 & \sin\theta_2 & \cos\phi_2 \\ \cos\theta_1 & -\sin\phi_1 & \cos\theta_2 & -\sin\phi_2 \\ \sin 2\theta_1 & \frac{\alpha_1}{\beta_1}\cos 2\phi_1 & \frac{\rho_2\beta_2^2\alpha_1}{\rho_1\beta_1^2\alpha_2}\cos 2\phi_1 & \frac{\rho_2\beta_2\alpha_1}{\rho_1\beta_1^2}\cos 2\phi_2 \\ -\cos 2\phi_1 & \frac{\beta_1}{\alpha_1}\sin 2\phi_1 & \frac{\rho_2\alpha_2}{\rho_1\alpha_1}\cos 2\phi_2 & -\frac{\rho_2\beta_2}{\rho_1\alpha_1}\sin 2\phi_2 \end{bmatrix}^{-1} \begin{bmatrix} \sin\theta_1 \\ \cos\theta_1 \\ \sin 2\theta_1 \\ \cos 2\phi_1 \end{bmatrix}$$

On the other hand, considering the inverse problem, the subsurface configuration can also be determined from the observed data. Over the years several approximations for Zoeppritz equations have been developed by various authors, which provide more intuitive insights into the energy partitioning problem by involving various elastic parameters. A graphical representation of angle of incidence ranging from 0 to 90 and reflection coefficient is presented in Fig 6.3 to give a better understanding of Zoeppritz equations and some of their most used approximations.

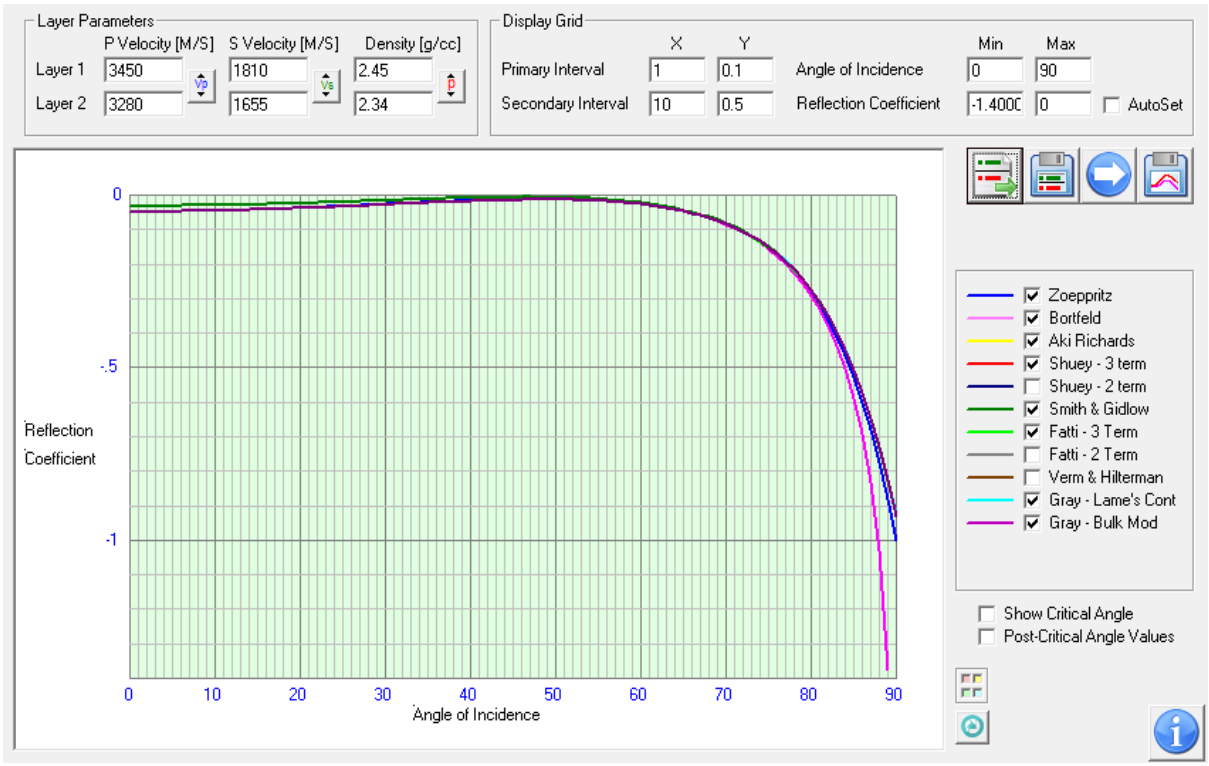

Fig 6.3: Reflection coefficient vs angle of incidence trend plotted by using Zoeppritz Calculator (Khan, K.A.).

6.3 AVA Synthetic Gather

An amplitude vs Angle synthetic gather was generated by using well data of Chak 5 Dim South 01. The three most basic parameters for AVA analysis are compressional velocity (Vp), Shear velocity (Vs) and Density (RHOB). AVA synthetic gather was generated by using these logs. The AVA effect at higher angles can be clearly observed in Fig 6.4 which is indicating Class 2 gas sands in the reservoir.

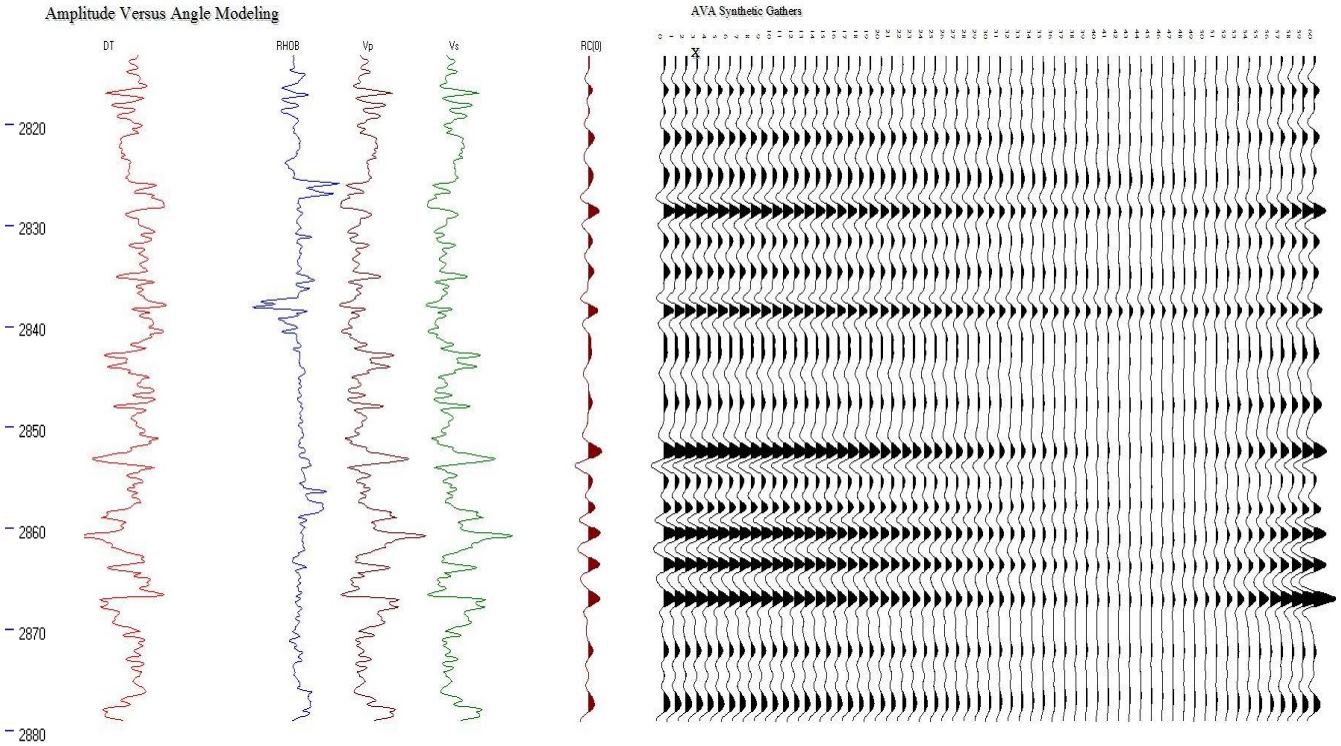

Fig 6.4: AVA Synthetic Gather for Well Chak 5 Dim South 01 showing Gas effect

Behavior of Reflection coefficient and angle of incidence is graphically represented in Fig 6.5. At lower angles reflection coefficient has higher negative values and started decreasing as the angle of incidence increases. The curve shows a different effect at angles between 40-49 degree and then started increasing from 50 degree.

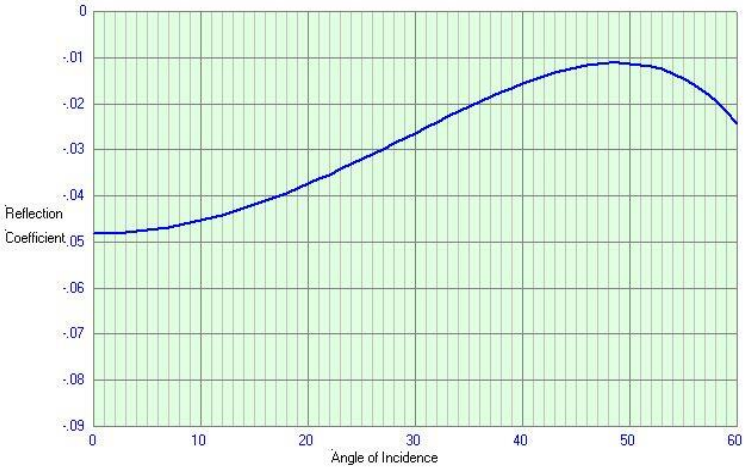

Fig 6.5: Behavior of Reflection co-efficient and Angle of Incidence

6.2.2 Post-stack inversion

The Post stack inversion methods use stacked (zero-offset) seismic data to produce images of the AI in depth or time. AI is one of the rock-physics parameters, which is influenced by the type of lithology, porosity, fluid content, depth, pressure, and temperature.

Conventional AI inversion methods include the direct inversion, e.g. trace integration (Oldenburg, Scheuer and Levy1983) and recursive inversion(Lavergne 1975; Lindseth1979),iterative inversion, e.g. model-based inversion(Cooke and Schneider1983), sparse spike inversion(Madiba and McMechan2003).The trace integration is easily implemented, but it cannot produce the absolute value of the AI. The recursive inversion can reserve well the characteristics of seismic reflection and clearly reflect lithology changes in space but is restricted by seismic bandwidth and interfered by noises (Sarwar1991), leading to a vertically low–resolution result. The result usually reflects relative changes of AI, and thus a given low-frequency component must be merged with it to obtain the associated absolute values (Cooke and Schneider1983). In addition, the inevitable accumulated errors in the conventional recursive method limit its retrieval accuracy. The model-based inversion suffers from the non-uniqueness problem more prominently, and its result is heavily dependent on the initial model. The sparse spike inversion is not sensitive to the smaller reflection coefficients, which may cause the possible loss of local details (Russell and Hampson1991). The nonlinear inversion and geostatistical inversion (de Almeida2010) are more inefficient because of the massive amount of computation, and difficult to be applied in the early stage of exploration when wells and geological information are insufficient.

In this research work AI is computed by using model-based inversion technique. Seismic line SNJ-20017-09 well CHAK 5 DIM SOUTH-01 was used to complete the process.

6.3 Methodology for Post-stack model-based inversion

In seismic exploration convolutional model provides basis for seismic inversion as reflectivity series is generated by convolution of the inverse of wavelet with seismic trace.

The most basic and commonly used one dimensional model for the seismic trace is referred to as the convolutional model. Seismic trace is generated by forward modelling it is the result of convolution between reflectivity series and bandlimited seismic source wavelet.

$$\boldsymbol{S(t) = RC * W(t) + noise}$$

S(t) is the seismic trace, W(t) us the seismic wavelet, RC is the reflection coefficient and noise component is added.

Seismic inversion uses inverse modelling phenomenon. In this technique inverse of the seismic wavelet is convolved with the seismic trace to generate reflectivity series which further use to generate acoustic impedance model. .

$$RC = S(t) * W(t)^{-1}$$

S(t) is seismic trace, RC is reflection coefficient, $W(t)^{-1}$is inverse of wavelet

Lindseth was one of the first geophysicist to show that if we assume that the recorded seismic signal is as given in Eq.1 below, it is possible to iteratively obtain the acoustic impedance in the next layer (Lindseth, R.O., 1979)

$$Z_{i+1} = Z_i \left[\frac{1+r_i}{1-r_i}\right] \qquad (1)$$

Applying above equation (1) to a seismic trace can effectively transform the seismic reflection data to P-impedance. The AI for the first layer needs to be estimated from a continuous layer above the target area. In this method the impedance for the n-th layer can be calculated as follows (Russell, B. Hampson D., Bankhead, B., 2006)

$$Z_n = Z_1 * \Pi \left[\frac{1+r_i}{1-r_i}\right] \qquad (2)$$

This procedure, however, is not free from problems. The most severe drawback is that the effect of band-limited wavelet is supposed to remove the low frequency component of the reflectivity. Another prime concern in inversion involves removing noise component and proper scaling of seismic data (Russell, B. Hampson D., Bankhead, B., 2006). To assure a more realistic result the low frequency component missing in the seismic data is added the logging data with stacked seismic data. An update approach to inversion is a model-based inversion in which an initial low frequency model is modified iteratively to give the best fit seismic data (Russell, B. Hampson D., Bankhead, B., 2006). The main steps in the inversion process include the data preparation and data input into the software, calibration by tying well logs to the seismic data, estimation of wavelet, generation of low frequency initial model, inversion analysis and inversion (Karim et al, 2015).

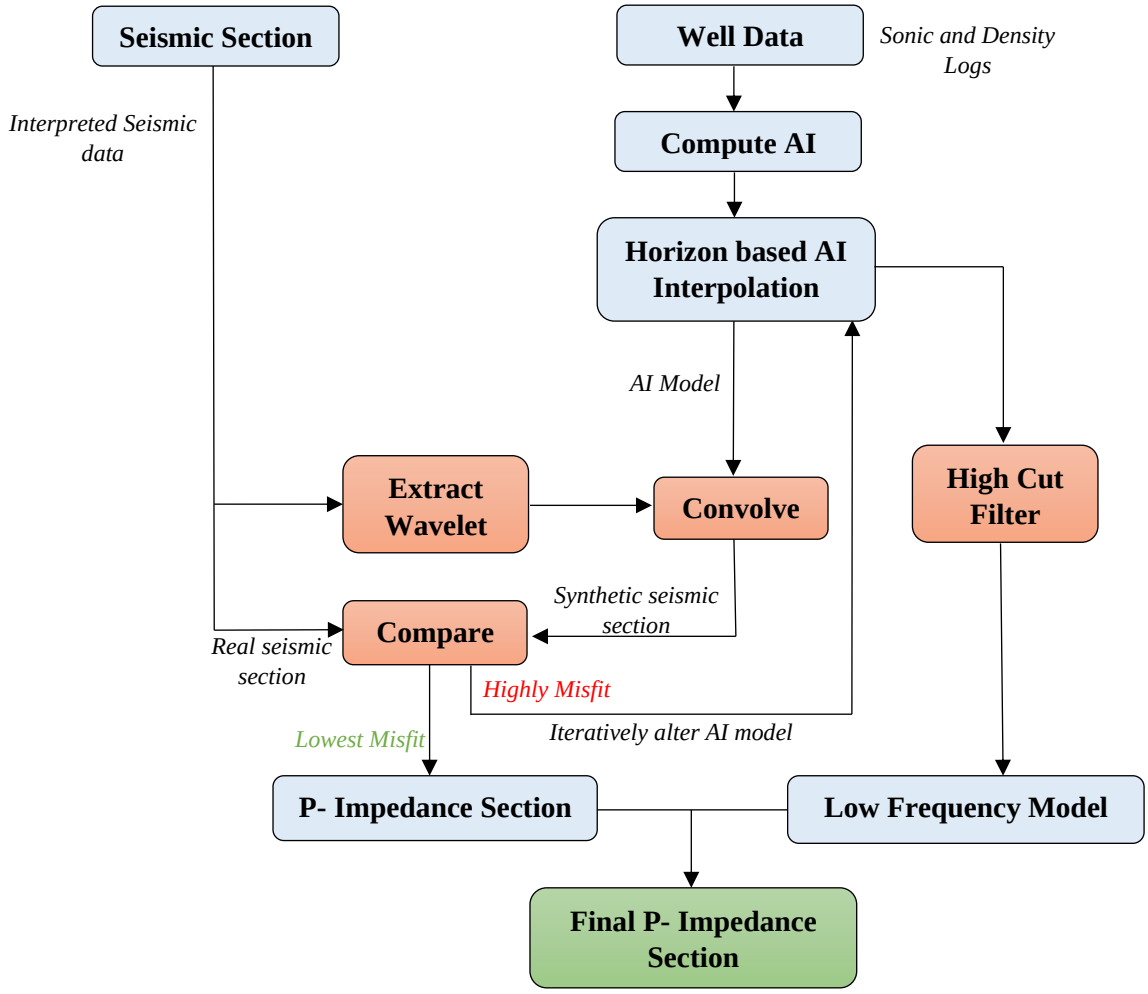

Fig 6.6: A generalized work flow for model-based inversion (Khan, K.A.).

6.4 Seismic Inversion

In this part a brief review of steps involved in model based seismic inversion are discussed. Well CHAK 05 DIM SOUTH and Seismic Line SNJ-20017-09 were used for inversion in Hampson Russell Suite (HRS9).

6.4.1 P-Impedance Calculation.

In the very first step a P-Impedance log was generated by using Hampson Russell P-Impedance Transform function. It simply multiplies density and sonic log (VP converted) to compute acoustic impedance.

6.4.2 Wavelet Extraction.

A seismic wavelet is nothing but the source signature, which is required during the inversion process of seismic data. A good wavelet is the core of inversion (Jain, C., 2013). A constant phase statistical wavelet was extracted from seismic data at well CHAK 05 DIM SOUTH. The

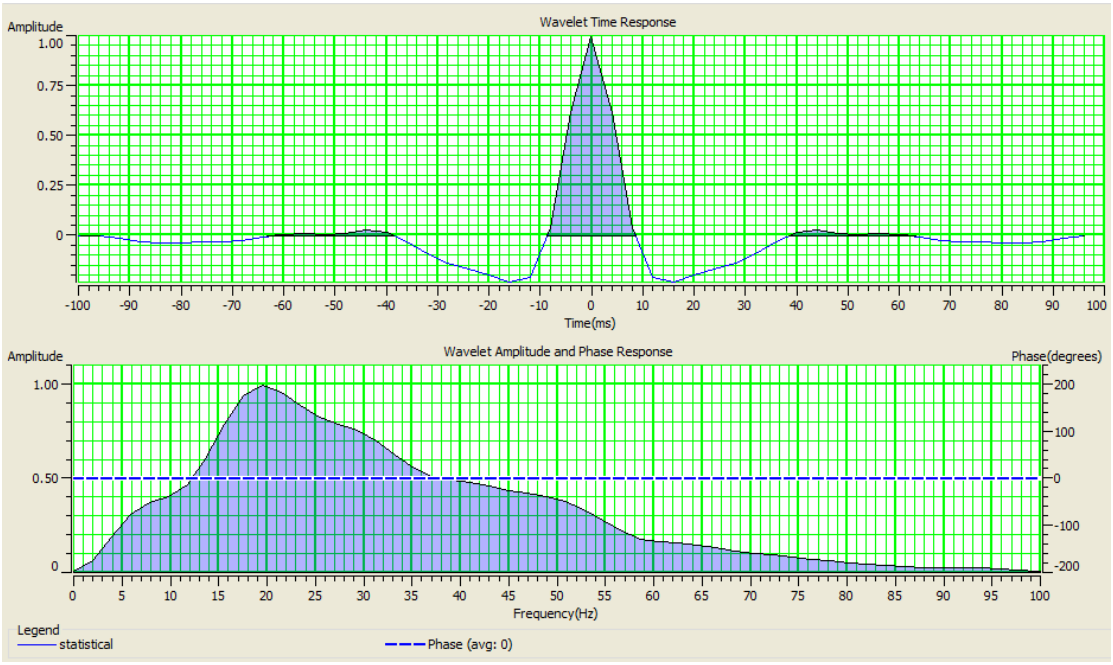

Fig 6.7: Extracted statistical wavelet from seismic traces around Well with time and amplitude spectrum. Phase of the wavelet is shown by dotted line.

window length used for extraction of wavelet ranges from 1000 to 2500 ms and wavelength of wavelet 200ms. Time and amplitude spectrum of wavelet shown in Fig 6.7.

To obtain reliable results from seismic interpretation and inversion, the wavelet should be at zero or minimum phase. The amount of phase shift in input wavelet greatly affects the inversion results. The greater the phase shift, the higher will be the error in the resulting impedance data (Jain, 2013).

6.4.3 Well Correlation

In well correlation a synthetic trace was generated to correlate with recorded seismic trace. The synthetic trace was stretched and squeezed for best matching with real seismic trace. Variations in the quality of well log data severely affects the final synthetic display. This correlation has been done with no phase rotation. Maximum coefficient was 0.683 at time shift 1ms down. Fig

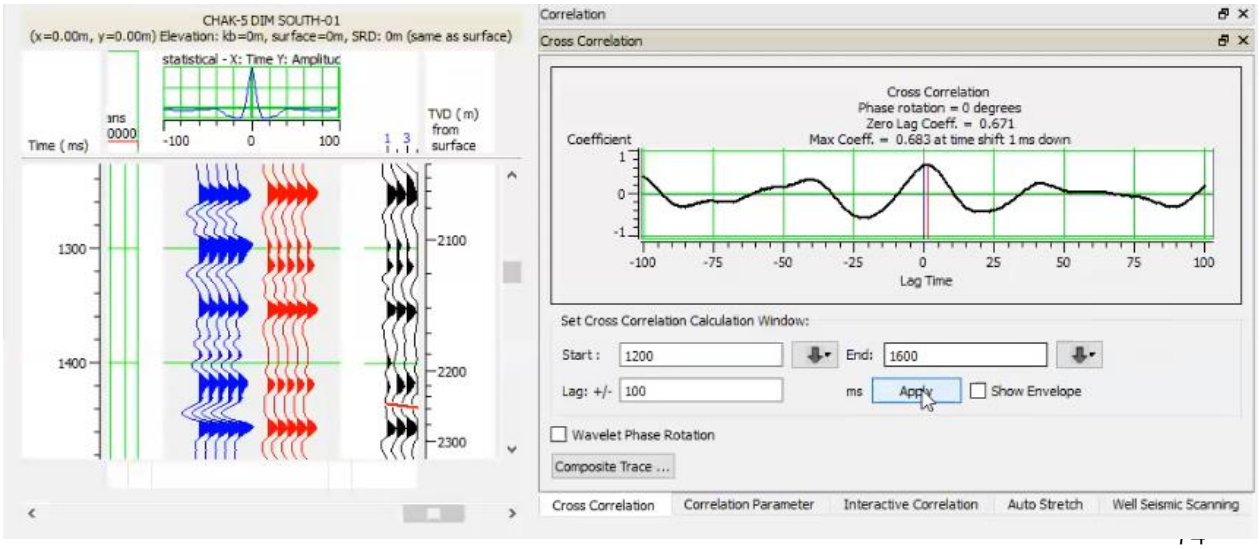

Fig 6.8: Cross Correlation window with synthetic and real seismic trace

6.8 shows final well correlation window in which synthetic gather is represented by blue color and seismic gather with red.

6.4.4 Initial Model

Initial model provides the low components missing from the seismic data which added to provide absolute acoustic impedance. Absolute acoustic impedance provides better interpretation opportunities. Absolute acoustic impedance is obtained when a proper low-frequency component (0-15 Hz) is incorporated in inversion algorithms (Cooke and Cant, 2010).

A low frequency model was generated by using the impedance curve generated by well data is shown in Fig 6.9 Initial model is generated within the time range of 1000ms to 2500ms in which the formation of interest lies. This initial model help to regain the lost low frequencies during processing and stacking of data and are important parameter for model-based inversion.

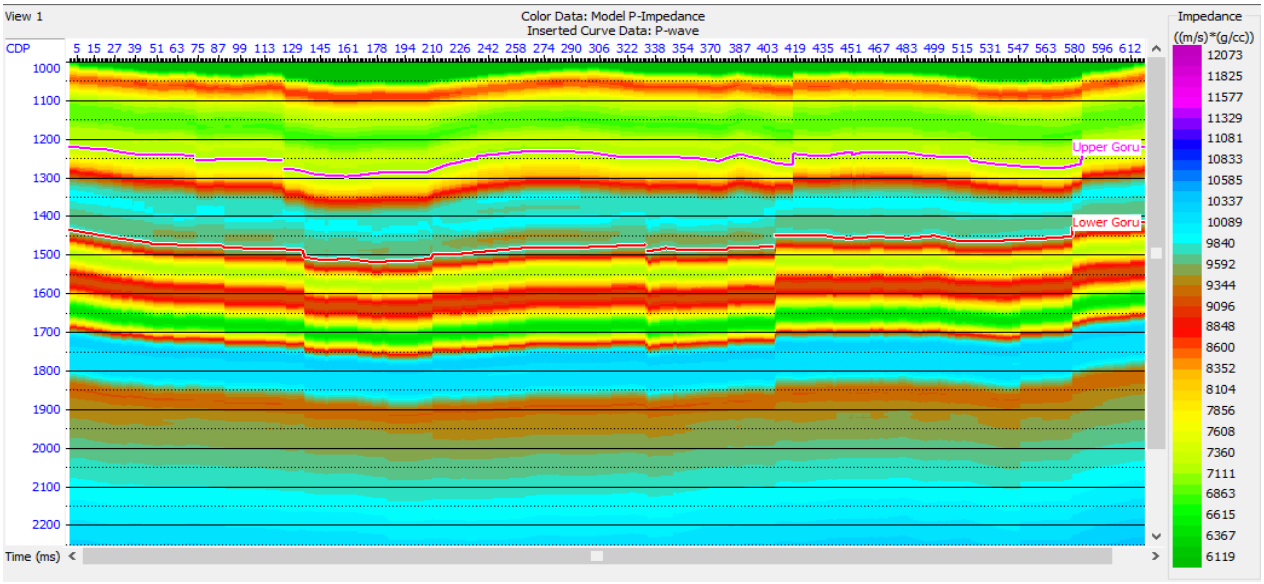

Fig 6.9: Initial Low Frequency Model generated by using the impedance curve

6.4.5 Model Based Inversion

In model-based inversion we start with a low frequency model of the P-impedance and then iteratively change this model until we obtain a good fit between the seismic data and synthetic trace. The basis of inversion analysis is the input data. In the post-stack seismic inversion, stacked seismic volume and the well logs are including velocity and density is required. Model based inversion.

In HRS software model-based inversion product is computed as above flow chart. Post-Stack parameter was set to soft constraints, pre whitening added 1% and after applying 20 iterations, the matching correlation comes to be nearly 0.9614 which is 96.1% with an error of 0.28 which is 2.8 %. This high percent of correlation will be led to the generation of good impedance model. Fig 6.10 shows Best fit correlation model of synthetic and real seismic trace

This correlation can be further improved by applying more iterations. This best fit model of synthetic and seismic is shown in Fig. Seismic traces from the formation tops of Upper and Lower Goru are showing best match with the synthetic traces.

This high percent of correlation then used to generate final impedance model for interpreted seismic line SNJ-20017-09. Fig 6.11 shows the final impedance model on the right side and low frequency model on the left. While Reservoir and Seal rock area is shown below.

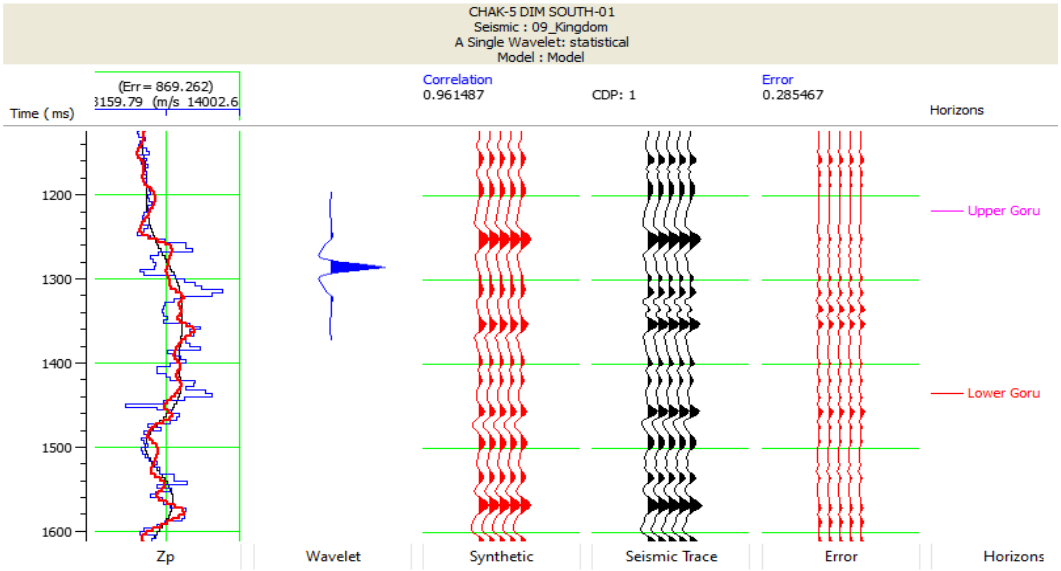

Fig 6.10: Best fit correlation model of synthetic and real seismic trace

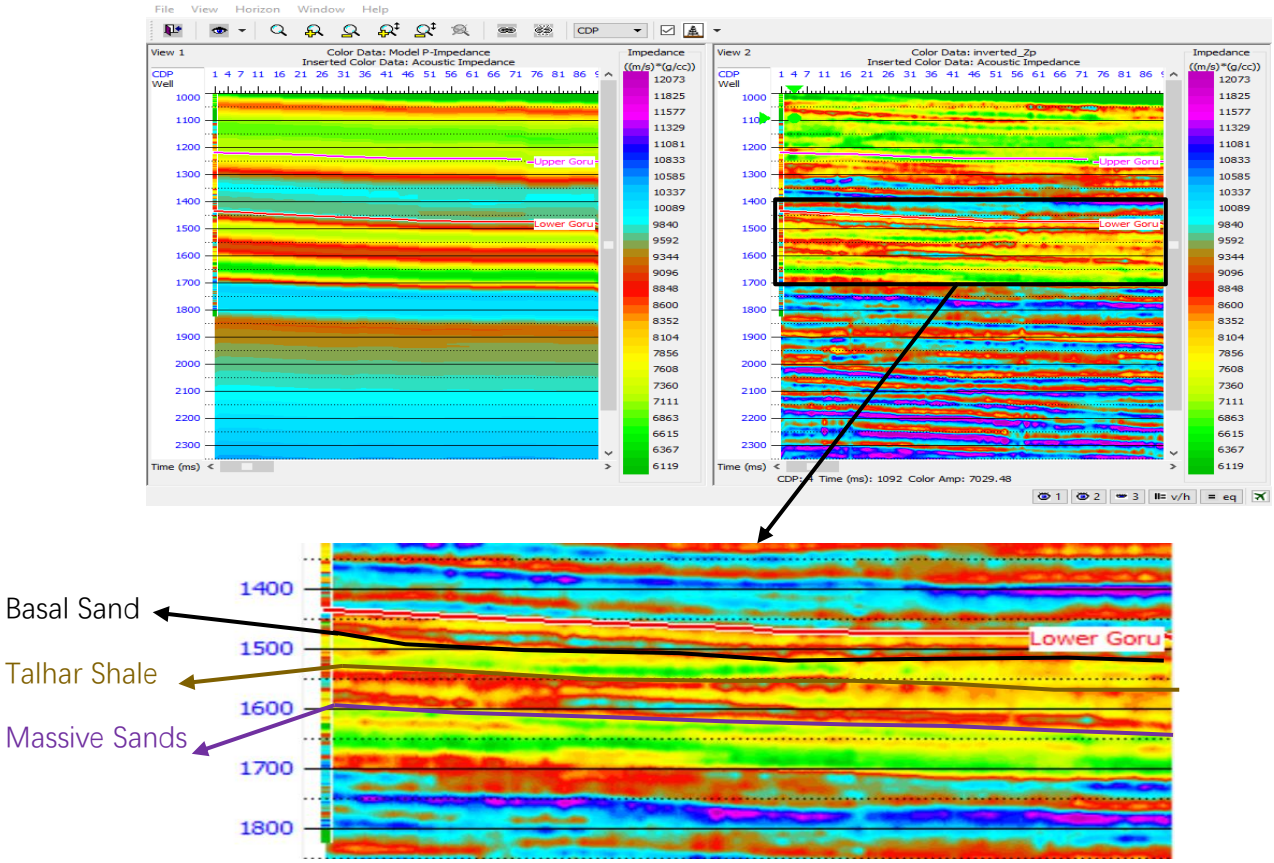

Fig 6.11: Final impedance model on the right side and low frequency model on the left. Reservoir and Seal rock area is shown below.

6.5 Results

Final impedance model successfully captured the reservoir zone i.e. Lower Goru which starts from 1430 milliseconds. In this model low impedance values represented by Red, Yellow and Green color clearly indicated the presence of hydrocarbons in this zone. Lower Goru formations is composed of shale and sand intervals. Sands of Lower Goru act as good reservoir in this area. The inversion model of Lower Goru also shows variations in impedance which indicates the presence of interbedded shale and sand in this zone.

Upper Goru act as seal in this area. High impedance values in the Upper Goru area represented by brown, sky blue and dark blue color confirms the presence of seal rock above reservoir.

Petrophysical analysis also showed that reservoir of Gas Sands lies at this zone. The depth column is shown at the extreme left side of the Fig 6.11. This portion is basically acoustic impedance generated by well data which corelates with the inverted seismic section and confirms the results of inversion. Impedance values for gas sands in other producing blocks in Lower Indus Basin are typically matches with these results.

Chapter 7: 3D Survey Planning

7.1 Introduction

Scientific technologies and tools are being used by oil and gas companies to obtain data improvements. Use of 3D seismic is among these technology for the energy sector. Success ratios for oil companies have been increased by using 3D data. In a worldwide study one large company registered an increase in their success rate for 13% in 1991 using 2D data to 44% in 1996 using 3D technology extensively (Ayler, 1997). The success rate using 2D data remained constant, the success rate using 3D seismic technology has shown a dramatic improvement.

3D seismic survey is a set of numerous closely spaced seismic lines that provide a high spatially sampled measure of subsurface reflectivity. A 3D seismic data for more thorough analysis than 2D seismic data. Shooting a 3D seismic survey has both exploration and exploitation benefits listed in Fig 7.1. A 3D survey is carried out for better interpretation than 2D to enhance production of oil and gas in a specific field.

The differences observed in 3-D seismic surveys recorded over the same field with a separation period of several years show the progress of depletion and flooding practices. Such “4-D” or “time lapse” surveys are becoming more common.

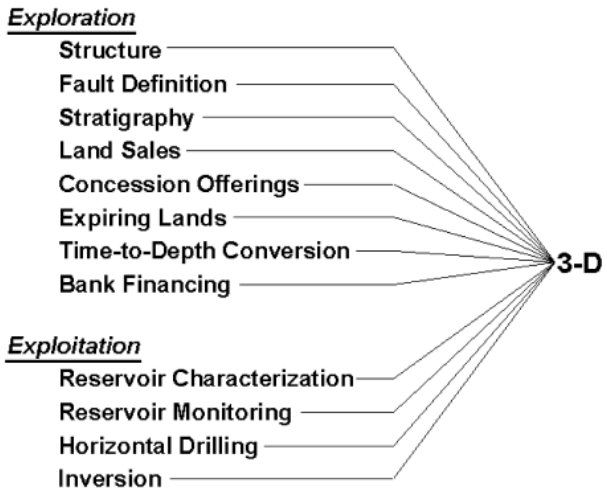

Fig 7.1: Different reasons for shooting a 3-D seismic survey

7.2 Differentiation of 2D and 3D seismic survey.

Seismic surveys are carried out in 2D, 3D and even 4D. Multiple 2D lines can be used to construct a contour map of horizon of interest but multiple 2D parallel lines if joined together do not for a 3D seismic grid as data in 2D is acquired only along one plane. 2D seismic survey is just like taking photographs from front and back as shown in Fig 7.2. Subsurface point is imaged only from front and back. It is just like a person standing at a point and photographer is capturing his front and back. While 3D seismic image has contributions from all the directions as shown in Fig 7.3. Subsurface point is imaged from all the directions along the grid. (Khan, 2013)

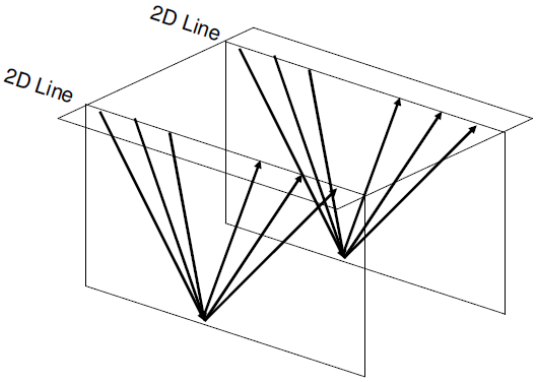

Fig 7.2: 2D seismic image

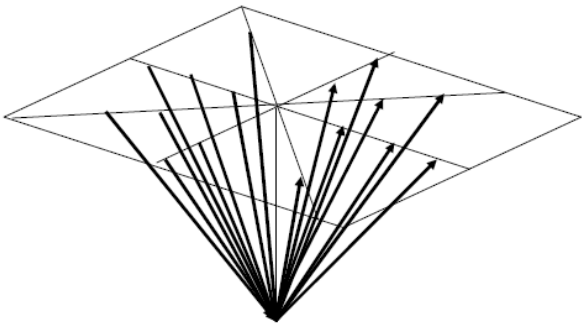

Fig 7.3: 3D seismic image

7.3 Financial Considerations for 3D.

3D seismic survey is costly than 2D so cost factors play an important role in making decisions about the expenditures for a 3D survey. The exploration team must prove to management that a dense grid of geophysical data tied to geological information from existing well provide significant economic benefits by reducing the number of dry holes and overall costs.

Head (1998) provides a more thorough analysis of the value of 3D data through decision tree analysis Fig 7.4. There are numerous decision points when deciding whether to drill and / or whether to acquire additional 2D 3D seismic data.

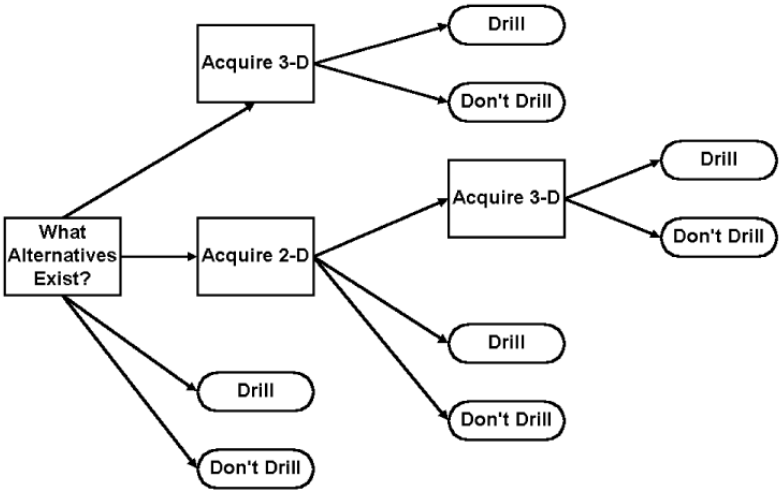

Fig 7.4: Decision tree analysis to guide the exploration decision process (3D

One can assign certain probabilities to particular exploration results that can be achieved with 3D seismic data by using expected value concepts. The probability of an economic success P_{es} is

$$\boldsymbol{P_{es} = P_{source} \times P_{migration} \times P_{reservoir} \times P_{trap}}$$

and the expected monetary value EMV is

$$\boldsymbol{EMV = NPV_{success} \times P_{es} \times NPV_{failure} \times P_{ef}}$$

P_{source}	Probability of hydrocarbon source
$P_{migration}$	Probability of migration of hydrocarbons
$P_{reservoir}$	Probability of reservoir/porosity
P_{trap}	Probability of seal/trap
$NPV_{success}$	Net present value of successful well
$NPV_{failure}$	Net present value of dry well
P_{es}	Probability of economic success
P_{ef}	Probability of economic failure
EMV	Expected monetary value

7.4 Definitions of 3D Seismic Terms.

For seismic exploration, it is the basis for better data acquisition to select better line layout. Orthogonal layout is the most common widely used geometry in 3D seismic. All the terms according to this layout are following

Receiver Line

A line on which receivers are located at a given Receiver Interval (RI) Fig 7.5.

Source Line

A line on which Source Point is located at a given Source Interval (SI). In an orthogonal geometry source lines are perpendicular to the receiver lines Fig 7.5.

Receiver Line Interval

The distance between successive Receiver lines Fig 7.5.

Source Line Interval

The distance between successive Source lines Fig 7.5.

Box

In an orthogonal 3D survey, the Box or Unit Cell is the area bounded by two adjacent source lines and two adjacent receiver lines Fig 7.5.

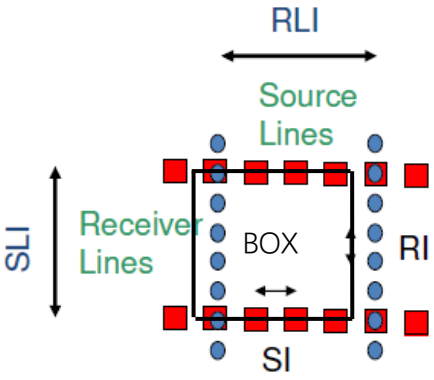

Fig 7.5: Basic 3D Seismic Terms

In-Line Direction

The direction that is parallel to receiver lines.

Usually set along the dip direction of target structure.

Crossline Direction

The direction that is orthogonal to receiver lines. Usually set along the strike direction of target structure. Fig 7.6

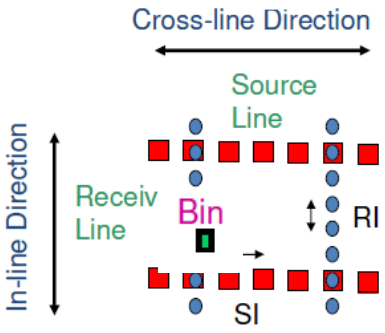

Fig 7.6: Basic 3D Seismic Terms

CMP Bin

A small rectangular area that usually has the dimensions of SI/2 x RI/2 Fig 7.6. All mid-points that lie inside this area are assumed to belong to the same common midpoint. Thus all traces that lie in the same bin will be CMP stacked and contribute to the fold of that bin.

Super Bin, Macro Bin or **Maxi Bin** is a group of neighbouring CMP Bins which are used for velocity analysis, residual static solutions, multiple attenuation & noise attenuation.

Source Point Density

(SD) is the number of source points/KM2 or source points/Mi2. Together with the number of channels (NC), and the size of the CMP Bin, SD determines the fold.

Xmin.

It is the largest minimum offset in a survey given by

$$X_{min} = \sqrt[2]{(RLI^2 + SLI^2)}$$

*X*min is necessary to record shallow events. It defines the largest minimum offset to be recorded in the bin that is in the centre of the box.

Xmax

It is the Maximum Recorded Offset and depends on the depth of the deepest targets that must be imaged. It is usually the half-diagonal distance of the patch.

Patch

A patch refers to all live receiver stations that record data from a given source point in the 3D survey Fig 7.7 (blue color). The patch usually forms a rectangle of several parallel receiver lines. The patch moves around the survey and occupies different template positions as the survey moves to

different source stations.

Salvo

A group of source points associated with a particular patch position. Fig 7.7 (red color).

Template

A particular receiver patch into which a number of sources points are recorded Fig 7.7 (yellow color). The source points may be inside or outside the patch.

Template = Patch + Salvo

A template moves along Swaths to cover the whole survey grid.

Swath

A Swath equals the width of the area over which source stations are recorded without any cross-line rolls. A template moves through the Swath in the in-line direction Fig 7.8.

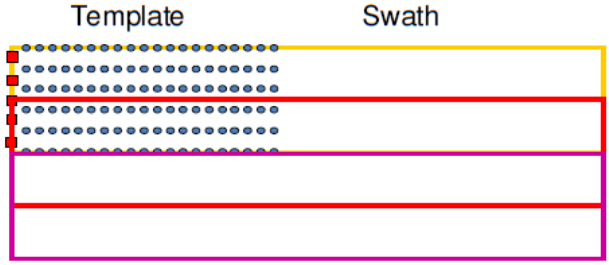

Fig 7.8: Patch (Blue), Salvo (Red) , Template (Yellow) and Swath

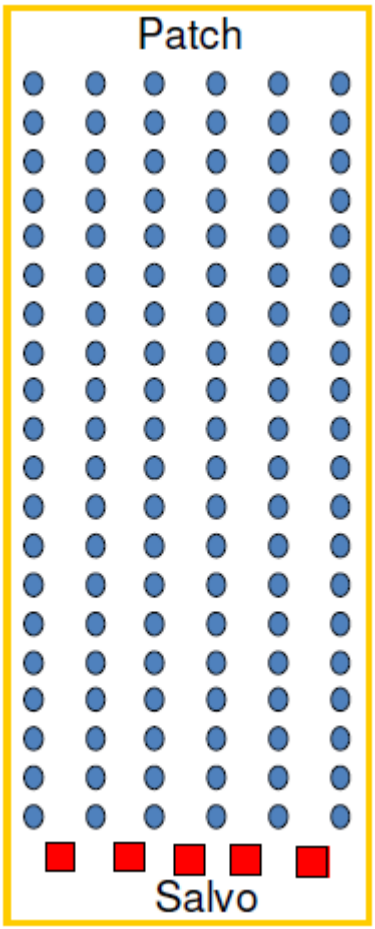

Fig 7.7: Patch (Blue) Salvo (Red) and Template (Yellow)

Grid

A Grid of equally spaced Receiver and Source line covers the whole survey area (orthogonal layout.) in Fig 7.9.

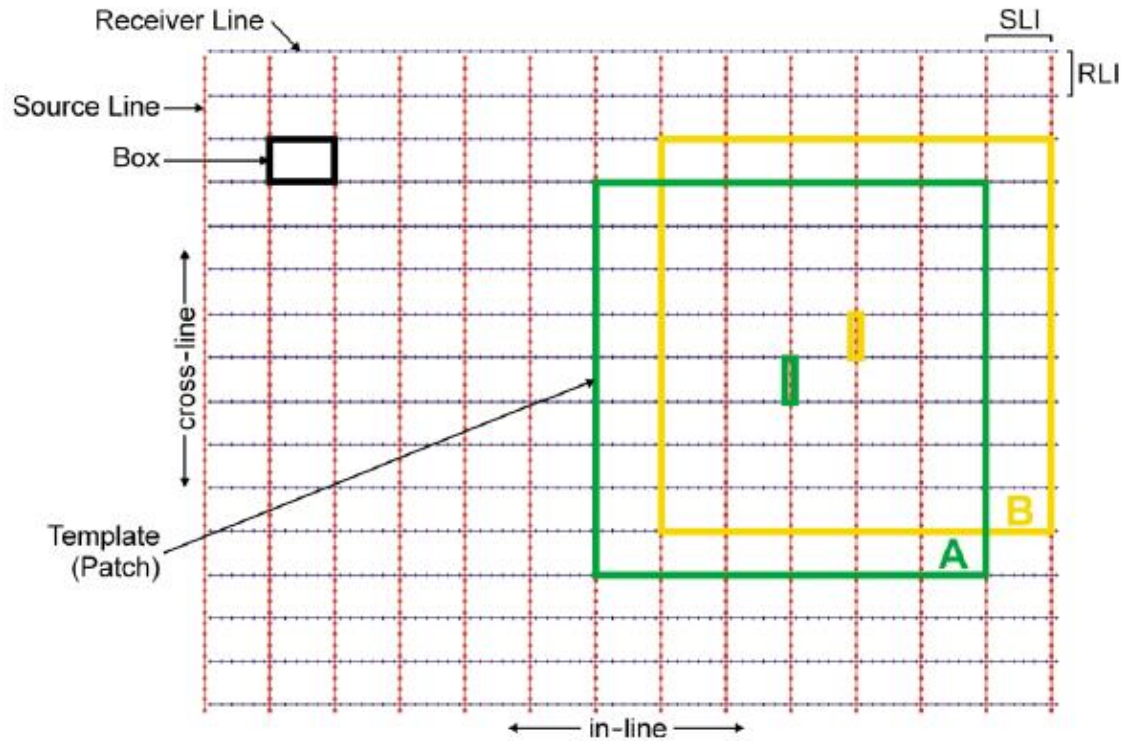

Fig 7.9: A grid of Receiver and Source lines

7.5 3D seismic survey design parameters and procedure.

Survey designing is dependent on so many input parameters and constraints that it has become quite an art. Considerations to design a survey are following

- Geologic Targets
- Economic Constraints
- Recording Equipment

Initial considerations to setup design parameters are dependent on objectives such as narrowest lateral dimensions of the geologic target that is to be imaged, depth of the shallowest target, depth of the deepest target, and required stacking fold to create an acceptable image at the depth of the principal target. (Khan K.A., 2013)

3D seismic recording grid geometry design parameter are following

- Recording Swath Size
- Source Station Spacing
- Receiver Station Spacing
- Source Line Spacing
- Receiver Line Spacing

A simplified flow chart for survey design is shown in the Fig 7.9

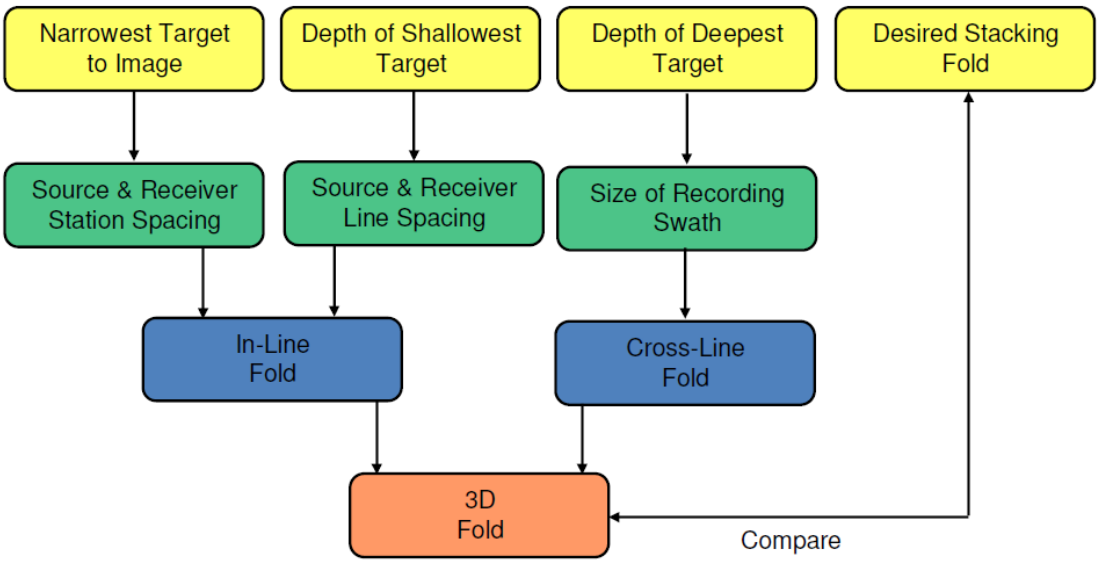

Fig 7.9: Flow Chart for Survey Design (Khan K.A., 2013).

7.5.1 Source and Receiver Station Spacing

Another important parameter is source and receiver station spacing for acquisition of 3D seismic survey. The dimension of a 3D stacking bin in the inline direction is one half of the receiver station spacing while its dimension along the crossline direction is one half of the source station spacing. So, for imaging of narrowest targets, in addition to the dimensions of stacking bins the source station and receiver station spacing are also defined. As the stacking-bin dimension are one-half of the station spacings, source-station and receiver station spacings should be one-half (or less) of the narrowest horizontal dimension that needs to be imaged. (Khan K.A., 2013)

7.5.2 Fold

Stacking fold (or fold-of-coverage) is the number of field traces that contribute to one stack trace i.e., the number of midpoints per CMP bin. It is also the number of overlapping midpoint areas. Fold controls the signal-to-noise ratio (S/N) Fig 7.10. If the fold is doubled, a 41% increase in S/N is accomplished. Keary (1987) showed that the ratio of 3-D to 2-D fold is frequency dependent and varies according to following equation

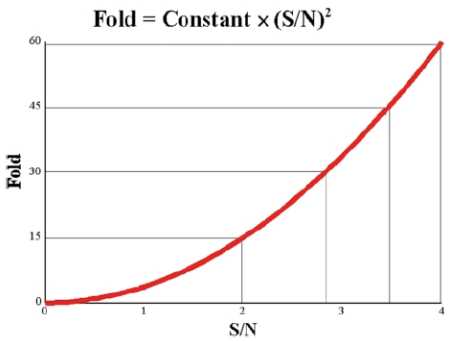

Fig 7.10: Relationship of Fold and S/N

$$\boldsymbol{3D\ fold = 2D\ fold \times frequency\ \times C}$$

Here C is an arbitrary constant.

Krey's (1987) more complete formula for 3-D fold is

$$\boldsymbol{3D\ fold = 2D\ fold \times \frac{3D\ bin\ spacing^2 \times frequency \times \pi \times 0.401}{2D\ CDP\ spacing \times Velocity}}$$

7.5.2.1 In Line Fold

For an orthogonal straight-line survey, in-line fold is defined similarly to the fold on 2-D data. The formula is as follows

$$\boldsymbol{In - line\ fold = \frac{number\ of\ receivers \times station\ spacing}{2 \times source\ interval\ along\ the\ receiver\ line}}$$

7.5.2.2 Crossline Fold

Similar to the calculation of in-line fold, the crossline fold is

$$\boldsymbol{Cross - line\ fold = \frac{source\ line\ length}{2 \times receiver\ line\ interval}}$$

7.5.2.3 Total Fold

The total 3-D nominal fold is the product of in-line fold and cross-line fold

$$\boldsymbol{Total\ fold = Cross - line\ fold \times In - line\ fold}$$

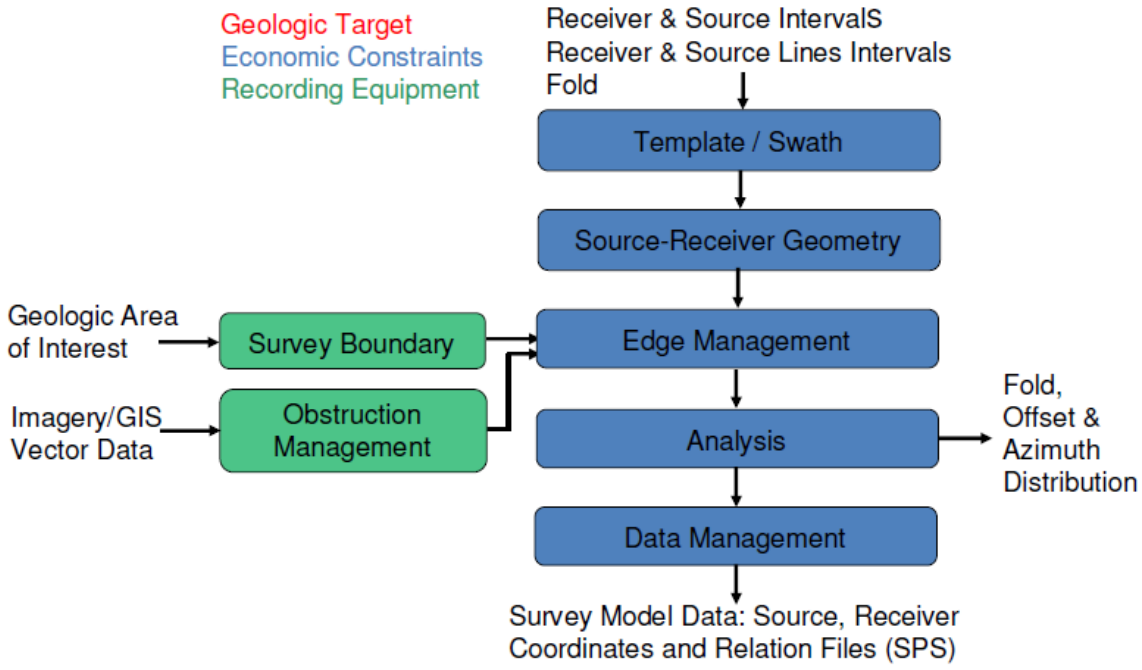

Fig 7.11: Complete Flow Chart for Survey Design (Khan, K.A., 2013)

7.5.2.4 Fold Coverage

Fold coverage map shows distribution of fold in the survey area. It shows the build-up of fold in the taper zone and the maintenance of full fold over the unmigrated area of interest Fig 7.12.

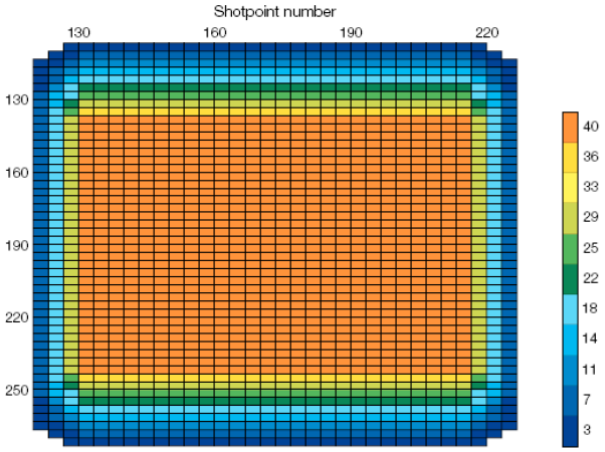

Fig 7.12: Fold Coverage map

7.6 Analysis of survey design

Design analysis is an integral part of survey design it helps in adjusting parameters to get optimum results. It has been done by analysis of fold coverage, offsets and azimuth.

7.6.1 Offset distribution

In 3D survey each CMP bin contains midpoints from many source-receiver pairs which contribute traces to the bin. Offset distribution in a stacking bin is most affected by fold. A lower fold gives poorer offset distribution, while increasing the fold improves the offset distribution Fig 7.13.

7.6.2 Azimuth Distribution

An azimuth is the deviation from 0° North or compass angle from source to receiver. An even Azimuth distribution map shows contributions to CMP Bins from all directions Fig 7.14.

It is important to consider offset and azimuth distribution not in single bins but in a "neighbourhood" of bins as Migration and DMO move trace energy across many surrounding bins. A good rule of thumb for the size of a neighbourhood is the first Fresnel zone. (Khan, K.A., 2013)

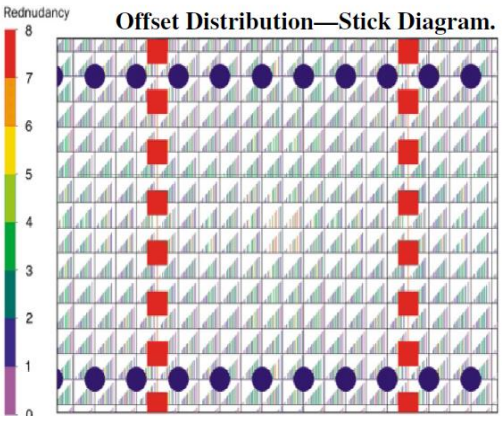

Fig 7.13: Offset distribution

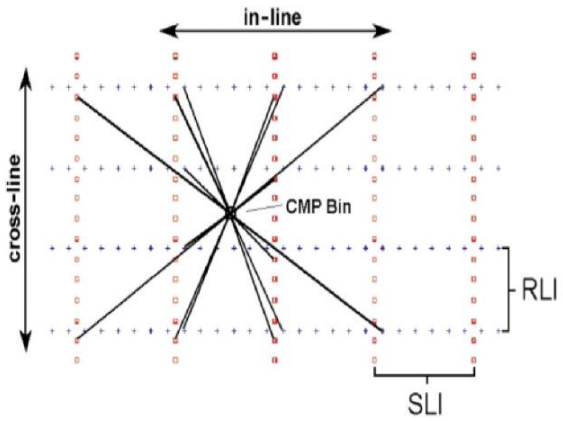

Fig 7.14: Azimuth distribution

7.7 Edge Management

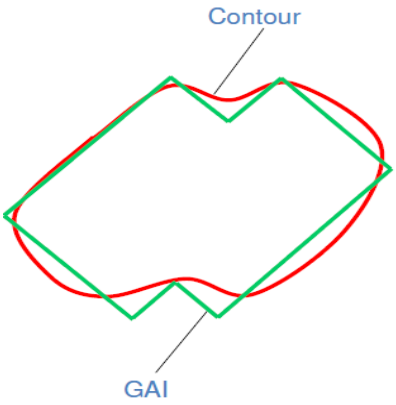

Fig 7.15: Geological Area Of Interest

In a 3-D design edge management specifies the width of the migration apron and the fold taper. The fold taper is the area at the edge of the survey where full-fold (or nearly full fold) at depth has not been reached before migration. The grid of 3-D design needs to be clipped at the sides according to an expanded boundary which follows the shape of the geologic area of interest. The Geologic Area of Interest (GAI) may be demarcated from an existing 2D Seismic base map or a geologic map. It may be in the form of a contour map Fig 7.15. The GAI is marked by a polygon which approximates the contour, with its sides along the dip and strike of the sub-surface structure.

7.7.1 Migration Apron

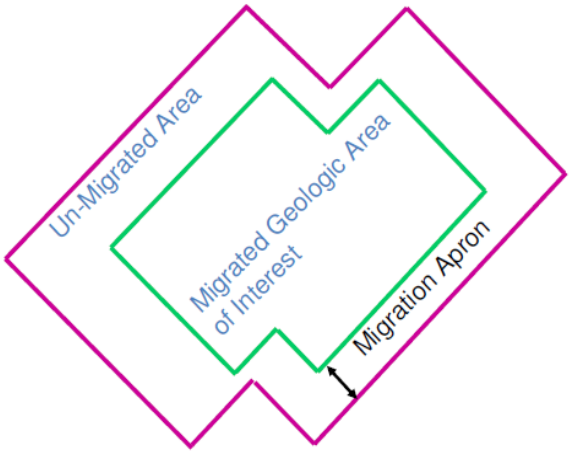

Fig 7.16: Migration Apron

The width of an area that needs to be added to the 3D survey to allow proper migration of any dipping events. This width does not need to be the same on all sides of the survey and depends on the dip of the structure in that direction and its depth Fig 7.16.

7.7.2 Fold Taper

The width of an additional area that needs to be added to the 3D surface area to build up full fold. Often there is some overlap between the fold taper and the migration apron because one can tolerate reduced fold on the outer edges of the migration apron Fig 7.17. Fig 7.18 shows migration apron and fold taper zone in association with seismic processes.

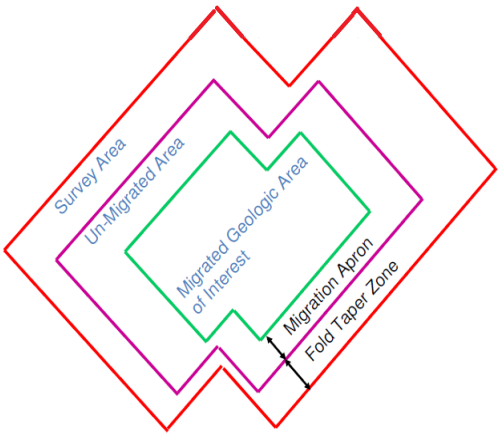

Fig 7.17 Complete edge management considerations

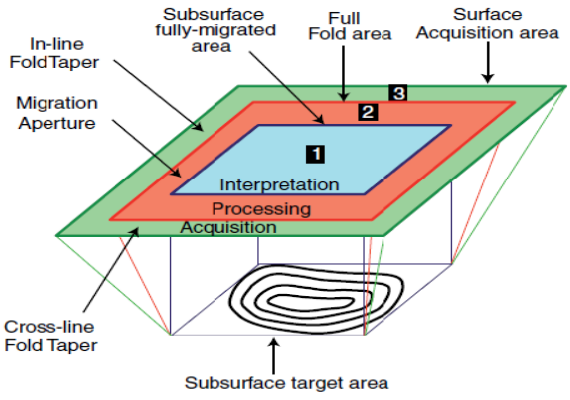

Fig 7.18: Migration Apron and Fold Taper zone

7.8 3-D Survey Planning of Sinjhoro area

The area is located at **25°30'-26°29' N, 68°25'-70°13' E**. Sinjhoro area is present in Sanghar district of Sindh, Pakistan, about 12 km from Sanghar city, along Sanghar-Shahdad Pur Road. Sinjhoro is Headquarter of Taluka Municipal Administration Sinjhoro. 3D-Survey has been planned for field development.

7.8.1 Input Parameters for 3-D Receiver Grid

Origin First point X	**466831**	**Origin First point Y**	**2870861**
Azimuth	**65**	**Starting Picket number**	**101**
Starting line number	**301**	**Picket number increment**	**1**
Line number increment	**1**	**Picket interval**	**50**
Line to Line interval	**300m**	**Max. Line Length**	**32000 m**
Number of line in project	**80**	**Receiver Line Color**	
		Receiver Line Name Color	

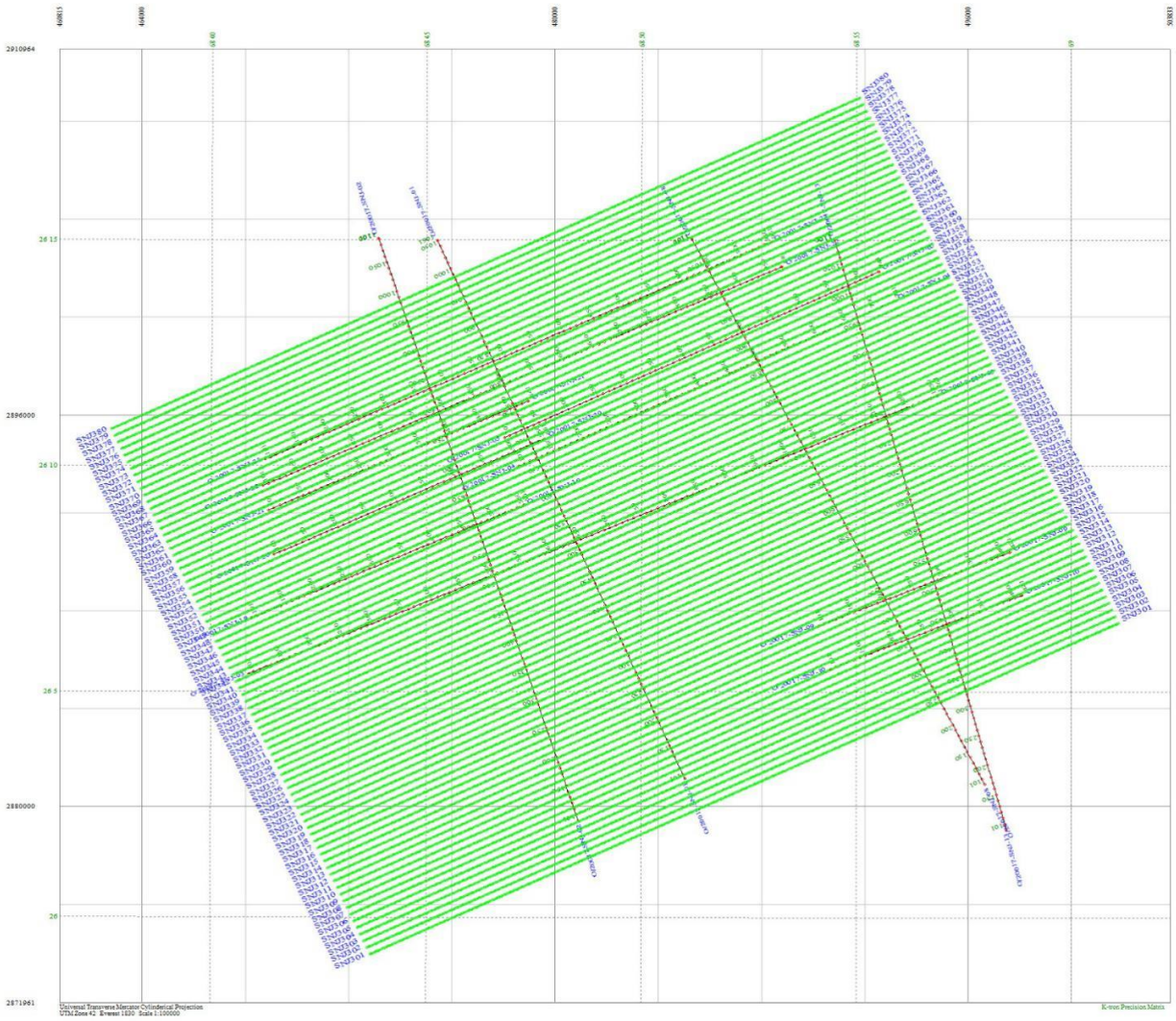

Fig 7.19: 3-D Receiver grid have been prepared using Sigma 3D (Khan, K.A.,)

7.8.2 Input Parameters for 3-D Shot Grid

Origin First point X	**473834**	**Origin First point Y**	**2875830**
Azimuth	**335**	**Starting Picket number**	**101**
Starting line number	**501**	**Picket number increment**	**1**
Line number increment	**1**	**Picket interval**	**100**
Line to Line interval	**300m**	**Max. Line Length**	**21150m**
Number of shot lines in project	**96**	**Shot Line Color**	
		Shot Line Name Color	

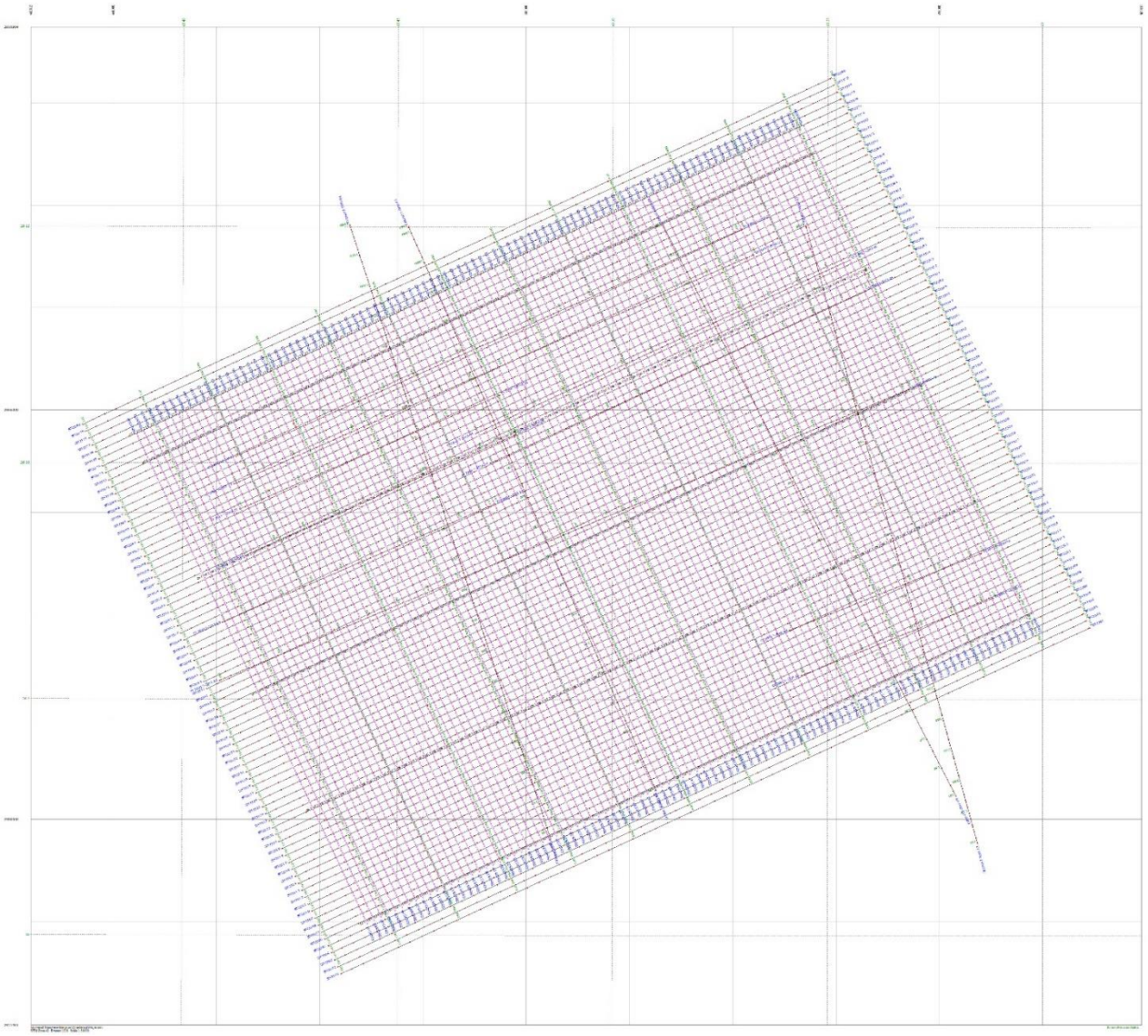

Fig 7.20: 3-D Shot Point grid prepared using Sigma 3D (Khan, K.A.,).

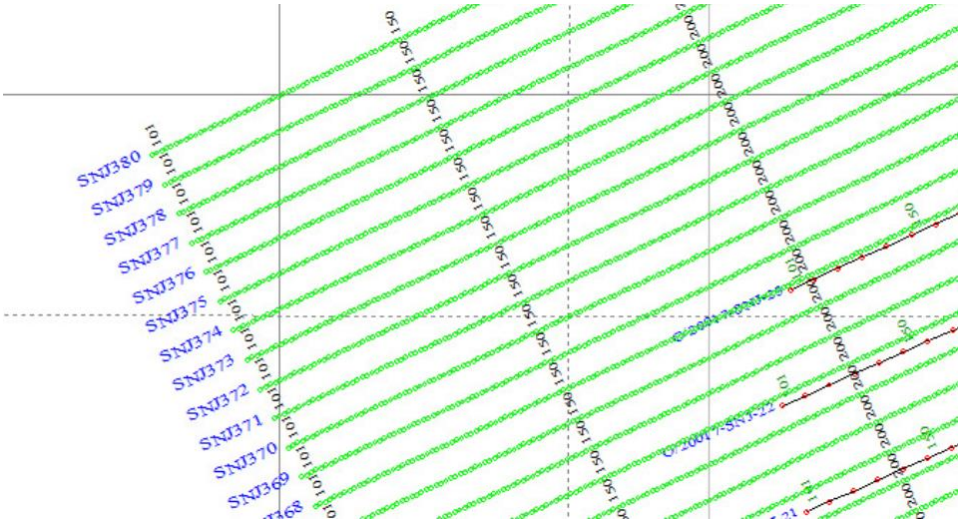

Fig 7.20: Close View of receiver grid

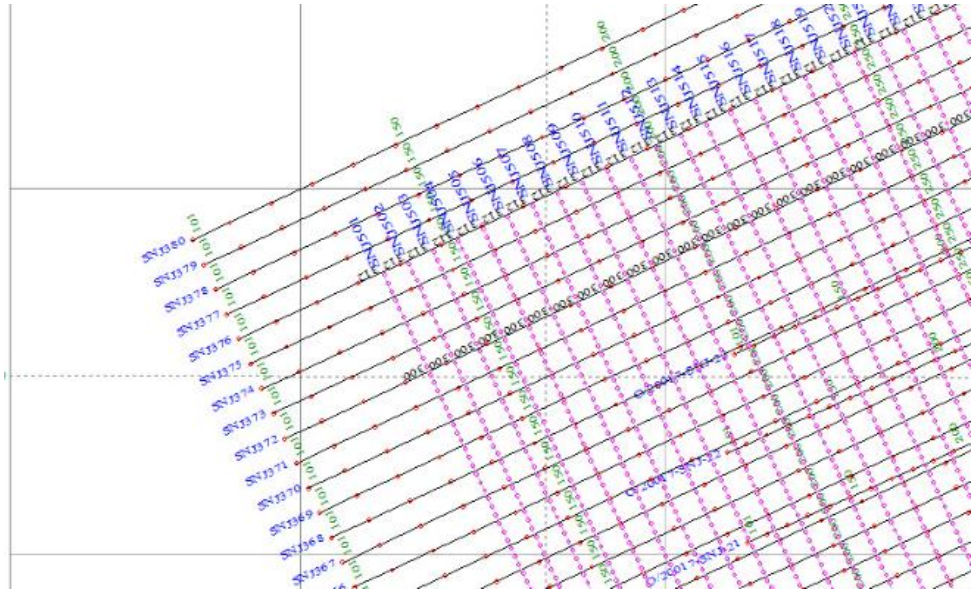

Fig 7.21: Close view of shot and receiver 3-D Grid

7.8.3 Edge Management

Geological Area of Interest marked from 2D interpreted data helped to calculate **Migration apron** and **fold taper zone** and their boundaries have been drawn Fig 7.22. Green color boundary is showing Geological area of interest. The area between green and blue boundary is unmigrated area. Red boundary is showing fold taper zone in the area. In Fig 7.23. 2-D receiver lines along with boundaries have been shown.

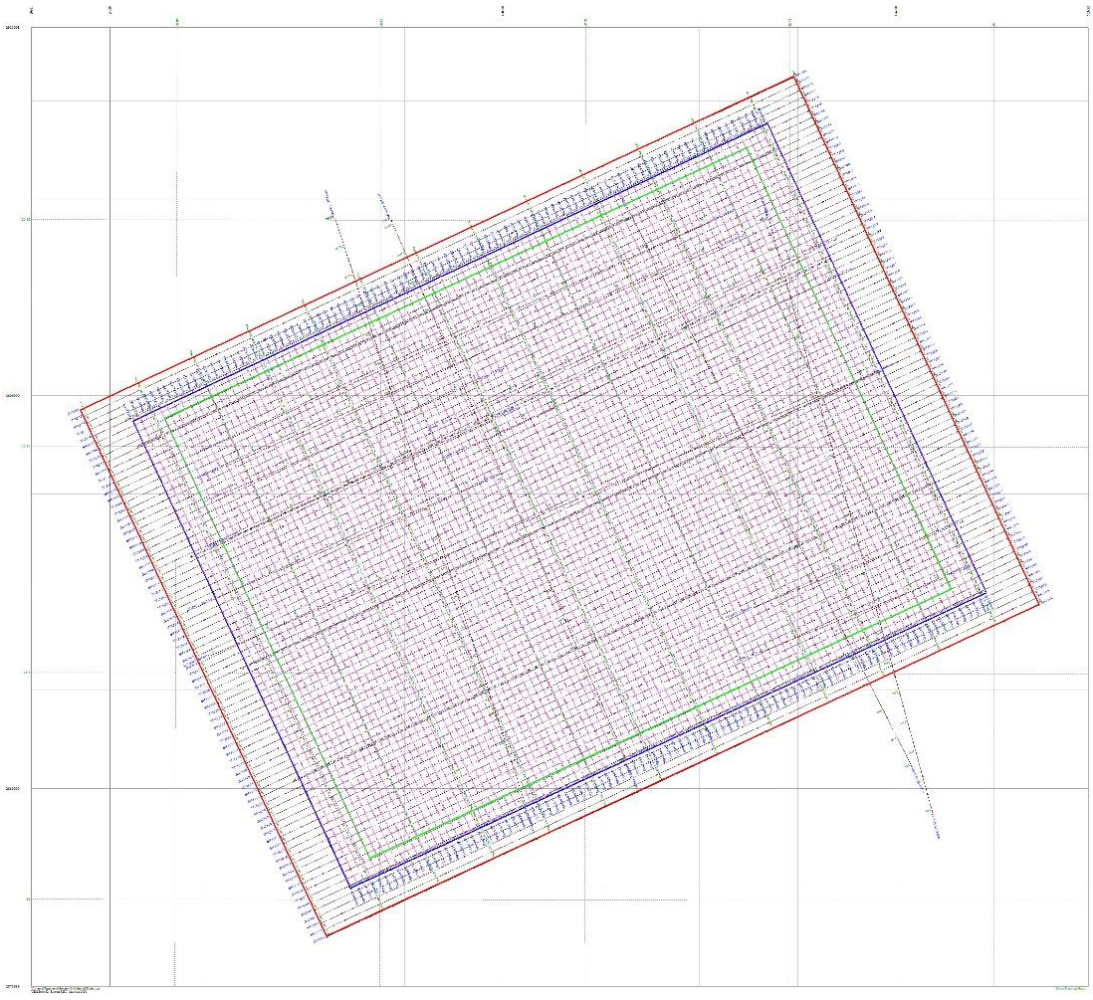

Fig 7.22: Geological Area of Interest(Green), Migration Apron (Blue) and Fold Taper zone (Red).

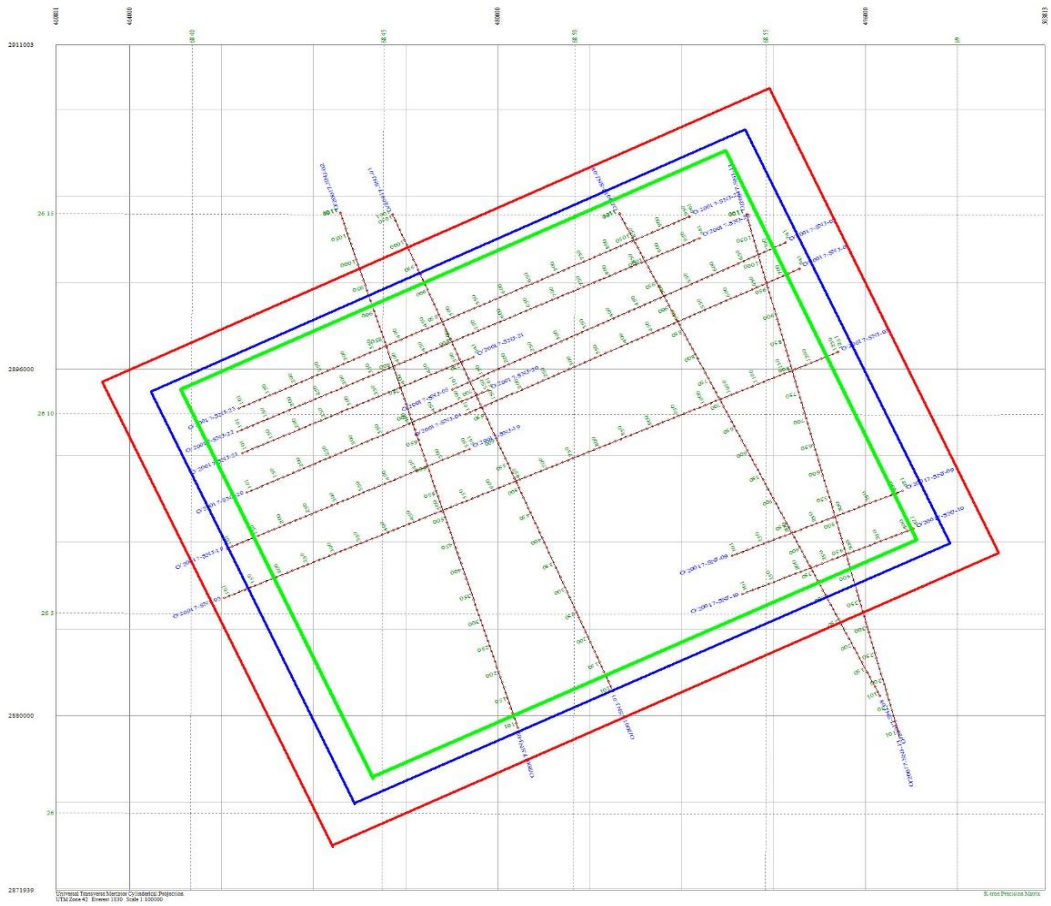

Fig 7.23: Geological Area of Interest (Green), Migration Apron (Blue) and Fold Taper zone (Red) with previous 2-D receiver lines.

7.8.4 Migration Aperture

2-D interpreted data helped to set parameters for calculation of migration apron. Lower Goru formation (GAI) is producing in this area, its depth, time and dip have been used to calculate migration aperture by using Seistein application (Khan, 2000) shown in Fig 7.24.

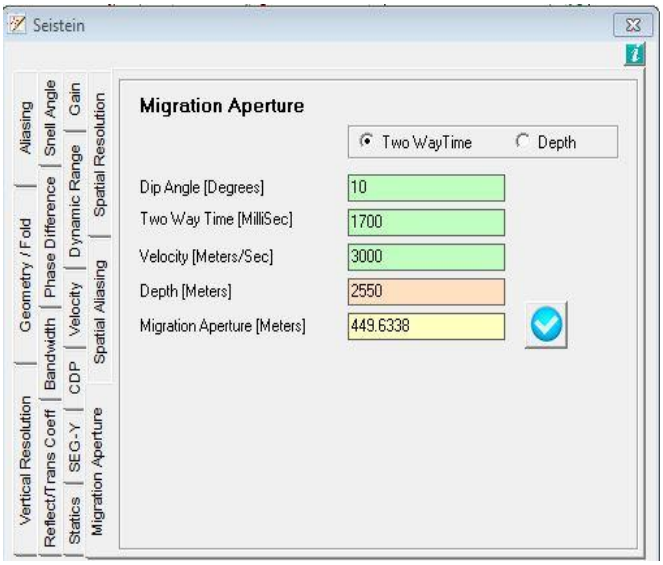

Fig 7.24: Migration Aperture Calculation (Khan, 2000).

Conclusions

- General Stratigraphic column and Formation Tops of well Chak 5 Dim South -01 were used to identify reflectors on seismic after seismic to well tie.
- The marked horizons are named as Ranikot, Upper Goru, Lower Goru and Chiltan. These horizons were identified with the help of synthetic seismogram of well Chak 5 Dim South-01. Synthetic seismogram was generated by using density and sonic log.
- Major Faults along with minor faults were marked in seismic section according to tectonics of the area. Normal faulting results in horst and graben structures which shows the area of research lies in the extensional regime. Crustal extension of rocks was also calculated
- Seismic Attributes such as Trace envelop confirm the major lithological changes such as top of Upper Goru and the instantaneous phase confirm the continuity of marked horizons on seismic section and the instantaneous frequency confirm the marked horizons are in reservoir rock by showing the low frequency signal.
- Petrophysical analysis used to calculate volume of shale, volume of sand water saturation and hydrocarbon saturation in the reservoir zone within the Lower Goru sands. Quantitative results show 13-14% porosity which is fair for the reservoir. 27-28% volume of shale, 33-34% water saturation, and 66-64% hydrocarbon saturation. These results show that the reservoir zones would be effective for the accumulation of the hydrocarbons.
- Elastic logs and petro-elastic cross plots have been generated for facies modeling which can effectively discriminate between Clean Sand, Shaly Sand and Shale sequences in Talhar formation. The facies modeling interpretation is confirmed through four cross plots, which provide the same interpretation.
- Velocity Analysis on interpreted geologic section 20017-SNJ-09 has been performed to generate a geologically realistic velocity model. 2D Modelling has been carried out on the velocity model to generate a 2D synthetic seismic section which further validates the velocity model.
- Seismic post stack inversion was carried out which show the low impedance values in the reservoir zone. These combined results confirmed the presence of gas sands in the reservoir zone.
- AVA synthetic gather confirmed the gas effect in the reservoir zone.

- 3D seismic survey was designed for Field development and reservoir characterization as 3D surveys increase the probability of success for next wells and provide a better image of the subsurface for reservoir characterization.

REFRENCES:

Aadil, N., Tayyab, M., & Naji, A. 2014. Source Rock Evaluation with Interpretation of Wireline Logs: A Case Study of Lower Indus Basin, Pakistan. *Nucleus*, *51*(1), 139-145.
-6

Ahmed, A., and Ahmed, N. 2005.Paleocene petroleum system and its significance for exploration in the southwest Lower Indus Basin and nearby offshore of Pakistan. Proceedings of Annual Technical Conference, Islamabad, Pakistan, November 28-29,p. 2.

Ahmed, Z, Akhter, G .,Bashir, F., khan, M.A, and Ahmed,M.2009. Structural interpretation of seismic profiles integrated with reservoir characterization of bitrisim block(Sindh Province),Pakistan. Energy Sources, Part A 32:303-314.

Al-Sadi, H.N. 1980 Seismic Exploration Technique and Processing

Andreas Cordsen, Mike Galbraith, and John Peirce, Planning Land 3-D Seismic Surveys: Soc. Expl. Geophys.

Asquith, G., and Krygowski, D.2004. Basic Well Log Analysis: AAPG Methods in Exploration, NO. 16, Tusla, OK: American Association of Petroleum Geologist, ppl. 31-35.

Ayler, 1997. The role of 3-D seismic in a world-class turnaround: 67th Ann.Internat. Mtg., Soc. Expl. Geophys., Expanded Abstracts, 725–729.

Aziz MZ, Khan MR. 2003. A Review of Infra Cambrian Source Rock Potential in Eastern Sindh, an analogue to Huqf Group of Oman. Infra – Cambrian play of Eastern Sindh, Pakistan.

Banks, C. J., & Warburton, J. 1986. 'Passive-roof 'duplex geometry in the frontal structures of the Kirthar and Suleiman mountain belts, Pakistan. Journal of Structural Geology, 8(3), 229-237.

Castagna, J. P., & Backus, M. M., 1993. Offset-Dependent Reflectivity Theory and Practice of AVO Analysis. Society of Exploration Geophysicists.

Chhajlani, R., Zheng, Mayfield, D., and MacArthur, B., 2002. Utilization of Geomechanics for Medusa Development, Deep water Gulf of Mexico, SPE Annual Technical Conference and Exhibition, Texas, 29 September-2 October 2002.

Cibin, P., Pizzaferri, L., and Marta, M. D., 2008. Seismic Velocities for Pore Pressure Prediction. Some Case Histories,SPG, 7th International Conference and Exposition on Petroleum Geophysics.

Coffeen, J.A., 1986, Seismic Exploration Fundamentals, PennWell Publishing Co.

Chang C-C, Yang M-H, Wen H-M & Chern J-C. 2002. Estimation of total flavonoid content in propolis by two complementary colorimetric methods. J Food Drug Anal

Dobrin and Savit. 1988, Geophysical Exploration, Hafner Publishing Co.

Dix, C. H., 1955. Seismic Velocities for Surface Managements, Geophysics, Vol. 20, pp. 68-86.

Fertl, W. H., & Rieke III, H. H. 1980. Gamma-ray spectral evaluation techniques identify fractured shale reservoirs and source-rock characteristics. Journal of Petroleum Technology, 32(11), 2-053.

Gadallah, J., and Fisher, I., 2009. Exploration Geophysics, Springer-Verlag Berlin Heidelberg. DOL:10.1007/978-540-85160-8.

Goodway B, Varsek J and Abaco C 2007 Isotropic AVO methods to detect fracture prone zones in tight gas resource plays *2007 CSPG CSEG Convention* pp 585–9.

Kadri, I.B. (1995) Petroleum Geology of Pakistan. p. 34.

Kazmi, A.H. and Jan, M.Q 1997. Geology & Tectonics of Pakistan. Graphic Publications, 650 p.

Kearey P., Hill I. and Brooks M. 2002. An Introduction to Geophysical Exploration (Ed). Tj International Ltd., Padstow, Cornwall, United Kingdom, 21-122.

Khan, K.A., 2013, Seismic - The Next Step Series: 3D Seismic Survey Design OIST, Islamabad.

Khan, K.A., 2007. Integrated Geo Systems - A Computational Environment for Integrated Management, Analysis and Presentation of Petroleum Industry Data, In: T. C. Coburn and J. M Yarus (Eds.), Geographic Information Systems in Petroleum Exploration and Development, American Association of Petroleum Geologists, AAPG Book on Computers in Geology, pp.215-226. M Yarus (Eds.), Geographic Information Systems in Petroleum Exploration and Development, American Association of Petroleum Geologists, AAPG Book on Computers in Geology, pp.215-226.

Khan, K.A., and Akhter, G., 2011. Work flow shown to develop useful seismic velocity models, Oil & Gas Journal,Vol.109(16), pp.52-61.

Khan, K.A., Akhter, G., and Ahmad, Z., 2011. An ActiveX control for embedding GPS capability in custom applications, GPS Solutions, Vol.15(4), pp.433-439.

Khan, K.A., 2007. Integrated Geo Systems - A Computational Environment for Integrated Management, Analysis and Presentation of Petroleum Industry Data, In: T. C. Coburn and J.

Khan, K. A., Akhtar, G., Ahmed, Z., Khan, M.A., and Naveed, A., 2006. Wavelets - A Computer Based Training Tool for Seismic Signal Processing, Pakistan Journal of Hydrocarbon Research, Vol.16(1), pp.37-43.

Khan, K.A., Khan, M.A., Abbas, G., Akhter, G., and Ahmad, Z., 2009. Algorithm helps define final 3D seismic survey polygon, Oil & Gas Journal, Vol.107(2), pp.34-38.

Michael E Badley, 1985. Practical seismic interpretation, International Human Resources Development Corporation

Raza, H. A., S. M. Ali, and R. Ahmed, 1990. Petroleum geology of Kirthar sub-basin and part of Kutch basin. Pak. J, Hydroc. Res., 2 (1): 68-76.

Robinson and coruh 1988, Basic Exploration Geophysics.

Shah, S.M.I. 1977. Stratigraphy of Pakistan, Geological Survey of Pakistan, Memories, (12): 71-72.

Yilmaz, O., 2001. Seismic Data Analysis—Processing, Inversion, and Interpretation of Seismic Data. Soc. of Expl. Geophys., Tulsa,OK